

Manuscript Number: GR-D-19-00480R1

Title: Hercynian anatexis in the envelope of the Beni Bousera peridotites (Alboran Domain, Morocco): implications for the tectono-metamorphic evolution of the deep crustal roots of the Mediterranean region

Article Type: Research Paper

Corresponding Author: Dr. Federico Rossetti,

Corresponding Author's Institution: Università di Roma Tre

First Author: Federico Rossetti

Order of Authors: Federico Rossetti; Federico Lucci; Thomas Theye; Mohamed Bouybaouenne; Axel Gerdes; Johachim Opitz; Andrea Dini; Christian Lipp

Abstract: The metamorphic core of the Betic-Rif orogenic chain (Alboran Domain) is made up of lower crustal rocks forming the envelope of the Ronda (Spain) and Beni Bousera (Morocco) peridotites. The deepest sections of the crustal envelopes are made of migmatitic granulites associated with diffuse acidic magmatic products, making these exposure and ideal site to investigate the textural and petrological connection between crustal anatexis and granite magmatism in the continental crust. However, still debated is the timing of intracrustal emplacement of the peridotite bodies, with models proposing either Alpine (early Miocene) or Hercynian ages, and still uncertain is the linkage between peridotite emplacement and crustal anatexis. In this study, by combining rock textures with whole-rock geochemistry, metamorphic thermobarometry, the U-Pb zircon geochronology and the analysis of the garnet and zircon REE chemistry, we document the P-T-t evolution of the granulite facies migmatites that form the immediate envelope of the Beni Bousera peridotites of the Rif belt. A main episode of Permo-Carboniferous (ca. 300-290 Ma) deep crustal anatexis, melt extraction and migration is documented that we link to the crustal emplacement of the Beni Bousera peridotites during collapse of the Hercynian orogen. Correlation at a regional scale suggests that the Beni-Bousera section can be tentatively correlated with the pre-Alpine (Permo-Carboniferous) basement units tectonically interleaved within the orogenic structure of the Alpine chain. The results of this study provide ultimate constraints to reconstruct the tectono-metamorphic evolution of the Alboran Domain in the Western Mediterranean and impose re-assessment of the modes and rates through which Alpine orogenic construction and collapse occurred and operated in the region.

Response to Reviewers: Roma, January 13 2020

To: Prof. Taras Gerya, Editor, Gondwana Research

Re: submission of the revised version ms. entitled: " Hercynian anatexis in the envelope of the Beni Bousera peridotites (Alboran Domain, Morocco): implications for the tectono-metamorphic evolution of the deep

crustal roots of the Mediterranean region" by Federico Rossetti, Federico Lucci, Thomas Theye, Mohamed Bouybaouenne, Axel Gerdes, Joachim Opitz, Andrea Dini, Christian Lipp

Dear Editor, please find attached the revised version of the ms. named above.

Both reviewers provide constructive comments and remarks that greatly contributed to improve the manuscript. We have carefully followed the reviewers' advice and comments to prepare this revised version. Below we provide a point-by-point response to the reviewers' comments. In the following, the response are typed in italics; changes in the original text are typed in red to allow to track the changes. Reference to the text pages refers to the uploaded revised Word file.

Reviewer #1 Prof. Laurent Jolivet: This paper presents a detailed study of migmatitic layers found along the contact with the Beni Bousera peridotites in the Sebides complex of the Betic-Rif orogen. The detailed up-to-date petrological approach is completed by geochemistry and U/Pb dating of zircons. Through the petrological and geochemical approach the authors make sure that the zircon they date represent the migmatitic event. The main finding is that the migmatites formed during the Late Carboniferous and Permian, thus during the collapse of the Hercynian Belt. The Beni Bousera granulitic migmatites formed along the Moho of the collapsing continental crust during post orogenic extension and they were much later integrated within the Betic-Rif orogen. The first exhumation from mantle depth thus occurred in the Late Paleozoic. The authors then correlate the Peri-Alboran peridotites massifs with the Alpine peridotites exhumed at the same period such as the well-known Ivrea peridotite body. This all makes a convincing proposal.

The paper is well written and easy to follow and the figures are self-explanatory. The only thing I really miss is a reconstruction (even tentative) all the way to the present-day situation that would help the reader to better understand how much the Alpine orogeny then modified the Late Paleozoic template and led to the observed structural position of the Beni-Bousera peridotite.

I also noted two very minor issues, below:

Page 9, line 10: which stratigraphic contact are referring to ? Between the granulites and the peridotites ? this is not a stratigraphic contact.

Page 9, line 28: "boudinaged" instead of "boudinated"

To conclude, this is an excellent paper that I wish to see published as soon as possible with only this suggestion of a more detailed reconstruction showing the post-Paleozoic evolution.

Response: We thank Prof. Jolivet for his positive evaluation of our study. We fully agree on the necessity to present a tectonic/geodynamic reconstruction. We have therefore re-organized the text of the final part of section 10.4 (see pg. 23-25 of the revised typescript) and proposed a new Figure 15, where we propose a new interpretation for the crust-mantle coupling in the Betic-Rif realm. A two-stage (Permo-Carboniferous and Early Miocene) crust-mantle coupling is tentatively proposed.

To provide the necessary background information to propose the new tectonic reconstruction shown in Fig. 15, we have also included complementary text in sections 2 and 3 of the revised manuscript (see the revised text at pg. 5 and 7-9).

The misprints at pg. 9 were corrected and revised following the Reviewer's advice.

Reviewer #2 (Dr. Antonio Acosta Vigil) : Review of "Hercynian anatexis in the envelope of the Beni Bousera peridotites (Alboran Domain, Morocco): implications for the tectono-metamorphic evolution of the deep crustal roots of the Mediterranean region", by Rossetti et al.

This is an interesting, well-written, though complex paper dealing with the anatexis of pelitic granulites located on top of the Beni Bousera peridotites, in the hinterland of an Alpine mediterranean orogen, the Rif of N Africa (Marocco). The paper deals with the age of anatexis and P-T conditions of the granulites and, from there, the authors provide some conclusions on the geodynamic implications. Despite being part of an Alpine orogen, authors conclude that anatexis in the granulites is Variscan in age, that anatexis was produced by the crustal emplacement of the peridotites, that the contact between granulites and underlying Beni Bousera peridotites represents a fossil continental crust-mantle transition during the Variscan, and that the granulites represent a transition from true lower crust to transient lower crust during the Variscan. The tools used are field relationships, petrography, geochronology (U-Pb on zircon) and thermobarometry (including thermodynamic modeling with Perplex). I recommend publication, though authors must first improve/clarify the paper regarding several issues. First, authors should include, in the appropriate place, and discuss, previous publications that are relevant to this problem (see comments below). Second, several of the interpretations/statements/conclusions, both on anatexis and on the geodynamic implications, are complex, and/or not clear, and/or not well articulated. Authors should improve these interpretations, and should warn readers about the limitations of the data/approach used (see comments below).

Response. We thank Dr. Acosta Vigil for his constructive review and comments. Following his recommendation, in the revised text we (i) include and discuss the relevant publications; and (ii) we re-organised data presentation and interpretation, particularly for what concerns zircon-garnet growth during rock anatexis and the history of crust-mantle coupling (see detailed responses below, the new section 10.4 and the new Fig. 15)

Page 4, lines 22-24. What do you mean with "how distributed are the effects of high grade metamorphism and crustal anatexis?" Re-write to clarify.

Response. We redacted the text

P. 5, l. 9-14. If Ghomaride is equivalent to Malaguide, and Alpujarride to Sebtide, the "respectively" is not correct; change the order.

Response. We redacted the text

P. 5, l. 20-25. I would not assign right away different metamorphic gradients to cover and basement rocks. This is the main issue you are investigating here, I think. In fact, you describe both metamorphic gradients in basement rocks later on, lines 51-59 of same page.

Response. Ok. We redacted the text

P. 6, l. 5-6. It should be Torres-Roldan (1983).
Response. fixed

P. 6, l. 58-59. Change to "through".
Response. fixed

P. 8, l. 18-23. This is correct, Melchiorre et al. (2017) report these U-Pb zircon ages in their abstract. But in their paper they conclude that they find two group ages of ~290-265 Ma and 23 Ma, that they associate with the HP-HT metamorphism in the granulites (similar to your results/interpretations), and to the LP-HT stage of the granulites (U-Pb ages similar to your data, but interpretation of the Alpine age different from yours), respectively. I think this is the main data to point out, in the appropriate place, from the work of Melchiorre et al (2017). Also, Montel et al (2000) and Rossetti et al. (2010) conducted geochronological studies on these rocks that are worth to mention here. All of these concluded that the granulite metamorphism in the kinzigites is Variscan.
Response. The reviewer is right. We redacted the text accordingly (see pg. 7-8 of the revised typescript).

P. 9, l. 18-19 versus l. 40-41. There is something strange in this description, as stromatic migmatites (l. 18-19) are a type of metatexites, whereas authors classify the migmatites as diatexites (l. 40-41). Please clarify the type of migmatite you are dealing with.
Response. The reviewer is right. We redacted the text: we are dealing with "metatexites"

P. 9, l. 44-45. Change to "Qz-Pl-Kfs-Ky-Gr-Rt"? Could you provide a reference for the mineral abbreviations?
Response. The reference for mineral abbreviations (Whitney and Evans, 2010) was provided in the Materials and Methods section of the early submitted typescript

P. 10, l. 3-6. Are you saying that you have found graphite-bearing fluid inclusions, and single mineral graphite inclusions, at the outer rim of Grt-1? If so, state it clearly.
Response. Yes. Following the reviewer's advice, we redacted the text

P. 10, l. 12-13. What do you mean by "Ky crystals embayed in Pl-Kfs-Qtz aggregates"? Do you mean that Ky is present, and apparently stable, within Pl-Kfs-Qtz aggregates, or that Ky is partially replaced by these aggregates and therefore looks unstable? Clarify.
Response. Following the reviewer's advice, we redacted the text

P. 10, l. 57-58. Replace by "instead".
Response. Done

P. 11, l. 51-55. I would not describe the chondrite-normalized profiles as "fractionated REE patters", but as rather flat.
Response. Ok. corrected

P. 12, l. 13-14. "...is from an intrafoliar..."?
Response. Ok. We meant "in situ melt segregation": we redacted the text

P. 14, l. 7-15. The Ti-in-Zrn thermometer depends on the activity of TiO₂ and SiO₂ I think (check Watson et al. 2006). Clarify in the text if you consider that rutile and quartz coexisted with the analyzed zircons (i.e. if the activity of TiO₂ and SiO₂ was 1). Otherwise, the activity will be

lower than 1, and this will affect the calculated temperature. If so, specify the activities of TiO₂ and SiO₂ used, and their influence on the calculation.

Response. This is an important point that impact on both the Zr-in-Rt and Ti-in-Zrc thermometry. We discussed this issue in section 10.3 in the submitted typescript. Following the reviewer's advice, we have redacted the text and moved the revised text to the end of the thermobarometry section (see the revised typescript at the end of pg 19)

P. 14, l. 38-45. REE of Grt-3 looks about the same as rims of Grt-2. Is that true, could you use shadow/grey domains to try to see this more clearly?

I think it would better if you provide here the results from the Kd of REE between Grt and Zrn, because these are results anyway. You can discuss these results later on, but can provide the data already here.

Response. Yes, the REE content of Grt-2 is similar to that of Grt-2. We would maintain the presentation of the partitioning coefficients among Zrc and Grt in the discussion section (section 10.3), since it implies interpretation of the crystallization histories of zircon and garnet during the prograde and retrograde history of metamorphism in the crustal envelope of the Beni Bousera peridotites. Following the reviewer's comments on the Zrc-Grt equilibrium relationships (see below), we have however re-organised section 10.3 to render more explicit the equilibrium relationships (see the revised typescript at pg. 20)

P. 15, l. 7-15. Acosta-Vigil et al. (2016) have dealt with melting reactions in kind of detail in similar granulites from Jubrique, Ronda. I think you should compare and refer to that work in this part of the paper.

Response. Yes. We redacted the text and referred to the mentioned paper P. 15, l. 17-19. The presence of melt at peak/HP conditions in similar granulites from Jubrique, Ronda, have been first reported and proposed by Barich et al. (2014), in direct connection with the study of melt inclusions in these rocks. That was a big step to understand the petrogenesis of these granulites. As far as I know, before that all studies considered that melting occurred at some point during decompression from peak HP conditions (e.g. Platt et al. JGeolSocLondon 2003). I think you should refer to Barich et al. (2014) in this part of the manuscript, around lines 16-19, when proposing that melt is present in the HP stage of the Beni Bousera granulites.

Response. Thanks. This is an important point to be emphasized in the discussion. We redacted the text accordingly both at the beginning of the discussion (see the revised typescript, pg. 15-16) and in section 10.2 section (see the revised typescript at pg 19, second paragraph)

P. 15, l. 32-39. I understand that you discuss about melting based on the presence of melt inclusions trapped in the garnet (e.g. lines 23-30). But I do not understand how can you discuss about conditions of crystallization of those melts, if you don't provide first any P-T calculations. I think you should move this part of the discussion to the appropriate place, after you provide info on the P-T of the retrograde path.

Response. Actually no info on the thermo-baric conditions is provided/discussed here. We are simply dealing with the sequence of metamorphic reactions as reconstructed from the inclusion assemblages and compositional zoning in garnet. This information provides the reference framework to guide the reader to the following sections where the

thermobarometric evolution of the studied rocks is presented. We would then preferred to maintain the sections 10.1 and 10.2 to the discussion section, since (i) the thermobarometry calculation (inverse and forward modelling) are based on the necessary assumptions done at the beginning of the discussion, and (ii) to clearly separate data from inference.

P. 16, l. 9-17. You provided T data from Ti in zircon before the discussion. Why did not you provide also T from Zr in rutile at that time? I suggest you place this data there too. In any case, as for Ti in zircon, you need to discuss if rutile crystallized in the presence of quartz and zircon, a requirement of this thermometer I think (check Tomkins et al. 2007).

Response. This choice based on the same rationale as explained in the above point. Following the reviewer's advice we discussed more deeply the results of the Zr-in-Rt and Ti-in-Zrc thermometry (see the revised typescript; last paragraph at pg 19)

P. 16, l. 25-26. What do you mean with "respectively", are you referring to the data from inclusions coming from Grt-1 and Grt-2?

Response. No, we are referring to the different pressure conditions adopted for pressure dependent Zr-in-Rt thermometry after Tomkins et al. (2007).

P. 16, l. 45-50. What I get, as a reader, is that based on the thermobarometers you have chosen to get the peak metamorphic conditions, P should be between 1.0-1.3 GPa. Hence 1.2-1.3 GPa is not a minimum P but, if any, a maximum P. Mostly because I would not think (all the previous literature, plus field appearance) that T in these granulites was higher than 1000C. Regarding T, what I get from the thermometer and your data, is that there is a large uncertainty between 800-1000C. Please explain to the reader then why you propose a minimum T of 900-950C. Maybe I am missing something. But for sure it is not straightforward how you go from your Zr in Rt and GASP data to a minimum P-T of 1.2-1.3 GPa and 900-950C.

Also, why these P-T are those of melt segregation, what do you mean? These are peak P-T, at which the rock was at some point, with melt likely present. How do you know that melt was segregating at these P-T conditions? If you think melt segregation occurred at peak P-T, please provide arguments.

Response. These estimates are based on inverse thermobarometry as derived from the Zr-in-Rt thermometry, coupled with the GASP barometry applied to the peritectic garnet (Grt-1 rim) and igneous (Grt-2 core) compositions and associated inclusion assemblages. These P-T estimates are intended to constrain the peak of metamorphism leading to crustal anatexis, i.e., incongruent melting and peritectic garnet growth. The peak conditions 1.2-1.3 GPa and 900-950 °C are derived by coupling the outcomes of Zr-in-Rt thermometry with the GASP barometry (colored fields in Fig. 12). Minimum temperature of 900-950°C are proposed due to the fact that we have the evidence of the change of the Als phase (Ky to Sil, from core to rim) hosted as inclusion in the peritectic garnet growth domains during prograde metamorphism: the prograde path is moving across the transition from the Ky (Grt-1 core) to the Sil (Grt-1 rim) stability (Fig. 12). An inference demonstrated from the results obtained from the forward modelling (cfr. section 10.2 and Fig. 13). We have tried to better explain these points in the revised text (see pg. 17 of the revised typescript)

P. 17, l. 7-9. This approach is a bit risky and I would introduce it as a first approximation, because you are dealing with anatexis in a highly dynamic environment (strongly foliated rocks). I think we are not sure if the melt you see at the outcrop scale is all produced in situ. I think you should warn readers about this.

Response. We agree. We have thus further stated the limitation of this approach (see red text at pg. 18)

P. 17, l. 36-37. Tentative also due to the uncertainty in starting bulk composition and proportion of melt loss.

Response. We agree. We have thus further stated the limitation of this approach (see red text at pg. 18, second paragraph)

P. 17, l. 38-41. "...escape of water-rich melt has likely occurred...". But you have already taken care of this, by reintegrating the amount of melt you considered has escaped, right? Or you are still referring to the uncertainty in H₂O in the starting bulk composition, that you are very likely underestimating in these calculations? Please re-write to clarify.

Response. We have redacted the text (see red text at pg. 18)

P. 17, l. 43-44. In this subsection you are basically getting info on the prograde path I think (e.g. lines 49-54). How did you get the peak conditions of 1.25-1.4 GPa and 950-1000C? Peak conditions in Fig. 13 do not correspond to those discussed/proposed in page 16 (lines 47-50). In theory you are getting peak P-T in the subsection of page 16. Again, I suggest to improve the discussion of peak P-T in page 16 (see previous comments) and then report appropriately the result in Fig. 13. Or explain better to the readers about all these P-T conditions reported and shown in Fig. 13.

Response. We used the forward modelling approach to refine the prograde path to the anatexis and the peak P-T conditions attained during incongruent melting. The output of the forward modelling provides first-order constraints on the path, as derived from the compositional zoning of Grt-1 garnet, and, in particular, by using the Ca and Mg isopleths, coupled with the change in the Als phases hosted in the different growth domains of the peritectic garnets. A further constraint is provided by the biotite stability field, which limits peak pressure to 1.5-1.6 GPa (Fig. 13).

P. 18, l. 1. Scales in Fig. 4 are absent or very difficult to see, please make them visible in all figure plates.

Response. We agree. Corrected

P. 18, l. 3-4. Again, where is this peak T of 950-1000C coming from exactly?

These results (higher peak T, if true; and the isobaric heating) are different from those reported in papers from Ronda (e.g. Platt et al. 2003, Barich et al. 2014). I think you should point it out and discuss it here or in the appropriate place.

Response. Following the reviewer's advice we have discussed the thermobarometry results with respect to the existing literature data (see the second paragraph at pg. 19 of the revised typescript).

P. 18, l. 25-26. Again, how do you get this peak T from the calculations presented in page 16? You really need to improve your discussion on peak P-T in page 16, and then stick to these numbers throughout the paper. Otherwise the reader won't know where the values for peak T are coming from.

Response. See above responses of this issue

P. 18, l. 47-48. I would replace "igneous" by "suprasolidus", unless you consider that all Grt crystallized from the melt, in which case you should explain/clarify it.

Response. Done

P. 18, l. 56-57. Why don't you use also the recent data from Taylor_Harley et al. JMG 2015?

Response. Many thanks for this suggestion. Following the reviewer's advice we have re-organised section 10.3 dealing with the zircon-garnet equilibria (see the new text at pag. 20-21 (third paragraph) and the new Fig. 14). We are confident that our argument is more straightforward

P. 19, l. 1-2. Re-write to clarify what do you exactly mean with "in the presence of plagioclase in the melt".

Response. done

P. 21, l. 13-17. You should include here two more references, related to Variscan metamorphism in Jubrique from the dating of garnets:

Response. Done

Barich, A. (2015) Unravelling the anatexis history of the lower continental crust throughout the petrology of melt inclusions and Lu-Hf garnet geochronology. A case study from the western Alpujarrides (Betic Cordillera, S. Spain). Ph.D. Thesis, Instituto Andaluz de Ciencias de la Tierra, CSIC-Universidad de Granada, 175 p.

Gómez-Pugnaire, M.T., Nieto, F., Abad, I., Velilla, N., Garrido, C.J., Acosta-Vigil, A., Barich, A., Hidas, K., Lopez Sanchez-Vizcaino, V. (2019) Alpine Metamorphism in the Betic Internal Zones. In: C. Quesada, J.T. Oliveira (eds.), *The Geology of Iberia: A Geodynamic Approach*, pp. 519-554, Springer Nature, Switzerland, https://doi.org/10.1007/978-3-030-11295-0_13

Response. done

Section 10.3 Zircon-garnet-melt equilibria and the age of crustal anatexis.

There is an important issue to deal with in this section. Checking the partitioning of REE between garnet and zircon is a technique used to couple ages from accessory minerals and P-T conditions of the host rock. In your study, you find that zircon did not crystallize in equilibrium with any of the garnet domains, so in theory you should not be able to couple zircon ages and garnet P-T conditions. But you conclude that, even if you cannot couple the crystallization of zircon and garnet, Variscan zircon cores, and not Alpine zircon rims, grew around the peak of metamorphism that produced most of the garnets and the high grade assemblages that we observed today in these granulites. So I think that you need to explain readers very clearly at the end of this section, what is then the main argument used to couple ages of zircon cores and peak metamorphic assemblages. This is a fundamental point to clarify in your manuscript.

Response. We agree and we thank the reviewer for the request to clarify this aspect in our study. Following the reviewer's advice, we have taken into account also the experimental results of Taylor et al. (2015) and implemented them in the revised manuscript. We have therefore revised the text (see pg. 20-211 of the revised typescript) and the corresponding

Figure (Figure 14). We clarified that the DREEZrn/Grt for the Grt-2 cores, showing nearly flat patterns for the HREE (from Dy to Lu) overlapping with the experimental data of Taylor et al. (2015) and Rubatto and Herman (2007) at higher temperatures, demonstrate that the analysed zircons crystallised at nearly equilibrium condition with the Grt-2 core and throughout the cooling history of the segregated melt. We can thus confidently propose an origin from the same melt/silicate system for both zircon and garnet sampled in the melt segregates from the inner granulite envelope of the Beni Bousera peridotites, in a scenario of prograde incongruent melting at high-pressure, melt production, extraction, crystallisation and cooling.

Section 10.4 A Hercynian granulite-granite suite: implications at regional scale.

There are a few issues that you should clarify here as well.

Regarding the nature and evolution of the continental crust at Beni Bousera, and associated with the isobaric heating and cooling paths you describe, you refer at some point (P. 22, l. 10-12) to true lower continental crust. But then you also say that the granulites arrived to the isobaric heating path after an early subduction type gradient (P. 18, l. 31-33). That would mean that these materials were not part, at least around that time, of a stable lower continental crust in the area, right? If yes, why do you bring the idea of a stable continental crust? To say that during the evolution of the Beni Bousera granulites some of the mechanisms that shape stable lower continental crust did occur? If yes, which are those mechanisms?

Another issue relates to the association of anatexis in the granulites with the intracrustal emplacement of the peridotites, and the idea of a fossil crust-mantle transition. I think you first clearly refer to the link between anatexis and crustal emplacement of the peridotite in P. 21, l. 38-44. But I did not find why do you link both phenomena, and/or any information on the mechanisms of emplacement. Please provide some information/discussion on both issues, at least to the main reason to link anatexis in the granulites and crustal emplacement of the peridotites. Also, if you think that the contact between granulites and peridotites reflects the crustal emplacement of the peridotites, then how could it represent a fossil crust-mantle transition? It would just be a tectonic contact within the continental crust, with the crust-mantle transition at that time being somewhere structurally below those rocks. Am I missing something?

Please re-write/improve this section to clarify all these issues.

Response. We thank the reviewer for the request to clarify this aspect in our study. This comment in part overlaps with what stated by reviewer#1 (Prof. Jolivet), when demanding for a tectonic reconstruction/model to synthesize the new findings. We agree that some misunderstanding arises from the early version of section 10.4 regarding the nature of the crust-mantle contact in the Beni Bousera units. We certainly agree that this is not stratigraphic but a tectonic contact. We therefore re-organise the text, explicitly speaking of crust-mantle tectonic coupling when dealing with the peridotite crustal envelope contact at Beni Bousera. Following the reviewers' advice we have thus re-organised the final part of section 10.4, presenting an original synthetic tectonic/geodynamic model for the Betic-Rif orogen since the Variscan (see pg. 22-25 and the new Figure 15).

In addition to what stated above, other amendments in the revised manuscript includes:

(i) change of the graphical abstract, to take into account the new tectonic/geodynamic model presented in Fig. 15; and (ii) the addition of essential literature data functional to the presentation of a tectonic reconstruction (see the sections 2 and 3 of the revised typescript).

We hope in the present form the manuscript may fulfill criteria for publication in Gondwana Research

Sincerely Yours,
Federico Rossetti

(on behalf of the co-authors)

Research Data Related to this Submission

There are no linked research data sets for this submission. The following reason is given:

Data will be made available on request

Roma, January 13 2020

To: Prof. Taras Gerya, Editor, Gondwana Research

Re: submission of the revised version ms. entitled: " Hercynian anatexis in the envelope of the Beni Bousera peridotites (Alboran Domain, Morocco): implications for the tectono-metamorphic evolution of the deep crustal roots of the Mediterranean region" by Federico Rossetti, Federico Lucci, Thomas Theye, Mohamed Bouybaouenne, Axel Gerdes, Joachim Opitz, Andrea Dini, Christian Lipp

Dear Editor, please find attached the revised version of the ms. named above.

Both reviewers provide constructive comments and remarks that greatly contributed to improve the manuscript. We have carefully followed the reviewers' advice and comments to prepare this revised version.

In the "Respond to Reviewers" section, we have provided a point-by-point response to the reviewers' comments and detailed how the original version of the manuscript was modified.

We hope in the present form the manuscript may fulfill criteria for publication in Gondwana Research

Sincerely Yours,

Federico Rossetti

(on behalf of the co-authors)

Roma, January 13 2020

To: Prof. Taras Gerya, Editor, Gondwana Research

Re: submission of the revised version ms. entitled: "*Hercynian anatexis in the envelope of the Beni Bousera peridotites (Alboran Domain, Morocco): implications for the tectono-metamorphic evolution of the deep crustal roots of the Mediterranean region*" by Federico Rossetti, Federico Lucci, Thomas Theye, Mohamed Bouybaouenne, Axel Gerdes, Joachim Opitz, Andrea Dini, Christian Lipp

Dear Editor, please find attached the revised version of the ms. named above.

Both reviewers provide constructive comments and remarks that greatly contributed to improve the manuscript. We have carefully followed the reviewers' advice and comments to prepare this revised version.

Below we provide a point-by-point response to the reviewers' comments. In the following, the response are typed in italics; changes in the original text are typed in red to allow to track the changes. Reference to the text pages refers to the uploaded revised Word file.

Reviewer #1 Prof. Laurent Jolivet: This paper presents a detailed study of migmatitic layers found along the contact with the Beni Bousera peridotites in the Sebides complex of the Betic-Rif orogen. The detailed up-to-date petrological approach is completed by geochemistry and U/Pb dating of zircons. Through the petrological and geochemical approach the authors make sure that the zircon they date represent the migmatitic event. The main finding is that the migmatites formed during the Late Carboniferous and Permian, thus during the collapse of the Hercynian Belt. The Beni Bousera granulitic migmatites formed along the Moho of the collapsing continental crust during post orogenic extension and they were much later integrated within the Betic-Rif orogen. The first exhumation from mantle depth thus occurred in the Late Paleozoic. The authors then correlate the Peri-Alboran peridotites massifs with the Alpine peridotites exhumed at the same period such as the well-known Ivrea peridotite body. This all makes a convincing proposal.

The paper is well written and easy to follow and the figures are self-explanatory. The only thing I really miss is a reconstruction (even tentative) all the way to the present-day situation that would help the reader to better understand how much the Alpine orogeny then modified the Late Paleozoic template and led to the observed structural position of the Beni-Bousera peridotite.

I also noted two very minor issues, below:

Page 9, line 10: which stratigraphic contact are referring to ? Between the granulites and the peridotites ? this is not a stratigraphic contact.

Page 9, line 28: "boudinaged" instead of "boudinated"

To conclude, this is an excellent paper that I wish to see published as soon as possible with only this suggestion of a more detailed reconstruction showing the post-Paleozoic evolution.

Response: We thank Prof. Jolivet for his positive evaluation of our study. We fully agree on the necessity to present a tectonic/geodynamic reconstruction. We have therefore re-organized the text of the final part of section 10.4 (see pg. 23-25 of the revised typescript) and proposed a new Figure 15, where we propose a new interpretation for the crust-mantle coupling in the Betic-Rif realm. A two-stage (Permo-Carboniferous and Early Miocene) crust-mantle coupling is tentatively proposed.

To provide the necessary background information to propose the new tectonic reconstruction shown in Fig. 15, we have also included complementary text in sections 2 and 3 of the revised manuscript (see the revised text at pg. 5 and 7-9).

The misprints at pg. 9 were corrected and revised following the Reviewer's advice.

Reviewer #2 (Dr. Antonio Acosta Vigil) : Review of "Hercynian anatexis in the envelope of the Beni Bousera peridotites (Alboran Domain, Morocco): implications for the tectono-metamorphic evolution of the deep crustal roots of the Mediterranean region", by Rossetti et al.

This is an interesting, well-written, though complex paper dealing with the anatexis of pelitic granulites located on top of the Beni Bousera peridotites, in the hinterland of an Alpine mediterranean orogen, the Rif of N Africa (Marocco). The paper deals with the age of anatexis and P-T conditions of the granulites and, from there, the authors provide some conclusions on the geodynamic implications. Despite being part of an Alpine orogen, authors conclude that anatexis in the granulites is Variscan in age, that anatexis was produced by the crustal emplacement of the peridotites, that the contact between granulites and underlying Beni Bousera peridotites represents a fossil continental crust-mantle transition during the Variscan, and that the granulites represent a transition from true lower crust to transient lower crust during the Variscan. The tools used are field relationships, petrography, geochronology (U-Pb on zircon) and thermobarometry (including thermodynamic modeling with Perplex). I recommend publication, though authors must first improve/clarify the paper regarding several issues. First, authors should include, in the appropriate place, and discuss, previous publications that are relevant to this problem (see comments below). Second, several of the interpretations/statements/conclusions, both on anatexis and on the geodynamic implications, are complex, and/or not clear, and/or not well articulated. Authors should improve these interpretations, and should warn readers about the limitations of the data/approach used (see comments below).

Response. We thank Dr. Acosta Vigil for his constructive review and comments. Following his recommendation, in the revised text we (ii) include and discuss the relevant publications; and (ii) we re-organised data presentation and interpretation, particularly for what concerns zircon-garnet growth during rock anatexis and the history of crust-mantle coupling (see detailed responses below, the new section 10.4 and the new Fig. 15)

Page 4, lines 22-24. What do you mean with "how distributed are the effects of high grade metamorphism and crustal anatexis?" Re-write to clarify.

Response. We redacted the text

P. 5, l. 9-14. If Ghomaride is equivalent to Malaguide, and Alpujarride to Sebtide, the "respectively" is not correct; change the order.

Response. We redacted the text

P. 5, l. 20-25. I would not assign right away different metamorphic gradients to cover and basement rocks. This is the main issue you are investigating here, I think. In fact, you describe both metamorphic gradients in basement rocks later on, lines 51-59 of same page.

Response. *Ok. We redacted the text*

P. 6, l. 5-6. It should be Torres-Roldan (1983).

Response. *fixed*

P. 6, l. 58-59. Change to "through".

Response. *fixed*

P. 8, l. 18-23. This is correct, Melchiorre et al. (2017) report these U-Pb zircon ages in their abstract. But in their paper they conclude that they find two group ages of ~290-265 Ma and 23 Ma, that they associate with the HP-HT metamorphism in the granulites (similar to your results/interpretations), and to the LP-HT stage of the granulites (U-Pb ages similar to your data, but interpretation of the Alpine age different from yours), respectively. I think this is the main data to point out, in the appropriate place, from the work of Melchiorre et al (2017). Also, Montel et al (2000) and Rossetti et al. (2010) conducted geochronological studies on these rocks that are worth to mention here. All of these concluded that the granulite metamorphism in the kinzigites is Variscan.

Response. *The reviewer is right. We redacted the text accordingly (see pg. 7-8 of the revised typescript).*

P. 9, l. 18-19 versus l. 40-41. There is something strange in this description, as stromatic migmatites (l. 18-19) are a type of metatexites, whereas authors classify the migmatites as diatexites (l. 40-41). Please clarify the type of migmatite you are dealing with.

Response. *The reviewer is right. We redacted the text: we are dealing with "metatexites"*

P. 9, l. 44-45. Change to "Qz-Pl-Kfs-Ky-Gr-Rt"? Could you provide a reference for the mineral abbreviations?

Response. *The reference for mineral abbreviations (Whitney and Evans, 2010) was provided in the Materials and Methods section of the early submitted typescript*

P. 10, l. 3-6. Are you saying that you have found graphite-bearing fluid inclusions, and single mineral graphite inclusions, at the outer rim of Grt-1? If so, state it clearly.

Response. *Yes. Following the reviewer's advice, we redacted the text*

P. 10, l. 12-13. What do you mean by "Ky crystals embayed in Pl-Kfs-Qtz aggregates"? Do you mean that Ky is present, and apparently stable, within Pl-Kfs-Qtz aggregates, or that Ky is partially replaced by these aggregates and therefore looks unstable? Clarify.

Response. *Following the reviewer's advice, we redacted the text*

P. 10, l. 57-58. Replace by "instead".

Response. *Done*

P. 11, l. 51-55. I would not describe the chondrite-normalized profiles as "fractionated REE patterns", but as rather flat.

Response. *Ok. corrected*

P. 12, l. 13-14. "...is from an intrafoliar...?"

Response. *Ok. We meant "in situ melt segregation": we redacted the text*

P. 14, l. 7-15. The Ti-in-Zrn thermometer depends on the activity of TiO₂ and SiO₂ I think (check Watson et al. 2006). Clarify in the text if you consider that rutile and quartz coexisted with the analyzed zircons (i.e. if the activity of TiO₂ and SiO₂ was 1). Otherwise, the activity will be lower than 1, and this will affect the calculated temperature. If so, specify the activities of TiO₂ and SiO₂ used, and their influence on the calculation.

Response. *This is an important point that impact on both the Zr-in-Rt and Ti-in-Zrc thermometry. We discussed this issue in section 10.3 in the submitted typescript. Following the reviewer's advice, we have redacted the text and moved the revised text to the end of the thermobarometry section (see the revised typescript at the end of pg 19)*

P. 14, l. 38-45. REE of Grt-3 looks about the same as rims of Grt-2. Is that true, could you use shadow/grey domains to try to see this more clearly?

I think it would better if you provide here the results from the Kd of REE between Grt and Zrn, because these are results anyway. You can discuss these results later on, but can provide the data already here.

Response. *Yes, the REE content of Grt-2 is similar to that of Grt-2. We would maintain the presentation of the partitioning coefficients among Zrc and Grt in the discussion section (section 10.3), since it implies interpretation of the crystallization histories of zircon and garnet during the prograde and retrograde history of metamorphism in the crustal envelope of the Beni Bousera peridotites. Following the reviewer's comments on the Zrc-Grt equilibrium relationships (see below), we have however re-organised section 10.3 to render more explicit the equilibrium relationships (see the revised typescript at pg. 20)*

P. 15, l. 7-15. Acosta-Vigil et al. (2016) have dealt with melting reactions in kind of detail in similar granulites from Jubrique, Ronda. I think you should compare and refer to that work in this part of the paper.

Response. *Yes. We redacted the text and referred to the mentioned paper*

P. 15, l. 17-19. The presence of melt at peak/HP conditions in similar granulites from Jubrique, Ronda, have been first reported and proposed by Barich et al. (2014), in direct connection with the study of melt inclusions in these rocks. That was a big step to understand the petrogenesis of these granulites. As far as I know, before that all studies considered that melting occurred at some point during decompression from peak HP conditions (e.g. Platt et al. JGeolSocLondon 2003). I think you should refer to Barich et al. (2014) in this part of the manuscript, around lines 16-19, when proposing that melt is present in the HP stage of the Beni Bousera granulites.

Response. *Thanks. This is an important point to be emphasized in the discussion. We redacted*

the text accordingly both at the beginning of the discussion (see the revised typescript, pg. 15-16) and in section 10.2 section (see the revised typescript at pg 19, second paragraph))

P. 15, l. 32-39. I understand that you discuss about melting based on the presence of melt inclusions trapped in the garnet (e.g. lines 23-30). But I do not understand how can you discuss about conditions of crystallization of those melts, if you don't provide first any P-T calculations. I think you should move this part of the discussion to the appropriate place, after you provide info on the P-T of the retrograde path.

Response. *Actually no info on the thermo-baric conditions is provided/discussed here. We are simply dealing with the sequence of metamorphic reactions as reconstructed from the inclusion assemblages and compositional zoning in garnet. This information provides the reference framework to guide the reader to the following sections where the thermobarometric evolution of the studied rocks is presented. We would then preferred to maintain the sections 10.1 and 10.2 to the discussion section, since (i) the thermobarometry calculation (inverse and forward modelling) are based on the necessary assumptions done at the beginning of the discussion, and (ii) to clearly separate data from inference.*

P. 16, l. 9-17. You provided T data from Ti in zircon before the discussion. Why did not you provide also T from Zr in rutile at that time? I suggest you place this data there too. In any case, as for Ti in zircon, you need to discuss if rutile crystallized in the presence of quartz and zircon, a requirement of this thermometer I think (check Tomkins et al. 2007).

Response. *This choice based on the same rationale as explained in the above point. Following the reviewer's advice we discussed more deeply the results of the Zr-in-Rt and Ti-in-Zrc thermometry (see the revised typescript; last paragraph at pg 19)*

P. 16, l. 25-26. What do you mean with "respectively", are you referring to the data from inclusions coming from Grt-1 and Grt-2?

Response. *No, we are referring to the different pressure conditions adopted for pressure dependent Zr-in-Rt thermometry after Tomkins et al. (2007).*

P. 16, l. 45-50. What I get, as a reader, is that based on the thermobarometers you have chosen to get the peak metamorphic conditions, P should be between 1.0-1.3 GPa. Hence 1.2-1.3 GPa is not a minimum P but, if any, a maximum P. Mostly because I would not think (all the previous literature, plus field appearance) that T in these granulites was higher than 1000C. Regarding T, what I get from the thermometer and your data, is that there is a large uncertainty between 800-1000C. Please explain to the reader then why you propose a minimum T of 900-950C. Maybe I am missing something. But for sure it is not straightforward how you go from your Zr in Rt and GASP data to a minimum P-T of 1.2-1.3 GPa and 900-950C.

Also, why these P-T are those of melt segregation, what do you mean? These are peak P-T, at which the rock was at some point, with melt likely present. How do you know that melt was segregating at these P-T conditions? If you think melt segregation occurred at peak P-T, please provide arguments.

Response. *These estimates are based on inverse thermobarometry as derived from the Zr-in-Rt thermometry, coupled with the GASP barometry applied to the peritectic garnet (Grt-1 rim) and igneous (Grt-2 core) compositions and associated inclusion assemblages. These P-T estimates*

are intended to constrain the peak of metamorphism leading to crustal anatexis, i.e., incongruent melting and peritectic garnet growth. The peak conditions 1.2-1.3 GPa and 900-950 °C are derived by coupling the outcomes of Zr-in-Rt thermometry with the GASP barometry (colored fields in Fig. 12). Minimum temperature of 900-950°C are proposed due to the fact that we have the evidence of the change of the Als phase (Ky to Sil, from core to rim) hosted as inclusion in the peritectic garnet growth domains during prograde metamorphism: the prograde path is moving across the transition from the Ky (Grt-1 core) to the Sil (Grt-1 rim) stability (Fig. 12). An inference demonstrated from the results obtained from the forward modelling (cfr. section 10.2 and Fig. 13). We have tried to better explain these points in the revised text (see pg. 17 of the revised typescript)

P. 17, l. 7-9. This approach is a bit risky and I would introduce it as a first approximation, because you are dealing with anatexis in a highly dynamic environment (strongly foliated rocks). I think we are not sure if the melt you see at the outcrop scale is all produced in situ. I think you should warn readers about this.

Response. We agree. We have thus further stated the limitation of this approach (see red text at pg. 18)

P. 17, l. 36-37. Tentative also due to the uncertainty in starting bulk composition and proportion of melt loss.

Response. We agree. We have thus further stated the limitation of this approach (see red text at pg. 18, second paragraph)

P. 17, l. 38-41. "...escape of water-rich melt has likely occurred...". But you have already taken care of this, by reintegrating the amount of melt you considered has escaped, right? Or you are still referring to the uncertainty in H₂O in the starting bulk composition, that you are very likely underestimating in these calculations? Please re-write to clarify.

Response. We have redacted the text (see red text at pg. 18)

P. 17, l. 43-44. In this subsection you are basically getting info on the prograde path I think (e.g. lines 49-54). How did you get the peak conditions of 1.25-1.4 GPa and 950-1000C? Peak conditions in Fig. 13 do not correspond to those discussed/proposed in page 16 (lines 47-50). In theory you are getting peak P-T in the subsection of page 16. Again, I suggest to improve the discussion of peak P-T in page 16 (see previous comments) and then report appropriately the result in Fig. 13. Or explain better to the readers about all these P-T conditions reported and shown in Fig. 13.

Response. We used the forward modelling approach to refine the prograde path to the anatexis and the peak P-T conditions attained during incongruent melting. The output of the forward modelling provides first-order constraints on the path, as derived from the compositional zoning of Grt-1 garnet, and, in particular, by using the Ca and Mg isopleths, coupled with the change in the Als phases hosted in the different growth domains of the peritectic garnets. A further constraint is provided by the biotite stability field, which limits peak pressure to 1.5-1.6 GPa (Fig. 13).

P. 18, l. 1. Scales in Fig. 4 are absent or very difficult to see, please make them visible in all

figure plates.

Response. *We agree. Corrected*

P. 18, l. 3-4. Again, where is this peak T of 950-1000C coming from exactly?

These results (higher peak T, if true; and the isobaric heating) are different from those reported in papers from Ronda (e.g. Platt et al. 2003, Barich et al. 2014). I think you should point it out and discuss it here or in the appropriate place.

Response. *Following the reviewer's advice we have discussed the thermobarometry results with respect to the existing literature data (see the second paragraph at pg. 19 of the revised typescript).*

P. 18, l. 25-26. Again, how do you get this peak T from the calculations presented in page 16?

You really need to improve your discussion on peak P-T in page 16, and then stick to these numbers throughout the paper. Otherwise the reader won't know where the values for peak T are coming from.

Response. *See above responses of this issue*

P. 18, l. 47-48. I would replace "igneous" by "suprasolidus", unless you consider that all Grt crystallized from the melt, in which case you should explain/clarify it.

Response. *Done*

P. 18, l. 56-57. Why don't you use also the recent data from Taylor_Harley et al. JMG 2015?

Response. *Many thanks for this suggestion. Following the reviewer's advice we have re-organised section 10.3 dealing with the zircon-garnet equilibria (see the new text at pag. 20-21 (third paragraph) and the new Fig. 14). We are confident that our argument is more straightforward*

P. 19, l. 1-2. Re-write to clarify what do you exactly mean with "in the presence of plagioclase in the melt".

Response. *done*

P. 21, l. 13-17. You should include here two more references, related to Variscan metamorphism in Jubrique from the dating of garnets:

Response. *Done*

Barich, A. (2015) Unravelling the anatexis history of the lower continental crust throughout the petrology of melt inclusions and Lu-Hf garnet geochronology. A case study from the western Alpujarrides (Betic Cordillera, S. Spain). Ph.D. Thesis, Instituto Andaluz de Ciencias de la Tierra, CSIC-Universidad de Granada, 175 p.

Gómez-Pugnaire, M.T., Nieto, F., Abad, I., Velilla, N., Garrido, C.J., Acosta-Vigil, A., Barich, A., Hidas, K., Lopez Sanchez-Vizcaino, V. (2019) Alpine Metamorphism in the Betic Internal Zones. In: C. Quesada, J.T. Oliveira (eds.), The Geology of Iberia: A Geodynamic Approach, pp. 519-554, Springer Nature, Switzerland, https://doi.org/10.1007/978-3-030-11295-0_13

Response. *done*

Section 10.3 Zircon-garnet-melt equilibria and the age of crustal anatexis.

There is an important issue to deal with in this section. Checking the partitioning of REE between garnet and zircon is a technique used to couple ages from accessory minerals and P-T conditions of the host rock. In your study, you find that zircon did not crystallize in equilibrium with any of the garnet domains, so in theory you should not be able to couple zircon ages and garnet P-T conditions. But you conclude that, even if you cannot couple the crystallization of zircon and garnet, Variscan zircon cores, and not Alpine zircon rims, grew around the peak of metamorphism that produced most of the garnets and the high grade assemblages that we observed today in these granulites. So I think that you need to explain readers very clearly at the end of this section, what is then the main argument used to couple ages of zircon cores and peak metamorphic assemblages. This is a fundamental point to clarify in your manuscript.

Response. *We agree and we thank the reviewer for the request to clarify this aspect in our study. Following the reviewer's advice, we have taken into account also the experimental results of Taylor et al. (2015) and implemented them in the revised manuscript. We have therefore revised the text (see pg. 20-211 of the revised typescript) and the corresponding Figure (Figure 14). We clarified that the $D_{REE}^{Zrn/Grt}$ for the Grt-2 cores, showing nearly flat patterns for the HREE (from Dy to Lu) overlapping with the experimental data of Taylor et al. (2015) and Rubatto and Herman (2007) at higher temperatures, demonstrate that the analysed zircons crystallised at nearly equilibrium condition with the Grt-2 core and throughout the cooling history of the segregated melt. We can thus confidently propose an origin from the same melt/silicate system for both zircon and garnet sampled in the melt segregates from the inner granulite envelope of the Beni Bousera peridotites, in a scenario of prograde incongruent melting at high-pressure, melt production, extraction, crystallisation and cooling.*

Section 10.4 A Hercynian granulite-granite suite: implications at regional scale.

There are a few issues that you should clarify here as well.

Regarding the nature and evolution of the continental crust at Beni Bousera, and associated with the isobaric heating and cooling paths you describe, you refer at some point (P. 22, l. 10-12) to true lower continental crust. But then you also say that the granulites arrived to the isobaric heating path after an early subduction type gradient (P. 18, l. 31-33). That would mean that these materials were not part, at least around that time, of a stable lower continental crust in the area, right? If yes, why do you bring the idea of a stable continental crust? To say that during the evolution of the Beni Bousera granulites some of the mechanisms that shape stable lower continental crust did occur? If yes, which are those mechanisms?

Another issue relates to the association of anatexis in the granulites with the intracrustal emplacement of the peridotites, and the idea of a fossil crust-mantle transition. I think you first clearly refer to the link between anatexis and crustal emplacement of the peridotite in P. 21, l. 38-44. But I did not find why do you link both phenomena, and/or any information on the mechanisms of emplacement. Please provide some information/discussion on both issues, at least to the main reason to link anatexis in the granulites and crustal emplacement of the peridotites. Also, if you think that the contact between granulites and peridotites reflects the crustal emplacement of the peridotites, then how could it represent a fossil crust-mantle transition? It would just be a tectonic contact within the continental crust, with the crust-mantle transition at that time being somewhere structurally below those rocks. Am I missing something?

Please re-write/improve this section to clarify all these issues.

Response. *We thank the reviewer for the request to clarify this aspect in our study. This comment in part overlaps with what stated by reviewer#1 (Prof. Jolivet), when demanding for a tectonic reconstruction/model to synthesize the new findings. We agree that some misunderstanding arises from the early version of section 10.4 regarding the nature of the crust-mantle contact in the Beni Bousera units. We certainly agree that this is not stratigraphic but a tectonic contact. We therefore re-organise the text, explicitly speaking of crust-mantle tectonic coupling when dealing with the peridotite crustal envelope contact at Beni Bousera. Following the reviewers' advice we have thus re-organised the final part of section 10.4, presenting an original synthetic tectonic/geodynamic model for the Betic-Rif orogen since the Variscan (see pg. 22-25 and the new Figure 15).*

In addition to what stated above, other amendments in the revised manuscript includes:
(i) change of the graphical abstract, to take into account the new tectonic/geodynamic model presented in Fig. 15; and (ii) the addition of essential literature data functional to the presentation of a tectonic reconstruction (see the sections 2 and 3 of the revised typescript).

We hope in the present form the manuscript may fulfill criteria for publication in Gondwana Research

Sincerely Yours,
Federico Rossetti



(on behalf of the co-authors)

Highlights

Hercynian granulite–granite suite preserved at the core of the Alboran Domain

Hercynian deep crustal anatexis linked to emplacement of the Alboran peridotites

The core of the Alboran Domain preserves a Hercynian fossil crust-mantle transition

Alboran Domain migmatites as part of the Hercynian basement of Mediterranean region

*Declaration of Interest Statement

Roma, October 22, 2019.

To: Editor, Gondwana Research

Re: submission of the ms. entitled: "*Hercynian anatexis in the envelope of the Beni Bousera peridotites, Alboran Domain, Rif belt (Morocco)*" by Federico Rossetti, Federico Lucci, Mohamed Bouybaouenne, Thomas Theye, Axel Gerdes, Joachim Opitz, Andrea Dini, Christian Lipp

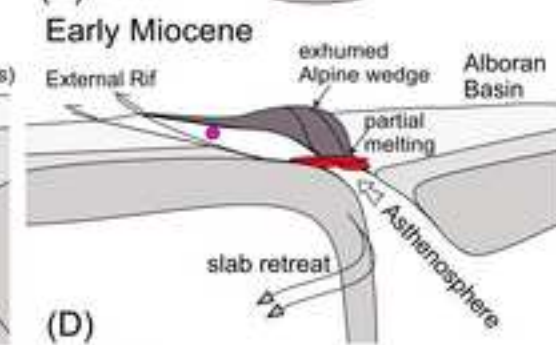
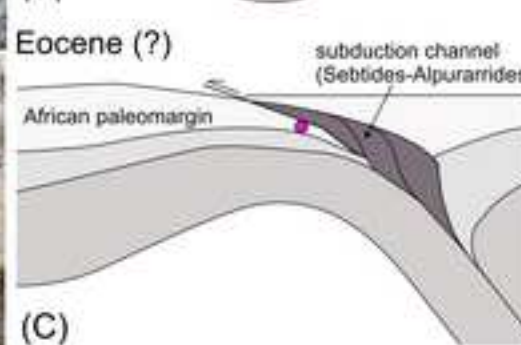
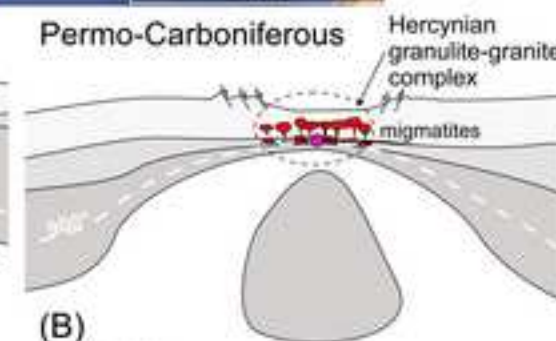
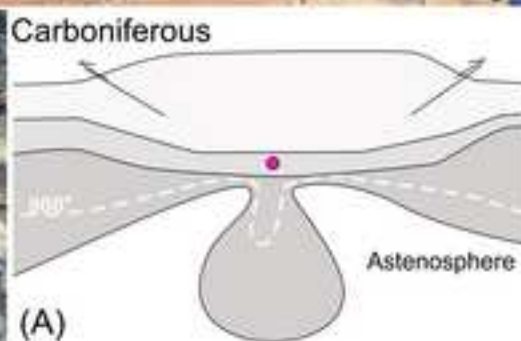
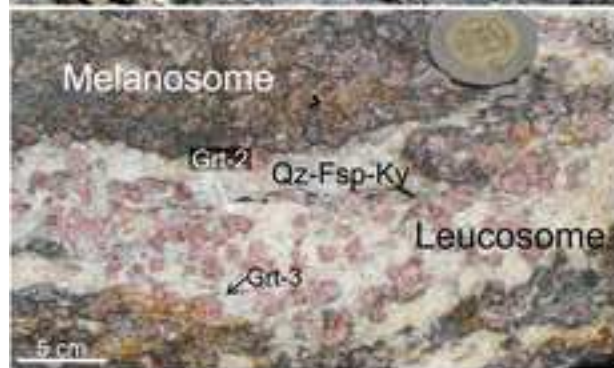
Declaration of interests

The authors declare that they have no known competing financial interests or personal relationships that could have appeared to influence the work reported in this paper.

Federico Rossetti



(on behalf of the co-authors)



- Beni Bousera units
- Crustal anatexis
- Upper crust
- Lower crust
- Mantle lithosphere

1
2
3
4
5
6
7
8
9
10
11
12
13
14
15
16
17
18
19
20
21
22
23
24
25
26
27
28
29
30
31
32
33
34
35
36
37
38
39
40
41
42
43
44
45
46
47
48
49
50
51
52
53
54
55
56
57
58
59
60
61
62
63
64
65

Hercynian anatexis in the envelope of the Beni Bousera peridotites (Alboran Domain, Morocco): implications for the tectono-metamorphic evolution of the deep crustal roots of the Mediterranean region

Federico Rossetti^{1(*)}, Federico Lucci¹, Thomas Theye², Mohamed Bouybaouenne², Axel Gerdes^{4,5}, Joachim Opitz², Andrea Dini⁶, Christian Lipp²

¹Dipartimento di Scienze, Università Roma Tre, Roma, Italy

²Institut für Anorganische Chemie, Universität Stuttgart, Stuttgart, Germany

³Département de Géologie, Université de Rabat, Rabat, Morocco

⁴Institute für Geowissenschaften, Goethe University, Frankfurt, Germany

⁵Frankfurt Isotope and Element Research Center (FIERCE), Goethe University Frankfurt, Germany

⁶Istituto di Geoscienze e Georisorse, CNR, Pisa, Italy

(*) Corresponding Author
Dipartimento di Scienze
Sez. Scienze Geologiche
Largo San Leonardo Murialdo, 1
010146 Roma (Italy)
e-mail: federico.rossetti@uniroma3.it
Tel: +390657338043

Abstract

1
2
3
4 The metamorphic core of the Betic-Rif orogenic chain (Alboran Domain) is made up of lower
5 crustal rocks forming the envelope of the Ronda (Spain) and Beni Bousera (Morocco) peridotites.
6
7 The deepest sections of the crustal envelopes are made of migmatitic granulites associated with
8
9 diffuse acidic magmatic products, making these exposure and ideal site to investigate the textural
10
11 and petrological connection between crustal anatexis and granite magmatism in the continental
12
13 crust. However, still debated is the timing of intracrustal emplacement of the peridotite bodies, with
14
15 models proposing either Alpine (early Miocene) or Hercynian ages, and still uncertain is the linkage
16
17 between peridotite emplacement and crustal anatexis. In this study, by combining rock textures with
18
19 whole-rock geochemistry, metamorphic thermobarometry, the U-Pb zircon geochronology and the
20
21 analysis of the garnet and zircon REE chemistry, we document the *P-T-t* evolution of the granulite
22
23 facies migmatites that form the immediate envelope of the Beni Bousera peridotites of the Rif belt.
24
25 A main episode of **Permo-Carboniferous (ca. 300-290 Ma)** deep crustal anatexis, melt extraction
26
27 and migration is documented that we link to the crustal emplacement of the Beni Bousera
28
29 peridotites **during collapse of the Hercynian orogen**. Correlation at a regional scale suggests that the
30
31 Beni-Bousera section can be tentatively correlated with the pre-Alpine (Permo-Carboniferous)
32
33 basement **units** tectonically interleaved within the orogenic structure of the Alpine chain. **The**
34
35 **results** of this study provide ultimate constraints to reconstruct the tectono-metamorphic evolution
36
37 of the Alboran Domain in the Western Mediterranean and impose re-assessment of the modes and
38
39 rates through which Alpine orogenic construction and collapse occurred and operated in the region.
40
41

42 **Keywords: Granulite; Anatexis; Hercynian; Alboran Domain; Western Mediterranean**
43
44
45
46
47
48
49
50
51
52
53
54
55
56
57
58
59
60
61
62
63
64
65

1. Introduction

The arcuate belt of the Betic-Rif chain forms the western termination of the peri-Mediterranean Alpine orogenic systems (Fig. 1a). This orogen is part of a mountain belt developed along the active margin of the western Mediterranean subduction zone, developed during the Alpine Mesozoic-Cenozoic convergence between African and Eurasian plates (Dewey et al., 1998; Faccenna et al. 2001, 2004; Jolivet et al., 2008; Lonergan and White 1997, Platt et al., 2013; Royden 1993; Vergés and Fernandez, 2012; Guerrera et al., 2019). The metamorphic core of this Alpine orogen is now dismembered in discontinuous outcrops located in the internal domains of the mountain fronts, where Neogene extensional tectonics overprinted the early crustal thickening event (e.g., Both-Rea et al., 2007; Comas et al., 1999; Dewey, 1988; Faccenna et al., 2001; 2004; García-Dueñas et al., 1992; Jolivet and Faccenna, 2000; Jolivet et al., 2008; Michard et al., 2006; Platt and Vissers, 1989; Platt and Whitehouse, 1999; Platt et al., 1998; 2003a,b; 2013; Guerrera et al., 2019; Van Hinsbergen et al., 2014).

The orogenic hinterland of the Betic-Rif chains consists of the continental-derived metamorphic units of the Alboran Domain (e.g., Andrieux et al., 1971; Casciello et al., 2015; Michard et al., 2006; Platt et al., 2013). Various models have been proposed in the literature with contrasting geodynamic and timing scenarios to frame the tectono-metamorphic evolution of the Alboran Domain. The major source of controversy comes from the pressure-temperature-time (P - T - t)-deformation history reconstructed from the Alpujarride-Sebtide Complex, which make-up the metamorphic envelope of the Ronda and Beni Bousera peridotite massifs (Fig. 1b). A distinctive feature of the Alpujarride/Sebtide Complex of the Alboran Domain is the presence of condensed metamorphic sequences with marked downward increase in the paleo-temperature gradients (Álvarez-Valero et al., 2014; Argles et al., 1999; Azanon et al., 1997; Balanya et al., 1997; Barich et al., 2014; Both Rea et al., 2007; Comas et al., 1999; García Casco and Torres Roldan, 1999; García-Dueñas et al., 1992; Gueydan et al., 2015; Haissen et al., 2004; Jolivet et al., 2008; Michard et al., 2006; Monié et al., 1994; Negro et al., 2006; Platt et al., 2013; Rossetti et al. 2005; Sanchez-Navas et al., 2014, 2017; Soto and Platt, 1999; Tubia et al., 1997; Zeck et al., 1992). Still debated is in particular, the timing of the high-grade metamorphism and associated crustal anatexis in the metamorphic rocks that make-up the inner envelopes of the peridotite bodies, with implications on the age and model of the intracrustal emplacement of the peridotites. Based on the available petrological, structural and geochronological data sets, two classes of models exist, with the high-grade metamorphism and magmatism referred either to the Alpine (Álvarez-Valero et al., 2014; Argles et al., 1999; Esteban et al., 2004, 2010; Frasca et al., 2017; Garrido et al., 2011; Gueydan et

1 al., 2015; 2019; Hidas et al., 2013; Homonnay et al., 2018; Janots et al., 2006; Mazzoli and Martín-
2 Algarra, 2011; Précigout et al., 2013; Platt and Vissers 1989; Platt et al., 1998; 2003a, b; Platt and
3 Whitehouse, 1999; Sánchez-Rodríguez and Gebauer, 2000; Soto and Platt, 1999; Tubia et al., 1997;
4 Whitehouse and Platt, 2003; Zeck et al., 1992) or the Hercynian (Acosta Vigil et al., 2014; Barich et
5 al., 2014; Bouybaouene et al., 1998; Michard et al., 1997; Montel et al., 2000; Rossetti et al., 2010;
6 2013; Ruiz Cruz and Sanz de Galdeano, 2014; Sánchez-Navas et al., 2014; Zeck and Williams,
7 2001; Zeck and Whitehouse, 2002) evolution. It is worth noting that disequilibrium textures and
8 disturbance of the isotopic systems are also reported from the high-grade basement rocks of the
9 Alboran Domain, suggesting a polyphase (Hercynian and Alpine) tectono-metamorphic evolution
10 (e.g., Acosta Vigil et al., 2014; García Casco and Torres Roldan, 1999; Gueydan et al., 2015;
11 Massonne, 2014; Rossetti et al., 2010; Sánchez-Navas et al., 2017, **Gómez-Pugnaire et al., 2019**).
12 Therefore, unanswered key questions regarding the tectono-thermal evolution of the Alboran
13 Domain remain; in particular: (i) the age of crustal anatexis: Alpine or Hercynian?; (ii) which the
14 link between crustal anatexis and the peridotite emplacement in the continental crust (**time and**
15 **mode of crust-mantle coupling**); and (iii) any correlations with the pre-Alpine lower crustal
16 exposures across the Alpine chain (e.g., Schmidt et al., 2004; von Raumer et al., 2013; Kunz et al.,
17 2018)? To answer to these questions it is essential to elucidate the space-time connection (if any)
18 between the partially **molten** source region (migmatites) and the extracted and migrated **melts** in the
19 crustal section of the Alboran Domain, i.e. the so-called granulite–granite connection (e.g., Brown,
20 1994, 2013; Vanderhaeghe, 1999; 2009; Vielzeuf et al., 1990).

21 In this paper, we investigate the Pressure-Temperature-time (*P-T-t*) evolution of the
22 granulite facies migmatites (kinzigites in Kornprobst, 1974) that form the immediate envelope of
23 the Beni Bousera peridotite at the core of the Alboran Domain of the Rif belt (Figs. 1b and 2). We
24 report a main Permo-Carboniferous deep crustal granulite-granite suite that we link to the crustal
25 emplacement of the Beni Bousera peridotites and discuss implications of these results for the
26 tectono-metamorphic evolution of the Alboran Domain and of the Alpine orogen in general.

27 **2. Geological Setting**

28 The Alboran Domain forms the metamorphic core of the Alpine Betic-Rif orogen. It consists
29 of continentally-derived metamorphic rock units that broadly correlate across the two arms of the
30 orogen (García Duenas et al., 1992; Michard et al., 2006) (Fig. 1b).

31 In Morocco, the Alboran Domain is made of the Ghomaride and Sebtime complexes that
32 tectonically overlie the Mesozoic carbonates of the Dorsale units (Figs. 1b and 2). In the Betics,
33 these metamorphic complexes correspond to the **Malaguide and Alpujarride complexes**,

1
2
3
4
5
6
7
8
9
10
11
12
13
14
15
16
17
18
19
20
21
22
23
24
25
26
27
28
29
30
31
32
33
34
35
36
37
38
39
40
41
42
43
44
45
46
47
48
49
50
51
52
53
54
55
56
57
58
59
60
61
62
63
64
65

respectively. The lower tectonic complex is the eclogite-bearing Nevado-Filabride Complex (Augier et al. 2005; Puga et al., 1999) of the Betics that is not exposed in the Moroccan side (Michard et al., 2006 and references therein) (Fig. 1b).

The metamorphic signature the Alpujarride-Septide complex has been classically referred to as a down-section transition from low-grade (subduction-type) to high-grade (Barrovian-type) thermo-baric environments, as recorded on Permian-Triassic and pre-Alpine protoliths, respectively (Azañon et al., 1997; Bouybaouene et al., 1998; El Maz and Guiraud, 2001; Michard et al., 1997; 2006). The age of the Alpine subduction zone metamorphism is still poorly constrained but referred to as Eocene (Platt et al., 2005). In the Moroccan Rif, this distinct metamorphic signature corresponds to the upper (Federico Group) and lower (Filali and Beni Bousera units) Sebtides, respectively (Kornprobst, 1974; Michard et al., 2006; Bouybaouenne et al, 1998; Negro et al., 2006; Gueydan et al., 2015) (see the tectono-stratigraphic column in Fig. 2a). This down-section change in the metamorphic signature is structurally associated with the presence of large peridotite bodies (Ronda and Beni Bousera; Fig. 1b), which are tectonically interlayered within the continental metamorphic sequence of the Alpujarride-Septide complex.

Field evidence documents similar contact relationships between the peridotite bodies and the hosting continental-derived Alpujarride-Sebtides units (e.g., Michard et al., 2006). High-grade metamorphic rocks characterise the upper and lower contacts of the peridotites with widespread evidence of rock anatexis close to these contacts. The upper tectonostratigraphic section corresponds to the Casares-Los Reales unit of the Betics (Monié et al., 1994; Haissein et al., 2004) and to the Lower Sebtides of the Rif (Kornprobst, 1974; Michard et al., 2006), consisting of basal acidic migmatitic granulites (kinzigites and Beni Bousera units) passing upward to lower-grade gneisses and metapelites of the Filali unit. Peak metamorphism in the Casares-Los Reales/Beni Bousera units is commonly framed within the HP granulite facies field (1.2-1.7 GPa and 750-850 °C), typified by the assemblage garnet-kyanite-rutile ± biotite, followed by a nearly isothermal decompression within the cordierite stability field (Bouybaouenne et al., 1998; Haissein et al., 2004; Alvarez-Valero et al., 2014).

The lower contact with the crustal envelope is well exposed in the western Betics, where the peridotites rest on top of the Blanca Group, a migmatitic, locally strongly mylonitised, inverse metamorphic sequence grading from granulite (top) to amphibolite (bottom) facies metamorphic conditions (Acosta-Vigil et al., 2014, Tubia et al., 1997; Torres-Roldàn, 1983). In the Moroccan Rif, the basal contact is exposed in the Ceuta area (Fig. 1b), where the peridotite bodies tectonically rest on top of the Monte Hacho gneiss (Kornprobst, 1974; Homonnay et al., 2018; see tectono-stratigraphic column in Fig. 2a). The lower and upper contacts of the peridotites and the associated

1 partial melting are interpreted as dynamothermal aureole developed during the intracrustal
2 emplacement of the peridotites, and considered as developed during hot thrusting and extensional
3 unroofing and decompression in Alpine times, respectively (e.g. Argles et al., 1999; Frasca et al.,
4 2017; Gueydan et al., 2019; Hidas et al., 2013; Homonnay et al., 2018; Mazzoli and Martin Algarra,
5 2011; Platt et al., 2003a-b; 2013; Tubia and Cuevas, 1986; Tubia et al., 1997). Evidence of an early
6 UHP evolution, assumed as Hercynian in age, has been also reported from the Jubrique zone of the
7 Alpujarride Complex in the Betic Cordillera (Ruiz Cruz and Sanz de Galdeano, 2014) and from the
8 orthogneiss of the Hacho unit in the Ceuta zone (Ruiz Cruz and Sanz de Galdeano, 2012; 2013).

9 **No definitive constraint on the granulite-granite connection issue has been derived since**
10 **now in the Betic-Rif realm.** The age of the anatexitic products and melt mobilisates found within the
11 immediate envelope of the peridotite bodies is still the subject of debate, **with Alpine and Hercynian**
12 **ages proposed so far (see Acosta Vigil et al., 2014 for a recent review).** Granite magmatism in the
13 Ronda area (**Betics**) is commonly attributed to the early Miocene (Rb-Sr, whole-rock (Priem et al.,
14 1979); Ar-Ar on biotite (Monié et al., 1994); U-Pb zircon dating (Esteban et al., 2010)). **However,**
15 **magmatic rocks of Hercynian age are also reported from the Betic Cordillera (Priem et al. 1966;**
16 **Platt and Whitehouse, 1999; Zeck and Williams, 1999).** Recently, through SHRIMP U-Pb zircon
17 **geochronology, Sanchez-Navas et al. (2014a) have documented Hercynian (286 ± 16 Ma) igneous**
18 **zircons and Alpine metamorphic resetting (early Miocene in age) in granitoid dykes intruded in the**
19 **Torrox unit of the Central Betics.**

20 This duality of Hercynian and Alpine ages for the granite magmatism is also documented in
21 the immediate envelope of the Beni Bousera peridotites in the Rif (Fig. 1), where two generation of
22 peraluminous granites with distinct isotopic signatures are recognised (Rossetti et al., 2010; 2013):
23 (i) an early *HP*, garnet-kyanite-bearing, granitic suite with highly radiogenic Sr isotope ratios
24 (0.736243–0.771449) (the so-called "leptinites" Kornprobst (1974) of Hercynian age (Permo-
25 Carboniferous, 290-300 Ma; U-Pb zircon dating); and (ii) a subsequent *LP*, andalusite-bearing, sub-
26 vertical granite dyke swarm with lower Sr radiogenic ratios (0.719753–0.722461), dated by
27 coupled U-Pb zircon/monazite and $^{40}\text{Ar}/^{39}\text{Ar}$ muscovite/biotite geochronology to the early Miocene
28 (c. 22 Ma).

29 **The** Hercynian and Alpine ages are also systematically derived from the U-Th-Pb zircon and
30 monazite geochronology of the migmatitic sequences of the Alboran Domain, where a significant
31 inheritance from Cadomian-Pan African (560–640 Ma), Grevillian (940–1020Ma), to Early
32 Archean (2-2.5 Ga) crustal sources are also reported (Zeck and Whitehouse, 2002; Zeck and
33 Williams, 2001; Platt and Whitehouse, 1999; Acosta-Vigil et al., 2014; Montel et al., 2000; Rossetti
34 et al., 2010; Sanchez-Navas et al., 2014; Melchiorre et al., 2017).

1 Based on U-Pb SHRIMP dating on structureless zircon rims from both the migmatitic
2 dynamothermal sole and syn-tectonic intrusives from the Blanca unit of Central Betics, Esteban et
3 al. (2010) proposed an age of 22-21 Ma for the intracrustal emplacement of the Ronda peridotites.
4 Similarly, U-Pb zircon and Ar-Ar datings of syn-tectonic and post-tectonic intrusive granitic dykes
5 constrain the crust-mantle coupling in the Ronda area during the Early Miocene (22.5-20 Ma;
6 Frasca et al., 2017). However, based on integrated petrographic/textural and SHRIMP U-Pb dating
7 of magmatic zircons, Acosta-Vigil et al. (2014) have constrained the age of anatexis at the footwall
8 of the Ronda peridotite to the late stages of the Hercynian orogeny (280–290 Ma), and documented
9 an Alpine-aged recrystallisation and Pb loss event in the Hercynian zircons. These Hercynian ages
10 are in line with the U-Pb zircon dating results derived from (i) the migmatitic portions of the Torrox
11 basement units, which provided mean ages of 285 ± 5 Ma, 313 ± 7 Ma (Zeck and Whitehouse
12 (2002) and 286 ± 11 Ma (Sanchez Navas et al., 2017), and (ii) the migmatitic sequences of the
13 Jubrique zone (mean ages of 330 ± 9 and 265 ± 4 Ma) (Ruiz Cruz and Sainz de Galdeano, 2014),
14 both structurally overlying the Ronda peridotites.
15

16 Regarding the high-grade migmatitic crustal envelope of the Beni Bousera peridotites,
17 Montel et al. (2000), have documented late Hercynian (284 ± 27 Ma) granulite metamorphism, as
18 derived from U-Th-Pb dating of monazite inclusions in garnet. The intrusive relationships between
19 Permo-Carboniferous granitoid bodies and the host Beni-Bousera units, allowed Rossetti et al.
20 (2010) to propose a pre-Alpine age for the crustal envelope of the Beni Bousera peridotites. On the
21 other hand, Platt et al. (2003a) provided a lower Miocene (22.7 ± 0.3 Ma) U-Pb zircon age for the
22 peak of metamorphism in the Beni Bousera units that is referred to as the main stage of crustal
23 thinning and exhumation. Finally, Melchiorre et al. (2017) reported new zircon U-Pb ages from the
24 Beni Bousera granulites, which provided ages spanning from Paleoproterozoic (1508 ± 23 Ma) to
25 Miocene (22.9 ± 0.7 Ma). In particular, two main groups of ages at ca. 286-264 and ca. 23 Ma are
26 derived, interpreted as the timing of the prograde *HP* metamorphism and the *LT* exhumation of the
27 granulite envelope, respectively (Melchiorre et al., 2017).
28

29 As a final point, it is worth noting that the early Miocene granite magmatism overlaps in
30 time with the wealth of the available radiometric geochronological and low-temperature
31 thermochronological data (apatite and zircon fission tracks) from the Sebtime-Alpujarride realm
32 that, regardless of the dating method, indicates a significant age clustering at 18-25 Ma, commonly
33 interpreted as the time of cooling and exhumation of the Alboran Domain (e.g., Michard et al ,
34 2006; Janots et al., 2007; Frasca et al., 2017; Gueydan et al., 2015; Homonnay et al., 2018;
35 Melchiorre et al., 2017; Monié et al. , 1994; Platt et al., 1998; 2003b; Platt and Whitehouse, 1999;
36
37
38
39
40
41
42
43
44
45
46
47
48
49
50
51
52
53
54
55
56
57
58
59
60
61
62
63
64
65

1 Rossetti et al., 2010; Sanchez-Rodriguez and Gebauer, 2000; Zeck et al. , 1992; Azdimousa et al.,
2 2014; Sosson et al., 1998; Esteban et al., 2004; 2007; 2011; Andriessen and Zeck, 1996).
3
4
5
6

7 **3. The Study area**

8
9 The study area corresponds to the north-western, high-grade envelope of the Beni Bousera
10 peridotites, where the lower Sebtides are exposed. The lithological units grade from granulite
11 migmatites (kinzigites) at the contact with the peridotite (collectively named as the Beni Bousera
12 units) to gneisses and micaschists of the Filali unit (Figs. 2a-b). The regional metamorphic foliation
13 wraps around the Beni Bousera peridotites, showing a general domal attitude (Alvarez-Valero et al.,
14 2014; Bouybaouenne et al., 1998; El Maz and Guiraud, 2001; Gueydan et al., 2015; Kornprobst,
15 1974; Melchiorre et al., 2017; Michard et al., 2006; Negro et al., 2006) (Figs. 2b-c). As documented
16 by Raman spectroscopic analyses of graphitic material from the Filali unit (Negro et al., 2006), the
17 metamorphic grade increases down-section from subsolidus andalusite to kyanite zones, with
18 melting occurring at the transition from the Filali mica schists to the Filali gneiss in correspondence
19 of the sillimanite + alkali feldspar isograd (El Maz and Guiraud, 2001). The metamorphic signature
20 of the Filali unit is described as acquired during a polyphase clockwise P-T path in response to a
21 transition from a Hercynian Barrovian stage (peak conditions of 550-670 °C and 0.5-08 GPa)
22 metamorphic gradient of 20–26 °C/km), followed and overprinted by a HT-LP one (equilibrated at
23 550-750 °C and 0.3-06 GPa; metamorphic gradient of 45 °C/km), Alpine in age (at ca. 21 Ma;
24 Gueydan et al., 2015).
25
26
27
28
29
30
31
32
33
34
35
36
37
38

39 The granulite envelope is dominantly made of felsic (metapelite-derived) and minor mafic
40 protoliths, the latter occurring as intercalations and boudins close to the contact with the peridotites
41 (Bouybaouene et al., 1998; Haisse et al., 2004; Alvarez-Valero et al., 20014; Melchiorre et al.,
42 2014). The thermobaric evolution of the granulite rocks is similarly framed within a nearly
43 isothermal decompressional evolution, starting at HP/HT conditions of 1.2-1.5 GPa (up to 2.0 GPa
44 in the basic granulites; Bouybaouenne et al., 1998) at ca. 800 °C, with a final re-equilibration at 0.4-
45 0.5 GPa for *T* below ca. 600 °C (Bouybaouenne et al., 1998; Haisse et al., 2004; Alvarez-Valero
46 et al., 2014). Age of the climax of metamorphism is still debated, referred either to the Hercynian
47 (Michard et al., 1997; Bouybaouene et al., 1998; Montel et al. 2000; Rossetti et al., 2010;
48 Melchiorre et al., 2017) or the Alpine (Early Miocene; Platt et al., 2003; Gueydan et al. 2015)
49 tectono-metamorphic evolution. Available zircon and apatite zircon fission-track data constrain the
50 final exhumation of the Beni Bousera peridotite massif during Burdigalian-Langhian times (ca.
51 19.5-15.5 Ma; Azdimousa et al., 2014).
52
53
54
55
56
57
58
59
60
61
62
63
64
65

4. Materials and Methods

This study investigates a suite of migmatitic granulites in the immediate envelope of the Beni Boussera peridotites, exposed on a ca. 500 metre long, continuous outcrop (known as Playa Smeila) located along the sea side, 1 km south-east of the Bouh Ahmed village (Figs. 2b and 3a). Meso- and micro-scale studies were carried out in order to investigate the petrology and geochronology of rock anatexis and melt formation.

Selected rock samples, representative of the different textures recognised in the field, were chosen for petrographical investigation, mineral and whole-rock chemistry (major and trace elements). Sample selection was based on the structure at the outcrop scale and on meso- and micro-scale textural and mineralogical features. Samples are shown in their structural context in Fig. 3a and listed in Table 1, where their location, fabrics, and constituent mineralogy are detailed. Electron microprobe analyses (EMPA) were used to define compositions of the constituent mineral assemblages. Inverse and forward modelling techniques (Powell and Holland, 2008) were used to assess the thermo-baric conditions associated with anatexis, magma segregation and emplacement. The U-(Th)-Pb zircon geochronology was adopted to constrain the timing of crustal anatexis and magmatism in the metamorphic envelope. Trace and rare earth element (REE) compositions (both in situ and on separates) of zircon and garnet were also investigated to link the U-Pb ages to the reconstructed tectono-metamorphic history.

Details on the analytical methods and protocols adopted in this study are provided in the Supplementary Material#1. In the following, mineral abbreviations are after Whitney and Evans (2010).

5. Structure and petrography of the granulites

The granulites are characterised by a north-eastward dipping foliation that is sub-parallel to the one in the underlying peridotites. A major, NW-SE steeply-dipping extensional fault, marked by a ca. 20 wide damage zone, cuts across the granulite-peridotite contact. The whole outcrop is affected by intense jointing that defines NW-SE striking sub-vertical fracture arrays associated with rock alteration in both the footwall and hangingwall rocks. A sub-parallel pegmatitic dyke swarm is observed to intrude the granulite rocks (Fig. 3a).

The granulites are extensively migmatitic, with an overall stromatic texture, made of centimetre- to decimetre-scale lithological banding parallel to the dominant foliation at the outcrop scale, and defined by alternating leucocratic and melanocratic portions (Figs. 3b-e). The granulites host dm-scale metabasite boundins, typically surrounded by leucocratic layers and lenses, and with

boudin necks providing dilatational sites for accumulation of leucocratic material (Fig. 3b).

Following Sawyer (2008), the leucocratic portions consist of both in situ and in-source leucosome types (up to 30-40 % vol.), associated with leucocratic sills (up to 10% vol.) (Fig. 3a-e). The latter are typically extensively **boundinaged** and stretched along the main foliation (Fig. 3c). The melt structures (leucosomes and sills) invariably contain high proportions of garnet. The melanocratic portions **are** here almost entirely constituted by mm to cm-thick porphyroblastic aggregates of garnet and interpreted as a melt residuum (Taylor and Stevens, 2010). In particular, garnet porphyroblasts (up to 3 cm in diameter) are surrounded by and embedded within diffuse leucocratic patches and layers (Fig. 3d-e), suggestive of in situ melting, likely developed through incongruent melting reactions in which the garnets are formed as the solid peritectic products (e.g., Brown, 2013). **Based on the overall rock texture, the Beni Bousera granulites can be classified as a metatexite migmatite (e.g., Brown, 1994; Sawyer, 1994).**

The rock mineralogy is dominated by modally abundant Grt (locally up to 60 vol%) in an igneous matrix made of Qz-Pl-Kfsp-Ky+Gr, Rt (see Supplementary Material#2 for representative EMPA of the mineral constituents). Accessories include Zrn, Ap, and Mnz. The igneous assemblage in the melt segregates (leucosomes and sills) resembles peraluminous granites (e.g. Clark, 1981) (Figs. 3d-f and 4). Three main generations of garnets can be recognised based on textural evidence, with distinct inclusion assemblages and composition zoning (see below). An early garnet generation (Grt-1), occurring **primarily** in the melanosome portions, consists of coarse-grained (up to 1-3 cm in diameter), anhedral grains, usually with distinct core and rim structures. The inner Grt-1 cores are typically devoid of mineral inclusion, whereas the outer core and rim domains are poikilitic, hosting numerous (10–200 μm) xenomorphic and round to lobate mono- and poly-mineralic inclusions typically made of Qz-Kfs (Ab_{13-17})-Pl (An_{35-45}) aggregates, usually associated with Rt, Gr and Bt with high TiO_2 (up to 7.76 wt %) and high X_{Mg} ($[\text{Mg}/(\text{Mg}+\text{Fe})]\times 100 = 51-60$). Significantly, the outer core domains are also characterized by dense arrays of **graphite-bearing fluid and solid inclusions**, where usually Ky occurs embayed in multiphase Pl-Kfs-Qz aggregates (Figs. 4a-d). The presence of Sil inclusions is instead systematically observed in the rim domains of the largest Grt-1 grains (Fig. 4e). A second generation (Grt-2), occurring in leucosomes, consists of large (up to 1-2 cm in diameter), still poikilitic and anhedral grains hosting Qz-Kfs-Pl inclusion assemblages, usually associated with Sil in the core domains (Figs. 4f). Ky crystals **either as single mineral inclusion or associated with** Pl-Kfs-Qz aggregates are commonly observed at the Grt-2 rims (Fig. 4g). The third garnet generation (Grt-3) occurs again only in the leucosomes and typically show anhedral grain shapes with a nearly uniform grain size (ca. 50-250 μm), interstitially distributed along Qz-Fsp grains boundaries, indicating that **Grt-3** directly crystallized from a melt

(Fig. 4h). Igneous textures are usually well preserved in the low strain domains, as documented by a well annealed polygonal texture made of inequigranular Qz-Fsp matrix, where Pl (An_{40-52}) and Kfs (Ab_{07-14}) form the framework microstructure (Figs. 4g-h).

Locally, an intense metamorphic overprint is documented in the melanosome portions and typified by symplectites of Crd-Sp-Pl-Qz \pm Ilm developed at the expenses of early Grt-Ky-Rt assemblages (Fig. 4i). A post-kynematic growth of Bt-Sil \pm Ms \pm late Chl aggregates also occurs in secondary foliation replacing the early Grt-Ky-bearing texture.

6. Chemical zoning in garnet

Garnet in both melanosomes and melt segregates is essentially a zoned almandine-pyrope-grossular solid solution with a minor content of spessartine. The zoning profiles are characterised by marked Ca and Mg compositional zoning as illustrated in Figure 5a. The Grt-1 grains are characterized by rather heterogeneous composition profiles, with a marked core-to-rim chemical zonation. When preserved, they show a broad core that is relatively homogeneous with respect to Fe and Mn ($Alm_{63-66}Pyr_{15-21}Grs_{15-17}Sps_{04-05}$), typically high in Ca and with the Mg content inversely correlated to the Ca content. In other cases, the Ca-rich core of Grt-1 is present only as relic (Fig. 5b) or completely lacking. The transition to the rim domains is characterized by a broad Ca-poor and Mg-rich domain ($Alm_{63-66}Pyr_{27-30}Grs_{05-07}Sps_{01-02}$), in conjunction with the transition from inclusion-free to inclusion-rich rim growth domains. The inclusion often contains a composite Qz-Fsp-Rt-Gr assemblage with Ky in addition. The occurrence of Sil is instead restricted to the outer rim zones of Grt-1 (Figs. 5a-b). The Grt-2 shows a nearly uniform core-to-rim composition with the core broadly corresponding to the Grt-1 outer rim compositions. Towards the rim, Ca increases at the expense of Mg and Fe. A variably developed (up to 50-70 μ m large) outer rim showing a strong decrease of Mg and Ca, concomitant with a slight increase in the Mn component ($Alm_{58-64}Pyr_{25-27}Grs_{15-17}Sps_{06-07}$) (Fig. 5c). The Grt-3 shows a contrasting zoning pattern being characterized by a large homogeneous core rich in Ca and Mg ($Pyr_{26}Grs_{15}$; similar to the composition of the Grt-2 rims) that grades into a relatively narrow rim with lower contents of Ca and Mg and higher Mn (Figs. 5d).

7. Whole-rock geochemistry

The chemical composition of four melanosome and five leucosome samples from the studied granulite migmatites (see Table 1 for sample location and constituent mineralogy) were analysed for major and trace element geochemistry. Data are reported in Table 2 and graphically shown in Fig. 6 for the leucosome compositions.

1 The leucosomes have acidic composition ($\text{SiO}_2 = 70.51\text{--}76.62$ wt%), associated with low
2 MgO (0.09-0.35 wt%), FeO_{TOT} (0.96-2.06 wt%), TiO_2 (0.01-0.14 wt%) and CaO (1.14-2.01 wt%)
3 contents. They are enriched in K_2O (5.29-5.57 wt%) with respect to Na_2O (1.7-2.78 wt%) and with
4 an Al_2O_3 content of 12.26-15.50 wt%. In the TAS (total alkali vs. silica) diagram, the leucosomes
5 fall in the granite field (Fig 6a). Significantly, the leucosome compositions fall within those derived
6 from experimental melts produced by biotite dehydration (Gao et al., 2016 and references therein)
7 (Fig. 6b). Leucosome compositions are however K-depleted and show higher $\text{Ca}/(\text{Ca} + \text{Na})$ ratios
8 than those of experimental and natural anatectic glasses (Fig. 6c-d; Taylor et al., 2014 and
9 references therein). Melanosomes show SiO_2 ranging 41-63 wt% with high Al_2O_3 (16.7-28.8 wt%)
10 and $\text{Fe}_2\text{O}_3^{\text{TOT}}$ (7.6-16.92 wt%) and low TiO_2 (1.0-1.4 wt%), associated with moderate MgO (2.1-4.2
11 wt%) and K_2O (2.1-3.1 wt%), variable CaO (0.8-4.1 wt%) and Na_2O (0.3-2.3 wt%). These
12 compositions are strongly Si and K depleted and strongly enriched in $\text{Ca}/(\text{Ca} + \text{Na})$ ratios and Fe +
13 Mg contents with respect to leucosomes (Fig. 6c-d).
14
15
16
17
18
19
20
21
22

23 The abundance of large-ion lithophile elements (LILEs, such as Ba, Rb, Sr) is positively
24 correlated with SiO_2 and it is higher in leucosomes. Conversely, high-field strength elements (such
25 as REE, Y, Nb and Zr) are negatively correlated with SiO_2 and their content is higher in
26 melanosomes. When normalized to chondrite (after Sun and McDonough, 1989), all samples are
27 generally enriched in light REE (LREE), with $(\text{La}/\text{Sm})_{\text{N}}$ and $(\text{La}/\text{Yb})_{\text{N}}$ ranging 3.09-7.40 and 1.73-
28 5.68 for the leucosomes and 3.87-4.33 and 6.35-12.57 for the melanosome, respectively. The Eu
29 anomaly ($\text{Eu}_{\text{N}}/[\text{Sm}_{\text{N}} \times \text{Gd}_{\text{N}}]^{1/2}$) is systematically positive for leucosomes (4.37-13.53), whereas in
30 melanosomes varies from positive (2.64) to slightly negative (0.47), when moving from
31 intermediate to low-silica compositions, respectively (Fig. 7).
32
33
34
35
36
37
38
39
40
41

42 8. U-Pb zircon geochronology

43 The zircon U-Pb geochronological study was carried out on zircon separates as obtained
44 from a melanosome-leucosome layering (sample K3L, representative of the in situ melt segregates)
45 and two leucosomes (sample Ma09/28L and Ma09/30L as representative of melt mobilisates).
46 Sample Ma09/28L is from an in situ melt segregation, while Ma09/30 is from a boudinated granite
47 (Fig. 3). Sample K3L is located within the alteration zone associated with dyke emplacement at the
48 base of the granulite exposure (Fig. 3).
49
50
51
52
53
54

55 Zircon grains were investigated through cathodoluminescence (CL) and back scattered
56 electron (BSE) imaging techniques and subsequently analysed in situ through a LA-ICP-MS system
57 at the Frankfurt Isotope and Element Research Center (FIERCE) of the Goethe University of
58
59
60
61
62
63
64
65

Frankfurt (see Supplementary Material#1). Analytical results are shown in Table 3a-c. Age calculations and graphical display were obtained through the ISOPLOT software (Ludwig, 2003).

8.1 Sample K3L

Zircons are generally euhedral to subhedral. Based on the BSE and CL imaging, two textural types are defined. The first and more abundant type consists of moderately luminescent, single-phase zircons with oscillatory zoning and planar growth banding (Fig. 8a). The second type comprises grains with distinct core and rim structures. The cores (inner and outer) show oscillatory and sector zoned growth zoning and are embayed by thin (10-30 μm wide), low-luminescent rims that commonly truncate the inner zoning (Fig. 8a). Minor metamict textures are also observed in some grains, documented by opaque, fractured domains. The Th/U values vary largely, with values significantly higher in the growth zoning domains (up to 0.70) with respect to the low-luminescent rims (<0.01) (Table 3a; Fig. 9).

The range of analytical zircon ages is very large, with apparent $^{206}\text{Pb}/^{238}\text{U}$ ages spanning from the Late Archean (ca. 2.5 Ga) in the cores to Cenozoic (ca. 22 Ma) in the structureless rim domains. However, a significant age cluster from the oscillatory growth domains is observed at c. 300 Ma (Table 3a; Fig. 8a). Taking into account the age population younger than 300 Ma, data array defines a Discordia with an upper intercept at 297 (+16/-17) Ma and a lower intercept of early Miocene age, at 20.0 (+4.4/-4.8) Ma. Eight analyses from the low-luminescent structureless rims form a nearly concordant age cluster at the lower end of the Discordia, yielding a weighted mean $^{206}\text{Pb}/^{238}\text{U}$ age of 22.1 ± 0.4 (Fig. 8a).

8.2 Sample Ma09/30L

Zircons are generally euhedral to subhedral. Most zircon grains show short to long prismatic habits (usually $>250 \mu\text{m}$), with length/width ratios up to 5:1. They appear as nearly homogeneous in BSE images. In CL images, zircons are weakly luminescent and show oscillatory to sector (soccer ball) growth zoning (Fig. 8b), typical of igneous zircons (Corfu et al., 2003; Harley et al. 2007). No inherited cores are present. The U content of these growth domains is moderate to high (330–1340 ppm) and the Th/U is generally low (0.02–0.01) (Table 3b; Fig. 9). The probability distribution plot of the cumulative eighty-six spots provides a mean cluster of $^{206}\text{Pb}/^{238}\text{U}$ ages at 294 ± 1 Ma (2σ ; 79% of the data). Thirty-three spots define a near concordant group, intercepting the Concordia curve at 301 ± 2 Ma (2σ , MSWD = 4.4) (Fig. 8b).

8.3 Sample Ma09/28L

1 Zircons are typically long prismatic in shape and euhedral. A minor aliquot shows a
2 pyramidal shape. They are homogeneous in BSE and the CL images reveal dominant oscillatory to
3 sector growth zoning (Fig. 8c), typical of igneous zircons. Also in this case, no inherited cores are
4 present. The Th/U values range 0.01–0.22 (Table 3c; Fig. 9). The probability distribution plot of the
5 cumulative thirty-two spots provides a mean cluster of $^{206}\text{Pb}/^{238}\text{U}$ ages at 290 ± 1 Ma (2σ ; 81% of
6 the data). Twenty-nine spots define a Concordia age at 291 ± 1 Ma (2σ , MSWD = 1.3) (Fig. 8c).
7
8
9

10 11 12 **9. Zircon and garnet REE chemistry**

13 Zircon and garnet crystals from the same samples used for U-Pb zircon geochronology
14 (Table 1), were analyzed both on mineral separates and in thin sections for REE and trace element
15 determination by LA-ICP-MS at the Institut für Mineralogie, Universität Stuttgart (see
16 Supplementary Material#1). The analyzed spots in zircons correspond to the oscillatory or sector
17 growth zoning domains analysed for the U-Pb geochronology. The different garnet growth domains
18 in igneous Grt-2 (core and rims) and Grt-3 (cores) grains were analysed. The results are presented
19 in Fig. 10 and Table 4.
20
21
22
23
24
25
26
27

28 29 **9.1 Zircon**

30 The analysed spots areas correspond to the same sector-zoned or oscillatory growth
31 domains investigated for the U-Pb geochronology. Irrespective of the sample, all the analysed
32 zircon domains (22 spots) are characterized by low LREE (ΣLREE of 0.74–6.9 ppm, with a mean
33 value of 2.4 ppm) and high HREE (ΣHREE ranging 335–1264 ppm, average value: 894 ppm)
34 contents, respectively. They show chondrite-normalised (Sun and McDonough, 1989) depleted
35 LREE (average $\text{La}_N = 0.40$ and $\text{La}_N/\text{Sm}_N < 0.15$) and enriched HREE (average Yb_N : 21745 and
36 Dy_N/Yb_N values of 0.19–0.38) patterns. All analyzed zircons show a systematic negative Eu
37 anomaly (0.05–0.11). The observed REE patterns are fully compatible with those presented in
38 Melchiorre et al. (2017) (Fig. 10a).
39
40
41
42
43
44
45
46
47

48 The Ti contents of the zircons were also analysed in order to constrain the temperature at
49 which the zircons grew using the Ti-in-zircon thermometer (Watson and Harrison, 2005; Watson et
50 al., 2006). The measured Ti values range between 3.4 and 13.8 ppm, corresponding to a temperature
51 estimate of 654–770 °C (Table 4), **provided that rutile was present at the time of zircon**
52 **crystallization.**
53
54
55
56
57
58

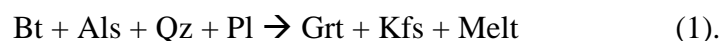
59 **9.2 Garnet**

1 The Grt-2 cores (6 spots) are characterized by low LREE (Σ LREE ranging 0.54-8.2 ppm,
2 average value of 2.8 ppm) and elevated HREE (Σ HREE ranging 552-1366 ppm) contents. They are
3 characterised by extremely depleted chondrite-normalised LREE ($La_N/Sm_N < 0.002$) and enriched
4 HREE patterns (Yb_N/Gd_N : 8-38) (Fig. 10b). The Grt-2 rims (9 spots) show comparable low LREE
5 (Σ LREE: 3.0-9.8 ppm) but lower HREE (Σ HREE of 81-219 ppm) contents. They show similar
6 LREE ($La_N/Sm_N < 0.007$) depletion, together with a less evident HREE enrichment (Yb_N/Gd_N :
7 0.42-2.9). Both the Grt-2 cores and rims show a systematic negative Eu/Eu* anomaly (0.17 and
8 0.19, average value of cores and rims, respectively) (Fig. 10b).

9 The Grt-3 garnets (cores, 22 spots) are characterised by moderate LREE (Σ LREE of 1.8-12
10 ppm) and elevated HREE (Σ HREE of 53-181 ppm) contents, with depleted chondrite-normalized
11 LREE ($La_N/Sm_N < 0.1$) and HREE ($Yb_N/Gd_N < 0.9$) patterns and negative Eu/Eu* anomaly (0.08-
12 0.37).

13 10. Discussion

14 The structures in the field and the petrographic evidence presented in this study provide
15 evidence of granulite-facies migmatitisation of the immediate crustal envelope of the Beni Bousera
16 peridotites. The presence of modally abundant garnet invariably characterises the mineral textures
17 of both the melt segregates and melanosomes. In particular, the systematic spatial association of
18 restitic garnet with leucosome segregations (Figs. 3e-f and 4a) is suggestive of incongruent melting
19 and peritectic garnet growth during crustal (Brown, 2013) anatexis in the immediate envelope of the
20 Beni Bousera peridotites. This is compatible with the presence of multiphase mineral inclusions of
21 overall granitic compositions (Qz-Pl-Kfs \pm Als) with lobate shapes and low-angle termination
22 hosted in Grt-1 and Grt-2 grains (Figs. 4a-d), which can be interpreted as melt inclusions (Cesare et
23 al., 2015), similarly to what already recognised for the migmatitic granulites of the Jubrique unit in
24 the envelope of the Ronda peridotites of the Betic Cordillera (Barich et al., 2014; Acosta-Vigil et
25 al., 2016). The evidence of high Ti^{4+} and high Mg# Bt inclusion in Grt-1 outer rims surrounded by
26 Pl-Kfsp-Qz aggregates supports a scenario of in situ dehydration melting of biotite and garnet
27 growth according to the following general reaction (Patiño Douce and Johnston, 1991; Vielzeuf and
28 Montel, 1994):



30 Accordingly, the peak metamorphic assemblage is assumed to be constituted by the anhydrous
31 assemblage made of Grt + Fsp + Qz + Rt \pm Als that was associated with melt. The pre-melting
32 metamorphic evolution in the crustal envelope of the Beni Bousera peridotites is dominantly
33 recorded by the Ca-rich and Mg-poor Grt-1 inner cores that are surrounded by the low (patchy
34
35
36
37
38
39
40
41
42
43
44
45
46
47
48
49
50
51
52
53
54
55
56
57
58
59
60
61
62
63
64
65

1 zoned) Ca- and Mg-rich rim domains. Remnants of the melt(s) produced at the peak stage are
2 preserved in the Grt-1 rim and Grt-2 growth domains as composite mineral/melt inclusions (Qz-
3 Fsp-Als), which document prograde melting, started within the Ky stability field and continued to
4 the Sil stability as recorded by the inner-to-outer rim inclusion assemblages in Grt-1. The Ca-poor
5 and Mg-rich growth domains of Grt-1 rim compositions are thus interpreted as peritectic
6
7 **crystallisation** products of prograde incongruent melting. Incipient crystallisation of the melt in the
8
9 stability field of sillimanite is documented by Grt-2 cores. (Figs. 11a-b) Progressive crystallisation
10
11 and cooling of the melt resulted in the formation of Ca-rich, Mg-poorer Grt-2 outer rims and Grt-3
12
13 grains during continuous cooling within the Ky stability field (Fig. 11c).
14
15

16 The post-peak retrograde evolution is attested by garnet resorption, Mn increase in garnet,
17 and complex symplectic intergrown of Crd-Qz-Pl-Sp (Fig. 4i). The symplectite formation can be
18 framed in a scenario of retrograde melt consuming reactions (e.g., White and Powell, 2002),
19 controlled by reactions such as (e.g., Cai et al., 2017):
20
21



25 The formation of texturally late Bt-Sil ± Ms aggregates around garnet can be explained as a
26
27 consequence of the reversal of reaction (1).
28

29 The almost complete preservation of the garnet porphyroblasts in the leucosomes and the
30 relatively minor replacement of garnet in the melanosome, also suggests that significant **hydrous**
31 melt extraction occurred after rocks anatexis in the envelope of the Beni Bousera peridotites. In
32 fact, in migmatitic granulites where no melt loss occurred, the replacement of the anhydrous
33 peritectic assemblage by hydrous phases (such as muscovite and biotite) in consequence of
34 retrograde melt-residuum chemical interactions is expected (White and Powell, 2002). In this view,
35 the melanosome is interpreted as the residuum produced by the passive accumulation of garnet after
36 partial melting and extraction of a significant amount of melt.
37
38
39
40
41
42
43
44

45 **10.1 Crustal anatexis: Inverse thermobarometry**

46 The *P-T* conditions attained during crustal anatexis are constrained through inverse
47 thermobarometry as derived from the inclusion assemblages hosted in the peritectic Grt-1 rim and
48 Grt-2 core growth domains, by coupling (i) the *P*-dependent Zr-in-rutile thermometry of Tomkins et
49 al. (2007), combined with (ii) the Grt-Pl-Qz-Als (GASP) barometry (Ghent, 1976) as calculated
50 with the THERMOCALC software v.3.33 (Powell et al., 1998).
51
52
53
54
55

56 The composition of the Rt grains found in different textural positions (as inclusion in Grt-1
57 (rims) and Grt-2 (cores and rims) and in the Qz-Fsp **leucosome portions**, respectively) were
58 investigated through EMPA. The Rt inclusions **in garnet** yielded Zr contents ranging 1975-8827
59
60
61
62
63
64
65

1 ppm ($n = 29$), which provided temperatures ranging $776-1015 \pm 40$ °C (analytical uncertainty) at
2 0.8 GPa and $826-1076 \pm 40$ °C at 1.7 GPa, respectively. The corresponding lower and upper limits
3 of the interquartile range values (Tomkins et al., 2007; Taylor Jones et al., 2015) are 799-887 and
4 850-921 °C with a median value of 844 ± 40 °C and 898 ± 42 °C, respectively (see Supplementary
5 Material#3). The Rt grains in the **leucosome portions** provided lower Zr contents, ranging 888-2053
6 ppm ($n = 64$), resulting in temperature estimates of $741-833 \pm 40$ °C at 0.8 GPa and $789-886 \pm 40$
7 °C at 1.7 GPa. The corresponding lower and upper limits of the interquartile range values are 774-
8 812 and 823-863 with a median value of 794 ± 19 and 845 ± 19 °C, respectively (see
9 Supplementary Material#3).

10 The GASP equilibria were calculated using the Grt-1 rim (Grt-2 core) composition
11 ($X_{\text{Grs}}=0.07-0.09$), combined with the Pl ($X_{\text{An}}=35-45\%$) inclusion, setting the Qz and Sil (**stable at**
12 **the Grt-1 rim**) activity to unit. The GASP barometry provided pressure estimates ranging from ca.
13 1.0 ± 0.1 GPa at 800 °C to 1.3 ± 0.1 GPa at 1000 °C.

14 **The results from inverse thermo-barometry** show that the **minimum** peak **P-T** conditions
15 associated with melt segregation in the granulite envelope of the Beni Bousera peridotites are ca.
16 $900-950$ °C **at 1.1-1.3 GPa, across the transition from the Ky (Grt-1 core) to the Sil (Grt-1 rim)**
17 **stability** (Fig. 12). These estimates are compatible with the results of melting experiments on pelitic
18 compositions, which indicate that biotite is fully consumed by reaction (1) at temperature in the
19 range $850-870$ °C and garnet is the **Fe-Mg** peritectic phase produced at high-pressure (≥ 1.0 GPa)
20 conditions (see reviews in Weinberg and Hasalová, 2015; Gao et al., 2016). The post-peak,
21 retrograde assemblage made of Crd-Qz-Pl-Sp-Bt-Sil \pm Ms indicates decompressional cooling and
22 constrains the final retrograde re-equilibration within the Crd stability field, below to ca. 0.5 GPa
23 (e.g. White and Powell, 2011) (Fig. 12).

24 **10.2 The path to crustal anatexis: forward modelling**

25 To refine the thermobaric evolution leading to crustal anatexis and magma production in the
26 granulite envelope of the Beni Bousera peridotites, we adopted a single-step melt re-integration
27 approach (e.g. Bartoli et al., 2017) by (i) estimating the relative fraction (vol%) of melt and residue
28 at the outcrop scale (see Supplementary Material#4); and (ii) re-integrating the measured bulk
29 average composition of leucosomes to that of a representative melanosome residue (Table 2). The
30 resulting bulk composition as derived by using a 45 vol% of melt composition is assumed as the
31 pre-melt bulk composition that is used for forward modelling thermobarometry using the software
32 program PERPLEX (Connolly, 2005). The model system MnNCaKFMASHTH (MnO–Na₂O–CaO–
33 K₂O–FeO–MgO–Al₂O₃–SiO₂–TiO₂–H₂O) was chosen. The Fe₂O₃ was not considered in the model
34
35
36
37
38
39
40
41
42
43
44
45
46
47
48
49
50
51
52
53
54
55
56
57
58
59
60
61
62
63
64
65

1 system, due to the presence of graphite in the mineral assemblage that is indicative of a reducing
2 environment. The analysed loss of ignition (LOI) was assumed as H₂O. The following solid-
3 solution models were used (details in the file solution.dat enclosed in the Perple_X package;
4 database: hp04ver.dat, an updated version of the Holland and Powell (1998) thermodynamic
5 dataset; Perple_X_6.8.7 version, downloaded July 27 2019): Grt(WPH) for garnet, Mica (CGH) for
6 white mica, Bio(TCC) for biotite, Omph(GHP) for clinopyroxene, Pl (h) for plagioclase, San for K-
7 feldspar and melt (HP) for the melt phase. Additional end-member phases considered in the
8 calculations comprise quartz, rutile, ilmenite, kyanite and sillimanite. The pseudosections were
9 constructed between 0.8 and 1.7 GPa and from 500 to 1100 °C.

10
11
12
13
14
15
16 **These calculations are to be considered as tentative, for the uncertainty on (i) the starting**
17 **bulk composition and proportion of melt loss, and (ii) the water content during progress of the**
18 **metamorphism and crustal melting.** Moreover, since the modal content of retrogressive biotite in the
19 melt products is very limited (ca 1% vol.), escape of water-rich melt has likely occurred, with a
20 consequent bias in the melt re-integration procedure (e.g. Bartoli et al., 2017).

21
22
23
24
25
26
27
28
29
30
31
32
33
34
35
36
37
38
39
40
41
42
43
44
45
46
47
48
49
50
51
52
53
54
55
56
57
58
59
60
61
62
63
64
65
The output of the pseudosection modelling is shown in Fig. 13. The isopleth plots of the
core-to-rim compositions as measured from garnet grains in the melanosome (Grt-1), combined
with the hosted inclusion assemblages are used as a proxy of the thermobaric evolution during
granulitisation and anatexis. Using the relevant Ca zoning in conjunction with the Mg content, the
Grt-1 core compositions ($X_{\text{Grs}} = 0.15-0.16$, $X_{\text{Py}} = 0.15-0.16$) constrains the pre-melting prograde
metamorphic evolution at ca. 550-600 °C and 1.3 GPa. These thermobaric estimates are well below
the temperature conditions compatible with muscovite- and/or biotite-dehydration melting (800-850
°C in the relevant pressure range) and compatible with the biotite stability field, which limits peak
pressure to 1.5-1.6 GPa (Fig. 13). Taking into account the abrupt rimward X_{Grs} decrease and X_{Py}
increase (to 0.05-0.06 and to 0.30-0.31, respectively), combined with the evidence of transition from
Ky to Sil inclusion from outer core to rim in Grt-1 (Figs. 4g), a nearly isothermal heating path is
proposed. Peak conditions are therefore attained within the Sil stability field for temperatures of
950-1000 °C (Fig. 13). The transition to Ca-richer (up to 0.10) outer rim domains in some Grt-2
garnets, coupled with the leucosome mineralogy documenting Ky as the stable Al₂SiO₅ polymorph
in melt segregates (Qz-Fsp-Grt-Ky + Rt + Gr), provide evidence of nearly isothermal cooling within
the Ky stability field during progressive crystallisation of the melt as monitored by the GASP
reaction $\text{An} = \text{Grs} + \text{Ky} + \text{Qz}$. The absence of retrograde Bt in most of the leucosomes constrains
the minimum P-T conditions of final melt crystallisation at ca. 1.1-1.2 GPa and 850-900 °C. **The**
presence of lately formed Sil after Ky in the leucosomes, coupled with the Ca-poor rim composition

1 of Grt-3 at a constant or even slightly increasing Mg content (Fig. 5d) impose a nearly isothermal
2 exhumation path at a temperature of ca. 800 °C (Fig. 13).

3
4 To sum up, integration of inverse and forward modelling thermobarometry (Figs. 12-13)
5 suggests that melt production in the envelope of the Beni Bousera peridotites occurred at HP-(U)HT
6 conditions with peak temperatures > 950° C and crustal depths of ca. 50 km (assuming a rock
7 density of 2800 kg/m³ at 1.3 GPa), followed by a nearly isobaric cooling at HP conditions (ca. 1.1-
8 1.2 GPa and 800-850 °C). Despite the different peak temperature conditions, this scenario confirms
9 what proposed for the granulites from Jubrique in the Betics, where the presence of melt at peak HP
10 conditions has been also documented (Barich et al., 2014), but contrasts with the scenario of
11 decompressional melting as earlier proposed both for the Ronda (Argles et al., 1999; Platt et al.
12 (2003a) and the Beni Bousera (Alvarez Valero et al. 2014) envelopes.

13
14 It is worth noting that the peak temperatures reconstructed in this study as derived from both
15 inverse (Zr-in-Rt thermometry) and forward thermobarometry (likely > 900-950 °C) are not
16 compatible with the Ti-in-zircon thermometry, which provided lower temperatures (ca. 654–770
17 °C ; Table 4). This is in accordance with the previous studies of HT and UHT migmatites, where
18 the Zr-in-Rt thermometry has been documented to be more robust than the Ti-in-zircon in retaining
19 the peak metamorphic conditions (Bin Fu et al., 2008; Clark et al., 2009; Ewing et al., 2013). The
20 convergence of the two thermometers requires the buffering assemblage of zircon-rutile-quartz
21 (Watson et al., 2006; Taylor Jones et al., 2015). In our samples, (i) the rutile grains found in the
22 inclusion assemblage of the peritectic and igneous garnets (Grt-1 and Grt-2) only occur in
23 equilibrium with quartz and not with zircon; (ii) zircon is instead dominantly observed in the matrix
24 assemblages representing the final melt crystallization. However, as discussed below, there are
25 good arguments suggesting that zircon was present at peak temperature as represented by the Grt-1
26 outer rim/Gtr-2 core domains crystallization.

27 28 29 30 31 32 33 34 35 36 37 38 39 40 41 42 43 44 45 ***10.3 Zircon-garnet-melt equilibria and the age of crustal anatexis***

46
47 In high-grade environments as the one documented in this study, garnet and zircon are the
48 primary competitors in controlling the MREE and HREE (from Sm to Lu) budget. In particular, the
49 REE partitioning between zircon and garnet has become an essential tool to decipher the history of
50 crustal anatexis and to link the U-Pb geochronology to the metamorphic evolution (e.g., Hokada
51 and Harley, 2004; Clark et al., 2009; Herman and Rubatto, 2003; Rocha et al., 2017; Rubatto, 2002;
52 Rubatto and Hermann, 2007; Taylor et al., 2015, 2017; Villaros et al., 2009; Whitehouse and Platt,
53 2003).

1 The REE contents of the different garnet growth domains during melt crystallisation (Grt-2
2 and Grt-3) can be thus compared to those of the zircon and the melts products in order to better
3 elucidate a possible timing of zircon growth with respect to the leucosome production,
4 crystallisation and cooling.
5

6
7 In order to verify equilibria between zircon and the two different suprasolidus (igneous)
8 garnet populations, zircon/garnet ($D_{\text{REE}}^{\text{Zrn/Grt}}$) REEs distribution coefficients were calculated from
9 the analyzed material. Due to the homogeneous REE abundances in zircons (Fig. 10a), an average
10 zircon composition was compared to those of the different garnet generations. Results are reported
11 in Table 4 and shown in Fig. 14, where $D_{\text{REE}}^{\text{Zrn/Grt}}$ are compared with those experimentally
12 determined for silicate melts at 900–1000 °C and 0.7 GPa (Taylor et al., 2015) and 800-1000 °C
13 and 2.0 GPa (Rubatto and Herman, 2007), conditions that are relevant for this study.
14
15

16
17 The elevated negative Eu anomalies in both zircon and garnet (Figs. 10) is mirrored by a
18 strong positive Eu anomaly in the leucosomes (Fig. 7), which together indicate that zircons and
19 garnet crystallised in equilibrium with plagioclase-bearing melts (e.g., Rubatto, 2002; Hoskin and
20 Schaltegger, 2003). Significantly, the melanosomes show neutral to negative Eu anomaly,
21 suggesting a fractionation process involving extraction of the Eu-rich phases from melanosome to
22 leucosome (Fig. 7). This is in line with the major element composition of the in situ melt segregates
23 (leucosomes), which are slightly K-depleted and enriched in Ca/(Ca + Na) with respect to
24 experimental melts (Figs. 6c-d), suggesting disequilibrium melting of plagioclase in the source and
25 melt loss from the sites of melt accumulation (Sanchez-Navas, 2014; Taylor et al., 2014).
26
27

28
29 Significantly, the $D_{\text{REE}}^{\text{Zrn/Grt}}$ for the Grt-2 cores show nearly flat patterns for the HREE (from
30 Dy to Lu), with the $D_{\text{REE}}^{\text{Zrn/Grt}}$ values varying close to the unity (Fig. 14; Table 4). These patterns
31 are overlapping with the experimental data of Taylor et al. (2015) and Rubatto and Herman (2007)
32 at HT (1000 °C) (Fig. 14). In contrast, Grt-2 rims and Grt-3 show a significant increase of the
33 HREE partitioning to zircon (Fig. 14; Table 4), essentially resulting from the HREE poor Grt-2 rim
34 and Grt-3 compositions (Fig. 10b). This suggests an impoverishment of HREE in the remaining
35 melt after major zircon crystallization simultaneously or shortly after Grt-2 core growth. It is
36 therefore suggested that the analysed zircons crystallised at nearly equilibrium conditions with the
37 Grt-2 core throughout the cooling history of the segregated melts. We can thus propose an origin
38 from the same melt/silicate system for both zircon and garnet sampled in the melt segregates from
39 the inner granulite envelope of the Beni Bousera peridotites, in a scenario of prograde incongruent
40 melting at high-pressure, melt production, extraction, crystallisation and cooling.
41
42
43
44
45
46
47
48
49
50
51
52
53
54
55
56
57

58 The internal structures (Fig. 8), together with the steep HREE patterns (Fig. 10a) of the
59 zircons recovered from the leucosomes are compatible with this reconstruction, being indicative of
60
61
62
63
64
65

1 crystallisation from a melt (e.g. Harley et al., 2007). The U-Pb geochronology on euhedral and
2 oscillatory to sector zoned growth domains constrains the partial melting event to Hercynian times
3 (300-290 Ma) (Fig. 8). The low Th/U values obtained from the Hercynian igneous domains of the
4 studied samples (Fig. 9) is compatible with the presence of monazite (Th-rich phase; e.g. Rubatto et
5 al., 2013) during zircon growth and progress of rock anatexis in the crustal envelope of the Beni
6 Bousera peridotites (Montel et al., 2000).
7
8
9

10 The few Cenozoic (ca. 20 Ma) U-Pb zircon ages derived from the low Th/U (typically
11 <0.01), structureless rims in zircons from the sample K3L (Fig. 8a) are instead compatible with
12 metamorphic overgrowth. We refer this overgrowth stage to the **low-pressure** Alpine
13 metamorphic/metasomatic event already documented in the inner envelope of the Beni Bousera
14 peridotites, associated with a renewed episode of crustal anatexis and acidic magmatism, early
15 Miocene in age (Rossetti et al., 2010; 2013). **Similarly, an Alpine-aged recrystallisation and Pb loss**
16 **event in the Hercynian zircons has been proposed for the polymetamorphic high-grade basement**
17 **units of the Alpujarride complex in the Betics (Acosta Vigil et al., 2014; Sanchez-Navas et al.,**
18 **2014; 2017).**
19
20
21
22
23
24
25
26
27
28

29 ***10.4 A Hercynian granulite-granite suite: implications at regional scale***

30
31
32
33 When integrated at **the** regional scale, the field, textural and geochronological data set
34 discussed above may contribute to elucidate the *P-T-t* conditions and the petrological/geodynamic
35 issues involved in the granulite-granite connection in the crustal section of the Alboran Domain.
36
37

38 The first **significant** result of our study is Hercynian **HP/(U)HT** granulite-facies migmatitic
39 event is preserved in the core of the Alboran Domain of the Rif chain. Significantly, the
40 crystallisation ages obtained from the melt segregates investigated in this study are, within error, the
41 same as those obtained from the peraluminous **HP (Grt-Ky-bearing)** Hercynian granitoids
42 (leptinites) that intrude the metamorphic core of the Alboran Domain of the Rif chain (Rossetti et
43 al., 2010) (Fig. 9a). This evidence supports a scenario of **HP/(U)HT** Hercynian anatexis in the Beni
44 Bousera envelope, synchronous with the segregation, crystallisation and emplacement of a suite of
45 leucogranitic bodies in the supracrustal metamorphic sequence of the Filali unit. We therefore
46 propose that a Hercynian granulite–granite suite is preserved in the Lower Sebides nappe stack of
47 the Moroccan Rif. **In particular, the documented Hercynian granulite–granite suite can be**
48 **coherently explained by a single metamorphic loop involving isobaric heating and cooling,**
49 **followed by decompression, without the need to introduce a second (Alpine) major anatectic event**
50 **in the high-grade basement of the Alboran Domain.** This reconstruction is coherent with the isotopic
51
52
53
54
55
56
57
58
59
60
61
62
63
64
65

1 data (Sr and Nd) available from both the Hercynian granitoids and the hosting granulite envelope of
2 the Beni Bousera peridotites (Rossetti et al., 2013). The Hercynian granitoids show a relatively high
3 $^{143}\text{Nd}/^{144}\text{Nd}$ values comparable with those of the coeval Iberian-French crustal magmas formed by
4 the partial melting of metasedimentary protoliths that experienced a significant juvenile addition
5 during the Cadomian events. Their origin by partial melting of the associated high-grade
6 metamorphic rocks of the Beni Bousera units is thus isotopically consistent. The Alpine (early
7 Miocene) crustal magmatism, being characterised by low $^{143}\text{Nd}/^{144}\text{Nd}$ values, is instead isotopically
8 distinct from both the Hercynian granitoids and the granulite host rocks (Rossetti et al., 2013), thus
9 attesting for a different metasedimentary source that is possibly identifiable in the metapelitic
10 sequences drilled in the Alboran Basin (Comas et al., 1992).

11 Similar Hercynian ages are also derived from partial melting products in migmatitic units
12 both at the footwall (Acosta Vigil et al., 2014) and hanging wall (Ruiz Cruz and Sains de Galdeano,
13 2014; Zeck and Williams, 2001; Zeck and Whitehouse, 2002; Sanchez Navas et al., 2014; 2017;
14 **Gómez-Pugnaire, 2019**) of the Ronda peridotites. Significant on this regard is the fact that the
15 crustal melting from the granulite envelope of the Beni Bousera peridotites as reconstructed in this
16 study is fully compatible, in terms of both textures and peak thermo-baric environments, with the
17 HP anatectic history of the Jubrique unit at the hanging-wall of the Ronda peridotites (Barich et al.,
18 2014; Acosta Vigil et al., 2016). This evidence further confirms that partial melting in the envelope
19 of the Alboran peridotites has occurred **before** the early Miocene Alpine decompressional evolution
20 (e.g. Argles et al., 1999; Platt et al., 2003a). Moreover, the pre-Hercynian U-Pb zircon ages derived
21 in this study from the high Th/U growth zoning domains (Fig. 9b-c) are also in agreement with
22 those recovered from the high-grade migmatitic units of the Alpujarride-Septide realm (Acosta-
23 Vigil et al., 2014; Melchiorre et al., 2017; Platt and Whitehouse, 1999; Rossetti et al., 2010;
24 Sanchez-Navas et al., 2014; Zeck and Whitehouse, 2002; Zeck and Williams, 2001), suggesting a
25 common crustal inheritance from wall-rock incorporation during the Hercynian anatectic event.
26 This reconstruction supports the presence of a Hercynian migmatized crustal domain in the
27 metamorphic core of the Alboran Domain, structurally associated with the intracrustal emplacement
28 of the Ronda and Beni Bousera peridotite bodies.

29 **The *P-T* evolution reconstructed for the migmatitic granulite envelope of the Beni Bousera
30 peridotite documents a significant isobaric temperature increase (ca. 400 °C, from ca. 600 to ca.
31 1000 °C) and anatectic melt production at deep crustal conditions (ca. 1.3 GPa), during the Permo-
32 Carboniferous transition from a subduction- (ca. 12 °C/km) to a Barrovian-type metamorphic
33 gradient. This is followed by nearly isobaric cooling (ca. 150 °C) and a major isothermal
34 decompression path (ca. 0.5 GPa at ca. 800 °C) during the final crystallisation history of the melt**

1 segregates (Fig. 13). This thermo-baric evolution implies a transient thermal input, followed by
2 cooling and exhumation, compatible with a geodynamic scenario dominated by the convective
3 removal of the deep roots of a mature orogen in a collisional setting (e.g., Dewey, 1988; Platt and
4 England, 1994). The Beni Bousera units can be thus tentatively interpreted as fossil zone of crust-
5 mantle coupling, developed after crustal thickening and intracrustal emplacement of hot peridotites
6 bodies at convergent plate margins. Significantly, the late Carboniferous-early Permian ages
7 documented in this study well fit with the late Carboniferous-early Permian tectono-magmatic
8 events framed within the orogenic collapse stage of the Hercynian chain (e.g. Burg et al., 1994;
9 Matte et al., 2001; Franke, 2015; Petri et al., 2017 and references therein). We can thus propose
10 that the transition from the isobaric prograde/retrograde metamorphism to the isothermal
11 exhumation in the Beni Bousera records the thermo-mechanical evolution of the deep roots of the
12 Hercynian orogeny during the shift from crustal thickening to crustal thinning and collapse of the
13 thermally-weakened orogen (Molnar and Lyon Caen, 1998; Platt and England, 1994;
14 Vanderhaeghe, 2012).

15
16 Despite still debated are the peak pressure conditions attained by the high-grade crustal
17 basement of the Alboran Domain (see Massonne et al., 2014), our results confirm previous
18 estimates pointing to HP conditions for the metamorphic climax (Haissein et al., 2004;
19 Bouybaouene et al., 1998) that we interpret as the evidence of a pre-Alpine (likely Hercynian in
20 age) crustal thickening event preserved in the Lower Sebtides units of the Rif (e.g., Michard et al.,
21 1997). Still unclear, however, is the linkage (if any) with the Hercynian UHP conditions proposed
22 by Ruiz Cruz and Sains de Galdeano (2012; 2013) for the metamorphic evolution of the Lower
23 Sebtides (Monte Hacho gneiss) exposed in the Ceuta region (Fig. 1).

24
25 The post-peak near-isothermal decompression led to the growth of a sequence of
26 symplectitic reaction textures that record exhumation to higher crustal levels of the Beni Bousera
27 units (within the cordierite stability field; below ca. 0.5 GPa; see also Alvarez Valero et al., 2014).
28 This final exhumation stage is geochronologically constrained during the Early Miocene (Rossetti et
29 al., 2010; Melchiorre et al., 2017; this study), which corresponds to the main stage of the Alboran
30 basin back-arc extension (Comas et al., 1999). Significantly, Early Miocene andalusite-bearing
31 dyke swarms are intruded in the Beni-Bousera units, indicating the exhumation of the high-grade
32 basement was almost already completed at that time (Rossetti et al., 2010; 2013).

33
34 Noteworthy are the implications of the above reconstruction for what concerns the impact of
35 the Late Paleozoic template into the Alpine orogeny at a regional scale. First of all, the definitive
36 demonstration of a polymetamorphic evolution of the high-grade basement of the Alboran Domain
37 of the Western Mediterranean region is given (see also Acosta Vigil et al., 2014; Sanchez-Navas et
38
39
40
41
42
43
44
45
46
47
48
49
50
51
52
53
54
55
56
57
58
59
60
61
62
63
64
65

al., 2017), providing evidence that an important Hercynian tectono-metamorphic inheritance contributed to the structuration of the metamorphic core of the Betic-Rif orogen. In such a scenario, taking into account and re-interpreting the existing *P-T-t* data and tectonic/geodynamic reconstructions for the crust-mantle tectonic coupling in the Betic-Rif realm (e.g., Melchiorre et al., 2017; Hidas et al., 2013; Gueydan et al., 2015; 2019; Mazzoli and Martin Algarra, 2011; Hidas et al., 2013; Frasca et al., 2016; 2017; Platt et al., 2003a, b; Platt and Vissers, 1989; Garrido et al., 2011), it is possible to propose a tentative re-appraisal of the tectono-metamorphic evolution of the high-grade basement the Betic-Rif realm from Late Paleozoic onward, including insights on the intracrustal emplacement of the Ronda and Beni-Bousera mantle bodies. In particular, two main stages of crust-mantle coupling can be recognised in the region, that can be framed in Permo-Carboniferous and Neogene times, at deep and shallow crustal conditions, respectively. The early stage occurred in the deep crust at the waning stage of the Hercynian orogeny, associated with diffuse crustal anatexis and associated granite magmatism (Fig. 15a-b). The Hercynian crust-mantle tectonic boundary then resided in the middle to shallow crustal conditions during the subsequent Early Mesozoic rifting phase associated with the formation of the oceanic Tethyan realm (Melchiorre et al., 2017; Gimeno Vives et al., 2019). During the Tertiary (Eocene), Alpine subduction and associated *HP/LT* metamorphism affected the Permo-Triassic supracrustal crustal rock units (upper Sebtides and Alpujarride complexes; Azanon et al. 1997, Bouybaouene et al., 1998; Michard et al., 2006), whereas the Hercynian basement largely escaped subduction and burial, being likely at the footwall of the main Alpine deformation front (Fig. 15c). Starting from the Neogene onward, the westward retreat of the Tethyan subduction caused back-arc extension, asthenosphere upwelling, lithosphere delamination and diffuse magmatism in the inner sectors of the chain, concurrently with the westward migration of the compressional fronts, thrusting the early structured and exhumed belt onto the external flysch domains (Royden et al., 1993; Frasca et al., 2016; 2017; Faccenna et al., 2004; Michard et al., 2006; Rossetti et al., 2013; Auguier et al., 2005; Platt et al., 2013; Van Hinsbergen et al., 2014) (Fig. 15d). This corresponds to the final stage of intracrustal emplacement of the Ronda peridotites, commonly framed in a scenario of hot thrusting/transpression at shallow crustal conditions during switching from crustal extension to shortening in the upper plate domain of the Tethyan subduction (Pregicout et al., 2013; Garrido et al., 2011; Hidas et al., 2011; Frasca et al., 2017; Gueydan et al., 2019; Mazzoli and Martin Algarra, 2011). The hypothesis of the two-stage (pre-Alpine and Alpine) crust-mantle coupling at different crustal depths in the Betic-Rif realm should be further validated through focused structural, petrological and geochronological investigations of the metamorphic envelopes of the Ronda and Beni Bousera peridotites.

1 On a wider scale, it is worth noting that the Hercynian (Permo-Carboniferous) signature
2 detected from the granulite facies migmatitic envelopes of the Alboran peridotites is a common
3 character of the pre-Alpine basement sections tectonically interleaved within the orogenic structure
4 of the Alpine chain. In particular, similar temporal relationships between the Permo-Carboniferous
5 granulite metamorphism and magmatism and are derived from the deep-crust/mantle transitions as
6 exposed in the Ulten (Del Moro et al., 1999; Tumiati et al., 2003; Langone et al., 2011) and Ivrea-
7 Verbano (e.g., Quick et al., 1995; Klötzli et al., 2014; Kunz et al., 2019; Guergouuz et al., 2018)
8 zones, Val Malenco (Herman et al., 1997; Herman and Rubatto, 2003), Calabria (Graessner and
9 Schenk, 2001) and the Northern Pyrenean Zone (Choukroune, 1992). This evidence is indicative of
10 the complex growth of the continental crust across the Alpine realm through the multiple
11 collisional-rifting events suffered by these basements since they were detached from northern
12 Gondwana paleo-margin (Early Palaeozoic), assembled along the Hercynian belt, then
13 fragmented/dispersed again during the Mesozoic and finally assembled and exhumed during the
14 Alpine orogenic cycle (e.g. Stampfli and Borel, 2002). The serendipitous spatial association of
15 Hercynian and Alpine migmatitic complexes and crustal-derived granites across the Alpine orogen is
16 **indicative** of this story and stresses the importance of detailed petrographic, geochronological,
17 geochemical and isotopic studies **of the exposed high-grade basement section** for the formulation of
18 a consistent geodynamic-petrologic interpretation.

11. Conclusion

The main results that can be extracted from this study are as follow:

- (i) A major Hercynian HP/(U)HT granulite-facies anatexis event associated with the intracrustal emplacement of the Beni Bousera peridotites is documented;
- (ii) A Hercynian granulite–granite suite is preserved in the Lower Sebides nappe stack of the Alboran Domain of the Moroccan Rif;
- (iii) A fossil Hercynian **crust-mantle coupling zone** is preserved at the core of the Alboran Domain, recording transition from orogenic construction to collapse;
- (iv) **The polymetamorphic nature of the high-grade basement of the Alboran Domain is confirmed, imposing the need to investigate further the *P-T-t*-deformation history associated with the crust-mantle coupling in the region;**
- (v) The crustal envelopes of the Alboran peridotites can be correlated to the pre-Alpine Permian–Carboniferous lower crustal exposures exposed within the Alpine orogen of the Mediterranean region.

1 Results of this study impose a re-assessment of the metamorphic gradients, exhumation rates
2 and thermo-baric environments associated with the Alpine construction of the Betic-Rif orogeny.
3 In particular, when integrated with the available data from the Alboran Domain of the Betic chain
4 our reconstruction fosters to re-consider the geodynamic significance of the Alpine high-grade
5 tectono-metamorphic event in the Betic-Rif realm, including the models of the intracrustal
6 emplacement of the Beni-Bousera and Ronda peridotites.
7
8
9

10 11 12 13 **Acknowledgements**

14 C. Faccenna, F. Tecce, D. Cozzupoli participated to the field work and are thanked for
15 fruitfull discussion and advice. N. Zaghoul is acknowledged for discussion and advice. H-J
16 Massonne is thanked for discussion and for allowing access to the analytical facilities at the Institut
17 für Mineralogie and Cristalchemie, Universität Stuttgart. M. Schmeltz is thanked for sample
18 preparation. The Grant to Department of Science, Roma Tre University (MIUR-Italy Dipartimenti
19 di Eccellenza, ARTICOLO 958 1, COMMI 314-337 LEGGE 232/2016) is gratefully
20 acknowledged. **This is FIERCE contribution No. XX. The constructive revision of L. Jolivet and A.
21 Acosta Vigil contributed to improve significantly the manuscript.**
22
23
24
25
26
27
28
29
30
31
32

33 **Supplementary Material#1:** Analytical methods and protocols.
34
35

36
37 **Supplementary Material#2:** Representative EMPA and structural fomulae of garnet, feldspar and
38 biotite.
39
40

41
42 **Supplementary Material#3:** Temperature estimates as derived from the Zr-in-rutile thermometer of
43 Tomkins et al. (2007). The results are presented in the form of box-plots showing the interquartile
44 range of the data for each textural setting (calculated @ 1.7 and 0.8 GPa): (a), (b), Rutile inclusion
45 in garnet; (c), (d) Rutile in the matrix. Data statistics obtained through Kirkman, T.W. (1996)
46 Statistics to Use; <http://www.physics.csbsju.edu/stats/> (16 Sept 2019).
47
48
49
50
51

52
53 **Supplementary Material#4:** Estimate of melt (leucosome)/restite (melanosome) proportions (vol%)
54 from outcrop observation
55
56
57
58

59 **References**

60
61
62
63
64
65

- 1 Acosta-Vigil, A., Rubatto, D., Bartoli, O., Cesare, B., Meli, S., Pedrera, A. Azor, A., Tajčmanová,
2 L., 2014. Age of anatexis in the crustal footwall of the Ronda peridotites, S Spain. *Lithos*
3 210–211, 147–167, doi:10.1016/j.lithos.2014.08.018.
- 4
5 Acosta-Vigil, A., Barich, A., Bartoli, O. Garrido, C. J., Cesare, B., Remusat, L., Poli, S., Raepsaet,
6 C., 2016. The composition of nanogranitoids in migmatites overlying the Ronda peridotites
7 (Betic Cordillera, S Spain): the anatectic history of a polymetamorphic basement. *Contrib*
8 *Mineral Petrol* 171, doi: 10.1007/s00410-016-1230-3.
- 9
10
11
12 Álvarez-Valero, A. M., Jagoutz, O., Stanley, J., Manthei, C., El Maz, A., Moukadiri, A., Piasecki,
13 A., 2014. Crustal attenuation as a tracer for the emplacement of the Beni Bousera ultramafic
14 massif (Bético-Rifean belt). *Geol. Soc. Am Bulletin* 126, 1614–1624, doi: 10.1130/B31040.1.
- 15
16
17
18 Andriessen, P.A.M., Zeck, H.P., 1996. Fission-track constraints on timing of Alpine Nappe
19 emplacement and rates of cooling and exhumation, Torrox area, Betic Cordilleras, S. Spain.
20 *Chem Geol* 131, 199–206.
- 21
22
23 Andrieux, J., Fontbote, J. M. Mattauer, M., 1971. Sur un modèle explicatif de l'arc de Gibraltar.
24 *Earth Planet. Sci. Lett.* 12, 191–198.
- 25
26
27 Argles, T. W., Platt, J. P., Waters, D. J., 1999. Attenuation and excision of a crustal section during
28 extensional exhumation: The Carratraca massif, Betic Cordillera, southern Spain. *J. Geol. Soc.*
29 *London* 156, 149–162, doi:10.1144/gsjgs.156.1.0149.
- 30
31
32 Augier, R., Agard, P., Moni[, P., Jolivet, L., Robin, C., and Booth-Rea, G., 2005. Exhumation,
33 doming and slab retreat in the Betic Cordillera (SE Spain): In situ $^{40}\text{Ar}/^{39}\text{Ar}$ ages and P–T–d–t
34 paths for the Nevado-Filabride complex. *Journal of Metamorphic Geology* 23, 357–381, doi:
35 10.1111/j.1525-1314.2005.00581.x.
- 36
37
38
39 Azañón, J.M., Crespo-Blanc, A., Garcíá-Dueñas, V., 1997. Continental collision, crustal thinning
40 and nappe-forming during the pre-Miocene evolution of the Alpujarride Complex (Alboran
41 Domain, Betics). *Journal of Structural Geology* 19, 1055–1071.
- 42
43
44
45 Azdimousa, A., Bourgois, J., Poupeau, G., Vazquez, M., Asebriy, L., Labrin, E., 2014. Fission track
46 thermochronology of the Beni Bousera peridotite massif (Internal Rif, Morocco) and the
47 exhumation of ultramafic rocks in the Gibraltar Arc. *Arabian Journal of Geosciences* 7, 1993–
48 2005.
- 49
50
51
52 Balanyá, J.C., Garcíá-Dueñas, V., Azañón, J.M., Sánchez-Gómez, M., 1997. Alternating
53 contractional and extensional events in the Alpujarride nappes of the Alboran Domain (Betics,
54 Gibraltar Arc). *Tectonics* 16, 226–238.
- 55
56
57
58
59
60
61
62
63
64
65

- 1 Barich, A., Acosta-Vigil, A., Garrido, C. J., Cesare, B., Tajčmanová, L., Bartoli,
2 2014. Microstructures and petrology of melt inclusions in the anatectic sequence of Jubrique
3 (Betic Cordillera, S Spain): implications for crustal anatexis. *Lithos* 206–207, 303–320.
4
5 Bartoli, O., 2017. Phase equilibria modelling of residual migmatites and granulites: An evaluation
6 of the melt-reintegration approach. *J Metamorph Geol.* 2017 35, 919–942, doi:
7 10.1111/jmg.12261
8
9 Booth-Rea, G., Ranero, C.R., Martínez-Martínez, J.M., Grevemeyer, I., 2007. Crustal types and
10 Tertiary tectonic evolution of the Alboran sea, westernMediterranean. *Geochem. Geophys.*
11 *Geosyst.* 8, doi: 10.1029/2007GC001639.
12
13 Bouybaouene, M.L., Michard, A., Goffé, B., 1998. High-pressure granulites on top of the Beni
14 Bousera peridotites, Rif Belt, Morocco: a record of an ancient thickened crust in the Alboran
15 domain. *Bull. Soc. Géol. Fr.* 169, 153–162.
16
17 Brown, M., 2013. Granite: From genesis to emplacement. *Geological Society of America Bulletin*
18 125, 1079-1113
19
20 Brown, M., 1994. The generation, segregation, ascent and emplacement of granite magma: the
21 migmatite-to-crustally-derived granite connection in thickened orogens. *Earth Science*
22 *Reviews* 36, 83-130.
23
24 Burg J-P, Van Den Drissche J, Brun J-P, 1994. Syn- to post-thickening extension in the Variscan
25 Belt of Western Europe: modes and structural consequences. *Geologie de la France* 3,33-51.
26
27 Cai, J., Liu, F., Liu, P., Wang, F., Liu, C., Shi, J., 2017. Anatectic record and P–T path evolution of
28 metapelites from the Wulashan Complex, Khondalite Belt, North China Craton. *Precambrian*
29 *Research* 303, 10–29.
30
31 Casciello, E., Fernández, M., Vergés, J., Montserrat, T., 2015. The Alboran Domain in the Western
32 Mediterranean evolution: the birth of a concept. *Bulletin de la Societe Geologique de France*
33 186, doi: 10.2113/gssgfbull.186.4-5.371
34
35 Cesare, B., Acosta-Vigil, A., Bartoli, O., Ferrero, S., 2015. What can we learn from melt
36 inclusions in migmatites and granulites?. *Lithos* 239, 186–216.
37
38 Choukroune, P., 1992. tectonic evolution of the Pyrenees. *Annual Review of Earth and Planetary*
39 *Sciences* 20, 143-158.
40
41 Clark, C., Collins, A. S., Santosh, M., Taylor, R., Wade, B. P., 2009. The P-T-t architecture of a
42 Gondwanan suture: REE, U–Pb and Ti-in-zircon thermometric constraints from the Palghat
43 Cauvery shear system, South India. *Precambrian Research* 174, 129–144.
44
45
46
47
48
49
50
51
52
53
54
55
56
57
58
59
60
61
62
63
64
65

- 1 Comas, M. C., Platt, J. P., Soto, J. I., Watts. A. B., 1999. The origin and tectonic history of the
2 Alboran Basin: insights from Leg 161 results. *Proc. Ocean Drill. Proj. Sci. Results* 161, 555–
3 79.
4
- 5 Connolly J.A.D., 2005. Computation of phase equilibria by linear programming: A tool for
6 geodynamic modeling and its application to subduction zone decarbonation. *Earth and*
7 *Planetary Science Letters* 236, 524-541.
8
- 9 Corfu, F., Hanchar, J.M., Hoskin, P.W.O., Kinny, P., 2003. Atlas of Zircon Textures. *Reviews in*
10 *Mineralogy and Geochemistry* 53, 469-500.
11
- 12 Del Moro, A., Martin, S., Prosser, G., 1999. Migmatites of the Ulten zone (NE Italy), a record of
13 melt transfer in deep crust. *Journal of Petrology* 40, 1803–1826.
14
- 15 Dewey, J. F., 1988. Extensional collapse of orogens, *Tectonics* 7 , 1123–1139, doi:
16 10.1029/TC007i006p01123.
17
- 18 Dewey, J. F., Helman M. L., Turco E., Hutton D. H. W., Knott S. D., 1989. Kinematics of the
19 western Mediterranean, In: *Alpine Tectonics*, edited by M. P. Coward, D. Dietrich, and R. G.
20 Park, *Geol. Soc. Spec. Publ.*, 45, 421–443.
21
- 22 El Maz, A., Guiraud, M., 2001. Paragenese à faible variance dans les métapelites de la sèrie de
23 Filali (Rif interne marocain): description, interpretation et conséquences géodynamiques.
24 *Bulletin de la Société Géologique de France* 172, 469–485.
25
- 26 Esteban, J. J., Sánchez-Rodríguez, L., Seward, D., Cuevas, J., Tubía, J.M., 2004. Late thermal
27 history of the Ronda area, southern Spain. *Tectonophysics* 398, 81–92.
28
- 29 Esteban, J.J., Cuevas, J., Tubía, J.M., Sergeev, S., Larionov, A., 2010. A revised Aquitanian age for
30 the emplacement of the Ronda peridotites (Betic Cordilleras, southern Spain). *Geol. Mag.*
31 147, doi:10.1017/S0016756810000737.
32
- 33 Esteban, J.J., Sánchez-Rodríguez, L., Seward, D., Cuevas, J. and Tubía, J.M., 2004. The late
34 thermal history of the Ronda area, southern Spain. *Tectonophysics* 389, 81–92.
35
- 36 Esteban, J. J., Cuevas, J., Tubía, J. M., Liati, A., Seward, D., Gebauer, D. 2007. Timing and origin
37 of zircon-bearing chlorite schists in the Ronda peridotites (Betic Cordilleras, Southern Spain).
38 *Lithos* 99, 121–135.
39
- 40 Ewing, T.A., Hermann, J., Rubatto, D., 2013. The robustness of the Zr-in-rutile and Ti-in-zircon
41 thermometers during high-temperature metamorphism (Ivrea-Verbano Zone, northern Italy).
42 *Contributions to Mineralogy and Petrology* 165, 757–779.
43
- 44 Faccenna, C., Becker, T.W., Lucente, F.P., Rossetti, F., 2001. History of Subduction and Back-arc
45 Extension in the Central Mediterranean. *Geophysical Journal International* 145, 1–21.
46
47
48
49
50
51
52
53
54
55
56
57
58
59
60
61
62
63
64
65

- 1 Faccenna, C., Piromallo, C., Crespo-Blanc, A., Jolivet, L., Rossetti, F., 2004. Lateral slab
2 deformation and the origin of the western Mediterranean arcs. *Tectonics* 23:TC1012
- 3 Franke, W., 2006. The Variscan orogen in Central Europe: construction and collapse. In: Gee, D.
4 G., Stephenson, R. A. (eds). *European Lithosphere Dynamics*. Geological Society, London,
5 Memoirs, 32, 333-343.
- 6
7
8
9 Frasca, G., Gueydan, F., Poujol, M., Brun, J.-P., Parat, F., Monié, P., et al., 2017. Fast switch from
10 extensional exhumation to thrusting of the Ronda Peridotites (South Spain). *Terra Nova* 29,
11 117–126, doi:10.1111/ter.12255.
- 12
13
14 Bin Fu, F., Page, Z., Cavosie, A. J., Fournelle, J., Kita, N. T., Lackey, J. S., Wilde, S. A., Valley, J.
15 W., 2008. Ti-in-zircon thermometry: applications and limitations. *Contrib Mineral Petrol* 156,
16 197–215.
- 17
18
19
20 Gao, P., Zheng, Y-F, Zhao, Z-F., 2016. Experimental melts from crustal rocks: A lithochemical
21 constraint on granite petrogenesis. *Lithos* 266–267, 133–157.
- 22
23
24 García-Dueñas, V., Balanyá J. C., Martínez-Martínez J. M., 1992. Miocene extensional
25 detachments in the outcropping basement of the northern Alboran Basin and their tectonic
26 implications, *Geo-Mar. Lett.*, 12, 88–95, doi:10.1007/BF02084917.
- 27
28
29 García-Casco, A., Torres-Roldán, R. L., 1999. Natural metastable reactions involving garnet,
30 staurolite and cordierite: Implications for petrogenetic grids and the extensional collapse of
31 the Betic-Rif Belt. *Contributions to Mineralogy and Petrology* 136, 131-153, doi:
32 10.1007/s004100050528.
- 33
34
35
36 Garrido, C.J., Gueydan, F., Booth-Rea, G., Precigout, J., Hidas, K., Padron-Navarta, J.A., Marchesi,
37 C., 2011. Garnet lherzolite and garnet-spinel mylonite in the Ronda peridotite: Vestiges of
38 Oligocene backarc mantle lithospheric extension in the western Mediterranean. *Geology* 39,
39 927-930. 10.1130/G31760.1.
- 40
41
42
43
44 Graessner, T., Schenk, V., 2001. An exposed Hercynian deep crustal Section in the Sila Massif of
45 northern Calabria: mineral chemistry, petrology and a P–T path of granulite-facies metapelitic
46 migmatites and metabasites. *Journal of Petrology* 42, 931-961.
- 47
48
49 Ghent, E.D., 1976. Plagioclase-garnet- Al_2SiO_5 -Quartz: A potential geobarometer-geothermometer.
50 *American Mineralogist* 61, 710-714.
- 51
52
53 **Gimeno-Vives, O., Mohn, G., Bosse, V., Haissen, F., Zaghloul, M. N., Atouabat, A., Frizon de**
54 **Lamotte, D., 2019. The Mesozoic margin of the Maghrebian Tethys in the Rif belt Morocco):**
55 **Evidence for polyphase rifting and related magmatic activity. *Tectonics* 38, 2894–**
56 **2918. <https://doi.org/10.1029/2019TC005508>**
- 57
58
59
60
61
62
63
64
65

- 1 Gómez-Pugnaire, M.T., Nieto, F., Abad, I., Velilla, N., Garrido, C.J., Acosta-Vigil, A., Barich, A.,
2 Hidas, K., Lopez Sanchez-Vizcaino, V., 2019. Alpine Metamorphism in the Betic Internal
3 Zones. In: C. Quesada, J.T. Oliveira (eds.), *The Geology of Iberia: A Geodynamic Approach*,
4 pp. 519-554, Springer Nature, Switzerland, https://doi.org/10.1007/978-3-030-11295-0_13.
5
6
7 Guergouz, C, Martin, L., Vanderhaeghe, O., Thébaud, N., Fiorentini, M. 2018. Zircon and monazite
8 petrochronologic record of prolonged amphibolite to granulite facies metamorphism in the
9 Ivrea-Verbano and Strona-Ceneri Zones, NW Italy. *Lithos* 308–309, 1–18.
10
11
12 Guerrera, F., Martín-Martín, M., Tramontana, M., 2019. Evolutionary geological models of the
13 central-western peri-Mediterranean chains: a review, *International Geology Review*, doi:
14 [10.1080/00206814.2019.1706056](https://doi.org/10.1080/00206814.2019.1706056)
15
16
17
18 Gueydan, F., Mazzotti, S., Tiberi, C., Cavin, R., and Villasenor, A., 2019. Western Mediterranean
19 sub-continental mantle emplacement by continental margin obduction. *Tectonics*,
20 doi:10.1029/2018TC005058.
21
22
23 Gueydan, F., Pitra, P., Afiri, A., Poujol, M., Essaifi, A., Paquette, J.-L., 2015. Oligo-Miocene
24 thinning of the Beni Bousera peridotites and their Variscan crustal host rocks, Internal Rif,
25 Morocco. *Tectonics* 34, 1244–1268, doi:10.1002/2014TC003769.
26
27
28
29 Harley, S. L., Kelly, N. M., Möller, A., 2007. Zircon behaviour and the thermal histories of
30 mountain chains, *Elements*, 3, 25–30, doi:10.2113/gselements.3.1.25.
31
32
33 Hermann, J., Rubatto, D., 2003. Relating zircon and monazite domains to garnet growth zones: age
34 and duration of granulite facies metamorphism in the Val Malenco lower crust. *Journal of*
35 *Metamorphic Geology* 21, 833–852.
36
37
38 Hidas, K., Booth-Rea, G., Garrido, C.J., Martínez-Martínez, J.M., Padrón-Navarta, J.A., Konc, Z.,
39 Giaconia, F., Frets, E., Marchesi, C., 2013. Backarc basin inversion and subcontinental mantle
40 emplacement in the crust: kilometre-scale folding and shearing at the base of the proto-
41 Alborán lithospheric mantle (Betic Cordillera, southern Spain). *Journal of the Geological*
42 *Society* 170, 47-55, doi: 10.1144/jgs2011-151.
43
44
45
46
47 Hokada, T., Harley, S.L., 2004. Zircon growth in UHT leucosome: constraints from zircon–garnet
48 rare earth elements (REE) relations in Napier Complex, East Antarctica. *Journal of*
49 *Mineralogical and Petrological Sciences* 99, 180–190.
50
51
52
53 Holland, T.J.B., Powell, R., 1998. An internally consistent thermodynamic data set for phases of
54 petrological interest. *Journal of Metamorphic Geology* 16, 309–343.
55
56
57 Homonnay, E., Corsini, M., Lardeaux, J-M, Romagny, A., Münch, P. Bosch D., Cenki-Tok, B.,
58 Ouazzani-Touhami, M., 2018. Miocene crustal extension following thrust tectonic in the
59 Lower Sebtides units (internal Rif, Ceuta Peninsula, Spain): Implication for the geodynamic
60
61
62
63
64
65

1 evolution of the Alboran domain, *Tectonophysics* 722, 507-535, doi:

2 10.1016/j.tecto.2017.11.028.

3 **Hoskin, P.W.O., Schaltegger, U., 2003. The composition of zircon and igneous and metamorphic**
4 **petrogenesis. In: Hanchar, J.M., Hoskin, P.W.O. (Eds.), *Zircon, 53. Mineralogical Society of***
5 ***America, Reviews in Mineralogy & Geochemistry, Washington, DC, pp. 27–62.***

6
7
8
9 Jolivet, L., Augier, R., Faccenna, C., Negro, F., Rimmelé, G., Agard, P., Robin, C., Rossetti, F.,
10 Crespo-Blanc, A., 2008. Subduction, convergence and the mode of backarc extension in the
11 Mediterranean region. *Bull. Soc. Géol. Fr.* 179, 525–550.

12
13
14 Jolivet, L., Faccenna, C. 2000. Mediterranean extension and the Africa-Eurasia collision.
15 *Tectonics*, 19, 1095-1106, doi:10.1029/2000TC900018.

16
17
18 Janots, E., Negro, F., Brunet, F., Goffè, B., Engi, M., Bouybaouene, M. L., 2006. Evolution of the
19 REE mineralogy in HP-LT metapelites of the Sebides complex, Rif, Morocco: Monazite
20 stability and geochronology. *Lithos* 87, 214–234.

21
22
23 Kotková, J., Harley, S. L., 2010. Anatexis during highpressure crustal metamorphism: evidence
24 from garnet–whole-rock REE relationships and zircon–rutile Ti–Zr thermometry in
25 leucogranulites from the Bohemian Massif. *Journal of Petrology* 51, 1967–2001

26
27
28 Kornprobst, J., 1974. Contribution à l'étude pétrographique et structurale de la zone interne du Rif
29 (Maroc septentrional); Petrography and structure of the Rif inner area, northern Morocco.
30 *Notes Mèm. Serv. Géol. Rabat*, 251, 256 pp.

31
32
33
34 Kunz BE, White RW. Phase equilibrium modelling of the amphibolite to granulite facies transition
35 in metabasic rocks (Ivrea Zone, NW Italy). *J Metamorph Geol.* 37, 935–950.

36
37
38 Klötzli, U.S., Sinigoi, S., Quick, J.E., Demarchi, G., Tassinari, C.C., Sato, K., Günes, Z., 2014.
39 Duration of igneous activity in the Sesia Magmatic System and implications for high-
40 temperature metamorphism in the Ivrea–Verbano deep crust. *Lithos* 206, 19–33.

41
42
43 Kunz, B. E., Manzotti, P., von Niederhäusern, B., Engi, M., Darling, J. R., Giuntoli, F., Lanari, P.,
44 2018. Permian high-temperature metamorphism in the Western Alps (NW Italy). *Int J Earth*
45 *Sci* 107, 203–229, doi:10.1007/s00531-017-1485-6.

46
47
48
49 Langone, A, Braga, R., Massonne H. J., Tiepolo, M., 2011. Preservation of old (prograde
50 metamorphic) U–Th–Pb ages in unshielded monazite from the high-pressure paragneisses of
51 the Variscan Ulten Zone (Italy). *Lithos* 127, 68–85.

52
53
54 Lonergan L., White N., 1997. Origin of the Betic-Rif mountain belt, *Tectonics* 16, 504–22

55
56 Ludwig, K. (2003), User's manual for Isoplot/Ex v3.0, a geochronological toolkit for Microsoft
57 Excel, Spec. Publ. 4, 25–31 Berkeley Geochronological Center, Berkeley, California

- 1
2
3
4
5
6
7
8
9
10
11
12
13
14
15
16
17
18
19
20
21
22
23
24
25
26
27
28
29
30
31
32
33
34
35
36
37
38
39
40
41
42
43
44
45
46
47
48
49
50
51
52
53
54
55
56
57
58
59
60
61
62
63
64
65
- Matte, P., 2001. The Variscan collage and orogeny (480-290 Ma) and the tectonic definition of the Armorica microplate: a review, *Terra Nova* 13, 122-128.
- Mazzoli, S., Martín-Algarra, A., 2011. Deformation partitioning during transpressional emplacement of a 'mantle extrusion wedge': The Ronda peridotites, western Betic Cordillera. Spain, *Journal of the Geological Society, London* 168, 373–382.
- Melchiorre, M., Álvarez-Valero, A.M., Vergés, J., Fernández, M., Belousova, E.A., El Maz, A., and Moukadiri, A., 2017. In situ U-Pb zircon geochronology on metapelitic granulites of Beni Bousera (Betic-Rif system, N Morocco), in Bianchini, G., Bodinier, J.-L., Braga, R., and Wilson, M., eds., *The Crust-Mantle and Lithosphere-Asthenosphere Boundaries: Insights from Xenoliths, Orogenic Deep Sections, and Geophysical Studies: Geological Society of America Special Paper 526*, 151–171, doi:10.1130/2017.2526(08).
- Michard, A., Goffé B., Bouybaouene M. L., Saddiqi O., 1997. Late Hercynian-Mesozoic thinning in the Alboran domain; metamorphic data from the northern Rif, Morocco, *Terra Nova*, 9, 171–174, doi:10.1046/j.1365-3121.1997.d01-24.x.
- Michard, A., Negro F., Saddiqi O., Bouybaouene M. L., Chalouan A., Montigny R., Goffé B., 2006. Pressure-temperature-time constraints on the Maghrebide mountain building: Evidence from the Rif-Betic transect (Morocco, Spain), Algerian correlations, and geodynamic implications, *C. R. Acad. Sci., Ser. II*, 338, 92–114.
- Molnar, P., Lyon-Caen, H., 1988. Some Physical Aspects of the Support, Structure, and Evolution of Mountain Belts, vol. 218. *Special Papers of the Geological Society of America*, pp. 179–207.
- Monié, P., Torres Roldan, R.L., Garcìa Casco, A., 1994. Cooling and exhumation of the Western Betic Cordilleras, $40\text{Ar}/39\text{Ar}$ thermochronological constraints on a collapsed terrane. *Tectonophysics* 238, 353–379.
- Montel, J.M., Kornprobst, J., Vielzeuf, D., 2000. Preservation of old U–Th–Pb ages in shielded monazite; example from the Beni Bousera Hercynian kinzigites (Morocco). *J. Metamorph. Geol.* 18, 335–342.
- Negro, F., Beyssac, O., Goffé, B., Saddiqi, O., Bouybaouene, M.L., 2006. Thermal structure of the Alboran Domain in the Rif (northern Morocco) and the Western Betics (southern Spain) constraints from Raman spectroscopy of carbonaceous material. *J. Metamorph. Geol.* 24, 309–327.
- Petri, B., · Mohn, G., · Skrzypek, E., · Mateeva, T., · Galster, F., · Manatschal, G., 2017. U–Pb geochronology of the Sondalo gabbroic complex (Central Alps) and its position within the Permian post-Variscan extension. *International Journal of Earth Sciences* 106, 2873–2893.

- 1
2
3
4
5
6
7
8
9
10
11
12
13
14
15
16
17
18
19
20
21
22
23
24
25
26
27
28
29
30
31
32
33
34
35
36
37
38
39
40
41
42
43
44
45
46
47
48
49
50
51
52
53
54
55
56
57
58
59
60
61
62
63
64
65
- Patiño Douce, A.E., Johnston, A.D., 1991. Phase equilibria and melt productivity in the pelitic system: implications for the origin of peraluminous granitoids and aluminous granulites. *Contrib. Miner. Petrol.* 107, 202–218.
- Platt, J.P., England, P.C., 1994. Convective removal of lithosphere beneath mountain belts: thermal and mechanical consequences. *American Journal of Science* 294, 307–336.
- Platt, J. P. , Behr, W. M., Johannesen K., Williams J. R, 2013. The Betic-Rif Arc and Its Orogenic Hinterland: A Review. *Annu. Rev. Earth Planet. Sci.*, 2013, 41, 14.1–14.45, doi: 10.1146/annurev-earth-050212-123951
- Platt, J.P., Vissers, R.L.M., 1989. Extensional collapse of thickened continental lithosphere: a working hypothesis for the Alboran Sea and Gibraltar Arc. *Geology* 17, 540–543.
- Platt, J.P., Whitehouse, M.J., 1999. Early Miocene high-temperature metamorphism and rapid exhumation in the Betic Cordillera (Spain): evidence from U–Pb zircon ages. *Earth Planet. Sci. Lett.* 171, 591–605.
- Platt, J.P., Soto, J.I., Whitehouse, M.J., Hurford, A.J., Kelley, S.P., 1998. Thermal evolution, rate of exhumation, and tectonic significance of metamorphic rocks from the floor of the Alboran extensional basin, western Mediterranean. *Tectonics* 17, 671–689.
- Platt, J.P., Argles, T.W., Carter, A., Kelley, S.P., Whitehouse, M.J., Lonergan, L., 2003a. Exhumation of the Ronda peridotite and its crustal envelope: constraints from thermal modelling of a P–T–time array. *J. Geol. Soc. Lond.* 160, 655–676.
- Platt, J.P., Whitehouse, M.J., Kelley, S.P., Carter, A., Hollick, L., 2003b. Simultaneous extensional exhumation across the Alboran Basin: implications for the causes of late orogenic extension. *Geology* 31, 251–254.
- Platt, J.P., Kelley, S.P., Carter, A., Orozco, M., 2005. Timing of tectonic events in the Alpujarride Complex, Betic Cordillera, southern Spain. *Journal of the Geological Society of London* 162, 451–462.
- Powell, R., Holland, T.J.B., 2008. On thermobarometry. *Journal of Metamorphic Geology* 26, 155–179.
- Powell, R., Holland, T.J.B., Worley, B, 1998. Calculating phase diagrams involving solid solutions via non-linear equations, with examples using THERMOCALC. *Journal of Metamorphic Geology* 16, 577–588.
- Priem, H.N.A., Boelrijk, N.A.I.M., Hebeda, E.H., Oen, I.S., Verdurmen, E.A.Th., Verschure, R.H., 1979. Isotopic dating of the emplacement of the ultramafic masses in the Serranía de Ronda, Southern Spain. *Contributions to Mineralogy and Petrology* 70, 103–109

- 1
2
3
4
5
6
7
8
9
10
11
12
13
14
15
16
17
18
19
20
21
22
23
24
25
26
27
28
29
30
31
32
33
34
35
36
37
38
39
40
41
42
43
44
45
46
47
48
49
50
51
52
53
54
55
56
57
58
59
60
61
62
63
64
65
- Priem, H.N.A., Boelrijk, N.A.I.M., Hebeda, E.H., Verschure, R.H., 1966. Isotopic age determinations on tourmaline granite-gneisses and a metagranite in the eastern Betic Cordilleras (southeastern Sierra de los Filabres), SE Spain. *Geol. Mijnbouw* 45, 184-187.
- Puga, E., Nieto, J.M., Diaz de Federico, A., Bodinier, J.L., and Morten, L., 1999. Petrology and metamorphic evolution of ultramafic rocks and dolerite dykes of the Betic Ophiolite Association (Mulhacen Complex, SE Spain): Evidence of eo-Alpine subduction following an ocean-floor metasomatic process. *Lithos* 49, 23–56.
- Quick, J. E., Sinigoi, S., A., Mayer, 1995 Emplacement of mantle peridotite in the lower continental crust, Ivrea-Verbano zone, northwest Italy. *Geology* 23, 739–742.
- Rocha, B.C., Moraes, R., Möller, A., Cioffi, C.R., Jercinovic, M.J., 2017. Timing of anatexis and melt crystallization in the Socorro–Guaxupé Nappe, SE Brazil: Insights from trace element composition of zircon, monazite and garnet coupled to U—Pb geochronology. *Lithos* 277, 337–355.
- Rossetti, F., Theye, T., Lucci, F., Bouybaouene, M.L., Dini, A., Gerdes, A., Phillips, D., Cozzupoli, D. 2010. Timing and modes of granites magmatism in the core of the Alboran Domain, Rif Chain, northern Morocco: Implications for the Alpine evolution of the Western Mediterranean. *Tectonics* 29,TC2017, doi:10.1029/2009TC002487.
- Rossetti, F., Faccenna, C., Crespo-Blanc, A. 2005. Structural and kinematic constraints to the exhumation of the Alpujarride Complex (Central Betic Cordillera, Spain). *J. Struct. Geol.*, 27, 199–216,.doi:10.1016/j.jsg.2004.10.008.
- Rossetti, F., Dini, A., Lucci, F., Bouybaouene, M. L., Faccenna, C., 2013. Early Miocene strike-slip tectonics and granite emplacement in the Alboran Domain (Rif chain, Morocco): significance for the geodynamic evolution of westernMediterranean. *Tectonophysics* 608, 774–791.
- Royden, L.H., 1993. Evolution of retreating subduction boundaries formed during continental collision. *Tectonics* 12, 629–38.
- Rubatto, D., 2002. Zircon trace element geochemistry: distribution coefficients and the link between U–Pb ages and metamorphism. *Chemical Geology* 184, 123–138.
- Rubatto, D., Hermann, J., 2007. Experimental zircon/melt and zircon/garnet trace element partitioning and implications for the geochronology of crustal rocks. *Chemical Geology* 241, 38–61.
- Rubatto, D., Chakraborty, S., Dasgupta, S., 2013. Timescales of crustal melting in the Higher Himalayan Crystallines (Sikkim, Eastern Himalaya) inferred from trace element constrained monazite and zircon chronology. *Contributions to Mineralogy and Petrology* 165, 349–372.

- 1 Ruiz Cruz, M. D., Sanz de Galdeano, C., 2014. Garnet variety and zircon ages in UHP meta-
2 sedimentary rocks from the Jubrique zone (Alpujarride Complex, Betic Cordillera, Spain):
3 Evidence for a pre-Alpine emplacement of the Ronda peridotite. *International Geology*
4 *Reviews* 56, 845–868.
5
6
7 Ruiz-Cruz, M.D., Sanz de Galdeano, C., 2012. Diamond and coesite in the ultrahigh-pressure–
8 ultrahigh-temperature granulites from Ceuta, Northern Rif, Northwest Africa *Mineralogical*
9 *Magazine*, 76 (2012), pp. 683-705
10
11
12 Ruiz-Cruz, M.D., Sanz de Galdeano, C., 2013. Coesite and diamond inclusions, exsolutions
13 microstructures and chemical patterns in ultrahigh-pressure garnet from Ceuta (Northern Rif,
14 Spain). *Lithos* 177, 184-206.
15
16
17 Sánchez-Navas, A., García-Casco, A., Martín-Algarra, A., 2014. Pre-Alpine discordant granitic
18 dikes in the metamorphic core of the Betic Cordillera: tectonic implications. *Terra Nova* 26,
19 477–486.
20
21
22 Sánchez-Navas, A., García-Casco, A., Mazzoli, S., Martín-Algarra, A., 2017. Polymetamorphism in
23 the Alpujarride Complex, Betic Cordillera, South Spain. *The Journal of Geology*, 125,
24 doi:10.1086/693862
25
26
27 Sánchez-Rodríguez, L., Gebauer, D., 2000. Mesozoic formation of pyroxenites and gabbros in the
28 Ronda area (southern Spain), followed by Early Miocene subduction metamorphism and
29 emplacement into the middle crust: U-Pb sensitive high-resolution ion microprobe dating of
30 zircon. *Tectonophysics* 316, 19–44.
31
32
33 Sawyer, E. W., 1994. Melt segregation in the continental crust. *Geology* 22, 1019- 1022.
34
35
36 Sawyer, E.W., 2008. Atlas of migmatites. The Canadian Mineralogist. In: Special Publication, vol.
37 9. NRC Research Press, Ottawa, Ontario, p. 371.
38
39 Schmid, S.M., Fügenschuh, B., Kissling, E., Schuster, R., 2004. Tectonic map and overall
40 architecture of the Alpine orogen. *Eclogae Geol Helv* 97, 93–117.
41
42
43 Sosson, M., Morrillon, A.-C., Bourgois, J., Feraud, G., Poupeau, G., Saint-Marc, P., 1998. Late
44 exhumation stages of the Alpujarride complex (western Betic Cordilleras, Spain): new
45 thermochronological and structural data on Los Reales and Ojen nappes. *Tectonophysics* 285,
46 253–273.
47
48
49 Soto, J.I., Platt, J.P., 1999. Petrological and structural evolution of high-grade metamorphic rocks
50 from the floor of the Alboran Sea basin, Western Mediterranean. *J. Petrol.* 40, 21–60.
51
52
53 Spear F. S., Daniel C. G., 2001. Diffusion control of garnet growth, Harpswell Neck, Maine, USA.
54
55
56 J. *Metamorphic Geol.* 19, 179-195.
57
58
59
60
61
62
63
64
65

- Stampfli, G.M., Borel, G.D., 2002. A plate tectonic model for the Paleozoic and Mesozoic constrained by dynamic plate boundaries and restored synthetic oceanic isochrones. *Earth and Planetary Science Letters* 196, 17-33, doi:10.1016/S0012-821X(01)00588-X
- Sun, S.S., McDonough, W.S., 1989. Chemical and Isotopic Systematics of Oceanic Basalts: Implications for Mantle Composition and Processes. Geological Society, London, Special Publications 42, pp. 313-345.
- Taylor, J., Nicoli, G., Stevens, G., Frei, D., Moyen, J.F., 2014. The processes that control leucosome compositions in metasedimentary granulites: perspectives from the Southern Marginal Zone migmatites, Limpopo Belt, South Africa. *Journal of Metamorphic Geology* 32, 713–742.
- Taylor, R. J. M., Harley, S. L., Hinton, R. W., Elphick, S., Clark, C., Kelly, N. M., 2015. Experimental determination of REE partition coefficients between zircon, garnet and melt: A key to understanding high-T crustal processes. *Journal of Metamorphic Geology* 33, 231–248.
- Taylor, R. J. M., Clark, C., Harley, S. L., Kylander-Clark, A. R. C., Hacker, B. R., Kinny, P. D., 2017. Interpreting granulite facies events through rare earth element partitioning arrays. *Journal of Metamorphic Geology* 35, 759–775, doi:10.1111/jmg.12254.
- Taylor-Jones, Powell, R., 2015. Interpreting zirconium-in-rutile thermometric results. *Journal of Metamorphic Geol.* 33, 115–122.
- Tomkins, H.S., Powell, R., Ellis, D.J., 2007. The pressure dependence of the zirconium-in-rutile thermometer. *Journal of Metamorphic Geology* 25, 703–713.
- Torres-Roldán, R.L., 1983. Fractionated melting of metapelite and further crystal-melt equilibria. The example of the Blanca Unit migmatite complex, north of Estepona (southern Spain). *Tectonophysics* 96, 95–123.
- Tubía, J., Cuevas, J., Ibarra, J. G., 1997. Sequential development of the metamorphic aureole beneath the Ronda Peridotites and its bearing on the tectonic evolution of the Betic Cordillera. *Tectonophysics* 279, 227 -252.
- Tubía, J., Cuevas, J., 1986. High-temperature emplacement of the Los Reales Peridotite nappe (Betic Cordillera, Spain). *Journal of Structural Geology* 8, 473–482.
- Tumiati, S., Thöni, M., Nimis, P., Martin, S., Mair, V., 2003. Mantle–crust interactions during Variscan subduction in the Eastern Alps (Nonsberg–Ulten zone): geochronology and new petrological constraints. *Earth and Planetary Science Letters* 210, 509–526.
- Vanderhaeghe, O., 1999. Pervasive melt migration from migmatites to leucogranite in the Shuswap metamorphic core complex, Canada: control of regional deformation. *Tectonophysics* 312, 35–55.

- 1
2 Vanderhaeghe, O., 2009. Migmatites, granites and orogeny: flow modes of partially molten rocks
3 and magmas associated with melt/solid segregation in orogenic belts. *Tectonophysics* 477,
4 119–134.
- 5 Vanderhaeghe, O., 2012. The thermal–mechanical evolution of crustal orogenic belts at convergent
6 plate boundaries: A reappraisal of the orogenic cycle. *Journal of Geodynamics* 56– 57, 124–
7 145.
- 8
9
10 **Van Hinsbergen, D.J.J., Vissers, R.L.M., Spakman, W., 2014. Origin and consequences of Western**
11 **Mediterranean subduction, rollback, and slab segmentation. *Tectonics* 33, 393–419.**
- 12
13
14 von Raumer, J.F., Bussy, F., Schaltegger, U., Schulz, B., Stampfli. G.M., 2013. Pre-Mesozoic
15 Alpine basements—their place in the European Paleozoic framework. *Geol Soc Am Bull*
16 125:89–108.
- 17
18
19
20 Vèrges, J, Fernàndez, M., 2012. Tethys-Atlantic interaction along the Iberia-Africa plate boundary:
21 the Betic-Rif orogenic system. *Tectonophysics* 579,144–72.
- 22
23 Vielzeuf, D. , Clemens, J.D., Pin, C., Moinet, E., 1990. Granites, granulites and crustal
24 differentiation In: Vielzeuf, D, Vidal, P. (eds) *Granulites and crustal evolution*. Kluwer
25 Academic Publishers, Dordrecht, 59-85.
- 26
27
28
29 Vielzeuf, D., Montel, J.M., 1994. Partial melting of metagreywackes part I. Fluid-absent
30 experiments and phase relationships. *Contrib. Miner. Petrol.* 117, 375–393.
- 31
32
33 Villarros, A., Stevens, G. Buick, I. S., 2009. Tracking S-type granite from source to emplacement:
34 Clues from garnet in the Cape Granite Suite. *Lithos* 112,217–235
- 35
36
37
38
39
40
41
42
43
44
45
46
47
48
49
50
51
52
53
54
55
56
57
58
59
60
61
62
63
64
65
- Watson, E.B., Harrison, T.M., 1983. Zircon saturation revisited: temperature and composition
effects in a variety of crustal magma types. *Earth Planet. Sci. Lett.*, 295-304.
- Watson, E.B., Wark, D.A., Thomas, J.B., 2006. Crystallization thermometers for zircon and rutile.
Contrib. Mineral. Petrol. 151, 413.
- Weinberg, R. F., Hasalová, P., 2015. Water-fluxed melting of the continental crust: A review.
Lithos 212–215, 158–188.
- White, R.W. & Powell, R., 2002. Melt loss and the preservation of granulite facies mineral
assemblages. *Journal of Metamorphic Geology* 20, 621–632.
- White, R. W., Powell, R., 2011. On the interpretation of retrograde reaction textures in granulite
facies rocks. *Journal of Metamorphic Geology* 29, 131-149, doi:10.1111/j.1525-
1314.2010.00905.x
- Whitehouse, M. J., Platt, J. P., 2003. Dating high-grade metamorphism - Constraints from rare-earth
elements in zircon and garnet. *Contributions to Mineralogy and Petrology* 145, 61-74.

- 1
2 Whitney, D.L., Evans, B.W., 2010. Abbreviations for Names of Rock-Forming Minerals. *American Mineralogist*, 95, 185-187, doi:10.2138/am.2010.3371.
- 3
4 Zeck, H.P., Monié, P., Villa, I.M., Hansen, B.T., 1992. Very high rates of cooling and uplift in the
5 Alpine belt of the Betic Cordilleras, southern Spain. *Geology* 20, 79–82.
- 6
7 Zeck, H. P., Whitehouse, M. J., 2002. Repeated age resetting in zircons from Hercynian–Alpine
8 polymetamorphic schists (Betic–Rif tectonic belt, S. Spain)—a U–Th–Pb ion microprobe
9 study. *Chemical Geology* 182, 275–292.
- 10
11
12 Zeck, H.P., Williams, I. S., 2001. Hercynian Metamorphism in Nappe Core Complexes of the
13 Alpine Betic–Rif Belt, Western Mediterranean—a SHRIMP Zircon Study. *Journal of*
14
15 *Petrology* 42, 1373-1385, doi: 10.1093/petrology/42.7.1373.
- 16
17
18 Zeck, H. P., Whitehouse, M.,J., 2002. Repeated age resetting in zircons from Hercynian–Alpine
19 polymetamorphic schists (Betic–Rif tectonic belt, S. Spain)—a U–Th–Pb ion microprobe
20 study, *Chemical Geology* 182, 275-292,doi: 10.1016/S0009-2541(01)00296-0.
- 21
22
23
24
25
26
27
28
29
30
31
32
33
34
35
36
37
38
39
40
41
42
43
44
45
46
47
48
49
50
51
52
53
54
55
56
57
58
59
60
61
62
63
64
65

Figure captions

1
2
3 Figure 1 – (a) The Mediterranean region with location of the Betic-Rif orogen. (b) Regional
4 geology of the western Mediterranean region and crustal-scale geological cross section across the
5 Rif chain (modified and re-adapted after Michard et al., 2002 and references therein). The study
6 area (Fig. 2) is also indicated.
7
8
9

10
11
12 Figure 2 - (a) Tectono-stratigraphic column of the Alboran Domain Complex in the Moroccan Rif ,
13 with indication of the migmatitic granulites (Mg) that are the focus of this study. (b) The geology
14 of the study area (modified after Kronmpbst, 1975). (c) General structural architecture across the
15 Beni Bousera peridotite bodies (geological cross-section A-B).
16
17
18
19
20

21 Figure 3 – Outcrop-scale rock textures in the field. (a) Geological sketch showing the across-strike
22 structure of the peridotite (β)-migmatitic granulites (Mg) contact (Beni Bousera units), showing
23 representative lithologies and the structural significance of the studied samples (see also Table 1).
24 (b) Stromatic leucosome layering within the granulites enveloping metabasite boudins. (c)
25 Coexistence of deformed (early segregated) leucosomes and stromatic leucosome layering within
26 the granulite foliation. (d) Coarse-grained garnet-bearing (Grt-1) residua (melanosome) hosting
27 stromatic and nebulitic leucosomes (stromatic metatexite). (e) Detail shown in (d) showing the
28 intimate relationships between garnet (Grt-1) and leucosomes. (f) The melanosome-leucosome
29 contact showing enclaves of grt-bearing melanosome portions and the two igneous garnet types
30 (Grt-2 and Grt-3, sample). Mineral abbreviations follow Whitney and Evans (2010).
31
32
33
34
35
36
37
38
39
40

41 Figure 4 - Microtextures and mineral assemblages. (a) Scanned thin section of a melanosome-
42 leucosome layering, showing the textural characteristics and arrangement of the Grt-1 types (sample
43 K3). (b) Enlargement of the garnet core shown in Fig. 4a, showing the inclusion assemblages
44 hosted at the garnet core. Plane polarised light. (c) Back-scattered electron (BSE) image showing of
45 the area indicated in (b) showing the polymineralic and single-phase inclusion assemblage made of
46 Rt, Qz, Kfs, Pl, Ky, Gr. (d) High-Ti Bt crystals hosted in poikiloblastic Grt-1 inner rim domain
47 (area indicated in Fig. 4a). Bt inclusions occur together with rounded, single-phase, Qz inclusions.
48 Plane polarised light. (e) Detail of a Grt-1 outer rim domain (area indicated in Fig. 4a), showing
49 sillimanite inclusion. Plane polarised light. (f) Grt-2 in leucosome. The enlargement shows the
50 sillimanite inclusion at the garnet core (sample Ma48). Plane polarised light. (g) The mineral
51 assemblage in leucosomes, showing a well annealed Qz-Fsp-Qz matrix showing equilibrium
52 textures with Ky and garnet (Grt-3; sample K3L). Crossed polarised light. (H) BSE image to
53
54
55
56
57
58
59
60
61
62
63
64
65

1 illustrate the leucosomes microtexture (sample Ma09/28L). Note the crystal framework made by
2 plagioclase, with K-feldspar, quartz. Garnet (Grt-3) occurs as an interstitial phase with subhedral
3 habit (sample Ma09/30L). (h) BSE image showing evidence of the retrograde metamorphism, as
4 documented by spinel–cordierite symplectic intergrowths that replaces early garnet-kyanite
5 assemblages (sample K3M). Mineral abbreviations follow Whitney and Evans (2010).
6
7
8
9

10 Figure 5 – Representative qualitative compositional maps and quantitative EMPA profiles showing
11 variation in cations (Mn, Mg, Fe, Ca) distribution in garnet grains from the Beni Bousera granulite
12 units. (a)-(b) Grt-1. (c) Grt-2. (c) Grt-3.
13
14
15
16

17 Figure 6 – Whole-rock major element composition of the studied samples. (a) Total alkali vs. silica
18 (TAS) chemical classification diagram (LeMaitre et al. 2002) for the melt products interlayered
19 within the Beni Bousera granulites. (b) The same samples plotted in the CaO–Na₂O–K₂O ternary
20 diagram and compared to experimental melts produced through fluid-absent biotite-dehydration
21 melting. (c)-(d) The major element compositions (100 wt% normalized) plotted as atomic K vs. Si
22 and Ca/(Ca + Na) and vs. Fe + Mg (after Taylor et al. 2014).
23
24
25
26
27
28
29
30

31 Figure 7: Chondrite-normalized (after Sun and McDonough, 1989) REE patterns of the studied
32 leucosome samples compared to the experimental S-type melts (after Taylor et al. 2014).
33
34
35

36 Figure 8 – (a)-(c) Cathodoluminescence images with location of the LA-ICPMS laser spots (white
37 circles) indicated (all ages are ²⁰⁶Pb/²³⁸U ages in Ma, with errors quoted at 2σ level) and
38 conventional Concordia diagrams of the analysed zircon grains from the studied samples (see Table
39 3). The inset in (a) shows the weighted average of ²⁰⁶Pb/²³⁸U ages for the data population at the
40 lower end of the Discordia.
41
42
43
44
45

46 Figure 9 – (a) Probability age distribution plot as obtained from the cumulative ²⁰⁶Pb/²³⁸U zircon
47 age data. (b)-(c) ²⁰⁶Pb/²³⁸U ages vs. U/Th diagram values for the analysed zircon ages. Data are
48 compared with those available from the Hercynian leptinites intruded into the Lower Sebtides units
49 (after Rossetti et al., 2010)
50
51
52
53
54
55

56 Figure 10: Chondrite-normalized (Sun and McDonough, 1989) REE pattern of the (a) analysed
57 zircons and (b) garnets.
58
59
60
61
62
63
64
65

1
2 Figure 11 – Conceptual evolutionary model for the textural and compositional characteristics of the
3 different garnet types recognised in the Beni Bousera migmatitic granulites.
4

5 Figure 12 –Pressure-Temperature diagram showing the thermo-baric conditions attained during
6 crustal anatexis in the Beni Bousera granulites as derived from inverse thermobarometry. The P-T
7 grid and the relevant mineral and melting reactions are after Kotková and Harley (2010) and
8 references therein.
9
10
11

12
13 Figure 13 - Representative P-T pseudosection calculated for the reconstructed bulk rock
14 composition (pre-melting) assuming a 45 vol% of melt loss in the system MnNKCFMASHT (MnO-
15 Na₂O-K₂O-CaO-FeO-MgO-Al₂O₃-SiO₂-H₂O-TiO₂) with a bulk composition (wt%) MnO = 0.27,
16 Na₂O = 1.54, K₂O = 4.19, FeO = 9.15, MgO = 2.44, Al₂O₃ = 22.98, SiO₂ = 55.43, H₂O = 1.46, TiO₂
17 = 0.86, using the Perple_X software. The dashed lines and arrows depict the inferred P-T path to
18 Biotite dehydration melting as as constrained from the X_{Grt} and X_{Pyr} isopleths in Grt-1 (core and rim
19 domains) and Grt-2 (core domains) garnets. The colored ellipses indicate the pre-melting and the
20 climax of metamorphism attained by the inner crustal envelope of the Beni Bousera **peridotites**.
21
22
23
24
25
26
27
28
29

30 Figure 14 - Calculated zircon/garnets REE partitioning coefficients for the different samples
31 compared with experimental data. **The coloured fields display the whole range of values, the**
32 **coloured continuous lines are the corresponding average values (see Table 4).**
33
34
35
36
37

38 **Figure 15 - Conceptual evolutionary model for the Beni Bousera Hercynian migmatitic granulites in**
39 **the framework of the Betic-Rif tectonics. A two-stage (Permo-Carboniferous and Early Miocene)**
40 **crust-mantle coupling is tentatively proposed.**
41
42
43
44
45
46

47 **Table captions**

48
49
50
51 Table 1 - Localisation of the samples, constituent mineralogy and analytical methods
52
53

54
55 Table 2 – Whole-rock chemical compositions
56
57

58
59 Table 3 - Results of U-Th-Pb LA-ICP-MS analyses and calculated ages for zircon separates from
60 the migmatitic granulites of the Beni Bousera unit
61
62
63
64
65

1
2
3
4
5
6
7
8
9
10
11
12
13
14
15
16
17
18
19
20
21
22
23
24
25
26
27
28
29
30
31
32
33
34
35
36
37
38
39
40
41
42
43
44
45
46
47
48
49
50
51
52
53
54
55
56
57
58
59
60
61
62
63
64
65

Table 4: Representative REE compositions of zircon and garnet with the corresponding $D_{\text{REE}}^{\text{Zrn/Grt}}$ coefficients.

1
2
3
4
5
6
7
8
9
10
11
12
13
14
15
16
17
18
19
20
21
22
23
24
25
26
27
28
29
30
31
32
33
34
35
36
37
38
39
40
41
42
43
44
45
46
47
48
49
50
51
52
53
54
55
56
57
58
59
60
61
62
63
64
65

Hercynian anatexis in the envelope of the Beni Bousera peridotites (Alboran Domain, Morocco): implications for the tectono-metamorphic evolution of the deep crustal roots of the Mediterranean region

Federico Rossetti^{1(*)}, Federico Lucci¹, Thomas Theye², Mohamed Bouybaouenne², Axel Gerdes^{4,5}, Joachim Opitz², Andrea Dini⁶, Christian Lipp²

¹Dipartimento di Scienze, Università Roma Tre, Roma, Italy

²Institut für Anorganische Chemie, Universität Stuttgart, Stuttgart, Germany

³Département de Géologie, Université de Rabat, Rabat, Morocco

⁴Institute für Geowissenschaften, Goethe University, Frankfurt, Germany

⁵Frankfurt Isotope and Element Research Center (FIERCE), Goethe University Frankfurt, Germany

⁶Istituto di Geoscienze e Georisorse, CNR, Pisa, Italy

(*) Corresponding Author
Dipartimento di Scienze
Sez. Scienze Geologiche
Largo San Leonardo Murialdo, 1
010146 Roma (Italy)
e-mail: federico.rossetti@uniroma3.it
Tel: +390657338043

Abstract

1
2
3
4 The metamorphic core of the Betic-Rif orogenic chain (Alboran Domain) is made up of lower
5 crustal rocks forming the envelope of the Ronda (Spain) and Beni Bousera (Morocco) peridotites.
6
7 The deepest sections of the crustal envelopes are made of migmatitic granulites associated with
8
9 diffuse acidic magmatic products, making these exposure and ideal site to investigate the textural
10
11 and petrological connection between crustal anatexis and granite magmatism in the continental
12
13 crust. However, still debated is the timing of intracrustal emplacement of the peridotite bodies, with
14
15 models proposing either Alpine (early Miocene) or Hercynian ages, and still uncertain is the linkage
16
17 between peridotite emplacement and crustal anatexis. In this study, by combining rock textures with
18
19 whole-rock geochemistry, metamorphic thermobarometry, the U-Pb zircon geochronology and the
20
21 analysis of the garnet and zircon REE chemistry, we document the *P-T-t* evolution of the granulite
22
23 facies migmatites that form the immediate envelope of the Beni Bousera peridotites of the Rif belt.
24
25 A main episode of Permo-Carboniferous (ca. 300-290 Ma) deep crustal anatexis, melt extraction
26
27 and migration is documented that we link to the crustal emplacement of the Beni Bousera
28
29 peridotites during collapse of the Hercynian orogen. Correlation at a regional scale suggests that the
30
31 Beni-Bousera section can be tentatively correlated with the pre-Alpine (Permo-Carboniferous)
32
33 basement units tectonically interleaved within the orogenic structure of the Alpine chain. The
34
35 results of this study provide ultimate constraints to reconstruct the tectono-metamorphic evolution
36
37 of the Alboran Domain in the Western Mediterranean and impose re-assessment of the modes and
38
39 rates through which Alpine orogenic construction and collapse occurred and operated in the region.
40
41

42 **Keywords: Granulite; Anatexis; Hercynian; Alboran Domain; Western Mediterranean**
43
44
45
46
47
48
49
50
51
52
53
54
55
56
57
58
59
60
61
62
63
64
65

1. Introduction

The arcuate belt of the Betic-Rif chain forms the western termination of the peri-Mediterranean Alpine orogenic systems (Fig. 1a). This orogen is part of a mountain belt developed along the active margin of the western Mediterranean subduction zone, developed during the Alpine Mesozoic-Cenozoic convergence between African and Eurasian plates (Dewey et al., 1998; Faccenna et al. 2001, 2004; Jolivet et al., 2008; Lonergan and White 1997, Platt et al., 2013; Royden 1993; Vergés and Fernandez, 2012; Guerrero et al., 2019). The metamorphic core of this Alpine orogen is now dismembered in discontinuous outcrops located in the internal domains of the mountain fronts, where Neogene extensional tectonics overprinted the early crustal thickening event (e.g., Both-Rea et al., 2007; Comas et al., 1999; Dewey, 1988; Faccenna et al., 2001; 2004; García-Dueñas et al., 1992; Jolivet and Faccenna, 2000; Jolivet et al., 2008; Michard et al., 2006; Platt and Vissers, 1989; Platt and Whitehouse, 1999; Platt et al., 1998; 2003a,b; 2013; Guerrero et al., 2019; Van Hinsbergen et al., 2014).

The orogenic hinterland of the Betic-Rif chains consists of the continental-derived metamorphic units of the Alboran Domain (e.g., Andrieux et al., 1971; Casciello et al., 2015; Michard et al., 2006; Platt et al., 2013). Various models have been proposed in the literature with contrasting geodynamic and timing scenarios to frame the tectono-metamorphic evolution of the Alboran Domain. The major source of controversy comes from the pressure-temperature-time (*P-T-t*)-deformation history reconstructed from the Alpujarride-Sebtide Complex, which make-up the metamorphic envelope of the Ronda and Beni Bousera peridotite massifs (Fig. 1b). A distinctive feature of the Alpujarride/Sebtide Complex of the Alboran Domain is the presence of condensed metamorphic sequences with marked downward increase in the paleo-temperature gradients (Álvarez-Valero et al., 2014; Argles et al., 1999; Azanon et al., 1997; Balanya et al., 1997; Barich et al., 2014; Both Rea et al., 2007; Comas et al., 1999; García Casco and Torres Roldan, 1999; García-Dueñas et al., 1992; Gueydan et al., 2015; Haissen et al., 2004; Jolivet et al., 2008; Michard et al., 2006; Monié et al., 1994; Negro et al., 2006; Platt et al., 2013; Rossetti et al. 2005; Sanchez-Navas et al., 2014, 2017; Soto and Platt, 1999; Tubia et al., 1997; Zeck et al., 1992). Still debated is in particular, the timing of the high-grade metamorphism and associated crustal anatexis in the metamorphic rocks that make-up the inner envelopes of the peridotite bodies, with implications on the age and model of the intracrustal emplacement of the peridotites. Based on the available petrological, structural and geochronological data sets, two classes of models exist, with the high-grade metamorphism and magmatism referred either to the Alpine (Álvarez-Valero et al., 2014; Argles et al., 1999; Esteban et al., 2004, 2010; Frasca et al., 2017; Garrido et al., 2011; Gueydan et

1 al., 2015; 2019; Hidas et al., 2013; Homonnay et al., 2018; Janots et al., 2006; Mazzoli and Martín-
2 Algarra, 2011; Précigout et al., 2013; Platt and Vissers 1989; Platt et al., 1998; 2003a, b; Platt and
3 Whitehouse, 1999; Sánchez-Rodríguez and Gebauer, 2000; Soto and Platt, 1999; Tubia et al., 1997;
4 Whitehouse and Platt, 2003; Zeck et al., 1992) or the Hercynian (Acosta Vigil et al., 2014; Barich et
5 al., 2014; Bouybaouene et al., 1998; Michard et al., 1997; Montel et al., 2000; Rossetti et al., 2010;
6 2013; Ruiz Cruz and Sanz de Galdeano, 2014; Sánchez-Navas et al., 2014; Zeck and Williams,
7 2001; Zeck and Whitehouse, 2002) evolution. It is worth noting that disequilibrium textures and
8 disturbance of the isotopic systems are also reported from the high-grade basement rocks of the
9 Alboran Domain, suggesting a polyphase (Hercynian and Alpine) tectono-metamorphic evolution
10 (e.g., Acosta Vigil et al., 2014; García Casco and Torres Roldan, 1999; Gueydan et al., 2015;
11 Massonne, 2014; Rossetti et al., 2010; Sánchez-Navas et al., 2017, Gómez-Pugnaire et al., 2019).
12 Therefore, unanswered key questions regarding the tectono-thermal evolution of the Alboran
13 Domain remain; in particular: (i) the age of crustal anatexis: Alpine or Hercynian?; (ii) which the
14 link between crustal anatexis and the peridotite emplacement in the continental crust (time and
15 mode of crust-mantle coupling)?; and (iii) any correlations with the pre-Alpine lower crustal
16 exposures across the Alpine chain (e.g., Schmidt et al., 2004; von Raumer et al., 2013; Kunz et al.,
17 2018)? To answer to these questions it is essential to elucidate the space-time connection (if any)
18 between the partially molten source region (migmatites) and the extracted and migrated melts in the
19 crustal section of the Alboran Domain, i.e. the so-called granulite–granite connection (e.g., Brown,
20 1994, 2013; Vanderhaeghe, 1999; 2009; Vielzeuf et al., 1990).

21 In this paper, we investigate the Pressure-Temperature-time (P - T - t) evolution of the
22 granulite facies migmatites (kinzigites in Kornprobst, 1974) that form the immediate envelope of
23 the Beni Bousera peridotite at the core of the Alboran Domain of the Rif belt (Figs. 1b and 2). We
24 report a main Permo-Carboniferous deep crustal granulite-granite suite that we link to the crustal
25 emplacement of the Beni Bousera peridotites and discuss implications of these results for the
26 tectono-metamorphic evolution of the Alboran Domain and of the Alpine orogen in general.

27 2. Geological Setting

28 The Alboran Domain forms the metamorphic core of the Alpine Betic-Rif orogen. It consists
29 of continentally-derived metamorphic rock units that broadly correlate across the two arms of the
30 orogeny (García Duenas et al., 1992; Michard et al., 2006) (Fig. 1b).

31 In Morocco, the Alboran Domain is made of the Ghomaride and Sebtime complexes that
32 tectonically overlie the Mesozoic carbonates of the Dorsale units (Figs. 1b and 2). In the Betics,
33 these metamorphic complexes correspond to the Malaguide and Alpujarride complexes,
34
35

1
2
3
4
5
6
7
8
9
10
11
12
13
14
15
16
17
18
19
20
21
22
23
24
25
26
27
28
29
30
31
32
33
34
35
36
37
38
39
40
41
42
43
44
45
46
47
48
49
50
51
52
53
54
55
56
57
58
59
60
61
62
63
64
65

respectively. The lower tectonic complex is the eclogite-bearing Nevado-Filabride Complex (Augier et al. 2005; Puga et al., 1999) of the Betics that is not exposed in the Moroccan side (Michard et al., 2006 and references therein) (Fig. 1b).

The metamorphic signature the Alpujarride-Septide complex has been classically referred to as a down-section transition from low-grade (subduction-type) to high-grade (Barrovian-type) thermo-baric environments, as recorded on Permian-Triassic and pre-Alpine protoliths, respectively (Azañon et al., 1997; Bouybaouene et al., 1998; El Maz and Guiraud, 2001; Michard et al., 1997; 2006). The age of the Alpine subduction zone metamorphism is still poorly constrained but referred to as Eocene (Platt et al., 2005). In the Moroccan Rif, this distinct metamorphic signature corresponds to the upper (Federico Group) and lower (Filali and Beni Bousera units) Sebtides, respectively (Kornprobst, 1974; Michard et al., 2006; Bouybaouenne et al, 1998; Negro et al., 2006; Gueydan et al., 2015) (see the tectono-stratigraphic column in Fig. 2a). This down-section change in the metamorphic signature is structurally associated with the presence of large peridotite bodies (Ronda and Beni Bousera; Fig. 1b), which are tectonically interlayered within the continental metamorphic sequence of the Alpujarride-Septide complex.

Field evidence documents similar contact relationships between the peridotite bodies and the hosting continental-derived Alpujarride-Sebtides units (e.g., Michard et al., 2006). High-grade metamorphic rocks characterise the upper and lower contacts of the peridotites with widespread evidence of rock anatexis close to these contacts. The upper tectonostratigraphic section corresponds to the Casares-Los Reales unit of the Betics (Monié et al., 1994; Haissein et al., 2004) and to the Lower Sebtides of the Rif (Kornprobst, 1974; Michard et al., 2006), consisting of basal acidic migmatitic granulites (kinzigites and Beni Bousera units) passing upward to lower-grade gneisses and metapelites of the Filali unit. Peak metamorphism in the Casares-Los Reales/Beni Bousera units is commonly framed within the HP granulite facies field (1.2-1.7 GPa and 750-850 °C), typified by the assemblage garnet-kyanite-rutile ± biotite, followed by a nearly isothermal decompression within the cordierite stability field (Bouybaouenne et al., 1998; Haissein et al., 2004; Alvarez-Valero et al., 2014).

The lower contact with the crustal envelope is well exposed in the western Betics, where the peridotites rest on top of the Blanca Group, a migmatitic, locally strongly mylonitised, inverse metamorphic sequence grading from granulite (top) to amphibolite (bottom) facies metamorphic conditions (Acosta-Vigil et al., 2014, Tubia et al., 1997; Torres-Roldàn, 1983). In the Moroccan Rif, the basal contact is exposed in the Ceuta area (Fig. 1b), where the peridotite bodies tectonically rest on top of the Monte Hacho gneiss (Kornprobst, 1974; Homonnay et al., 2018; see tectono-stratigraphic column in Fig. 2a). The lower and upper contacts of the peridotites and the associated

1 partial melting are interpreted as dynamothermal aureole developed during the intracrustal
2 emplacement of the peridotites, and considered as developed during hot thrusting and extensional
3 unroofing and decompression in Alpine times, respectively (e.g. Argles et al., 1999; Frasca et al.,
4 2017; Gueydan et al., 2019; Hidas et al., 2013; Homonnay et al., 2018; Mazzoli and Martin Algarra,
5 2011; Platt et al., 2003a-b; 2013; Tubia and Cuevas, 1986; Tubia et al., 1997). Evidence of an early
6 UHP evolution, assumed as Hercynian in age, has been also reported from the Jubrique zone of the
7 Alpujarride Complex in the Betic Cordillera (Ruiz Cruz and Sanz de Galdeano, 2014) and from the
8 orthogneiss of the Hacho unit in the Ceuta zone (Ruiz Cruz and Sanz de Galdeano, 2012; 2013).

9 No definitive constraint on the granulite-granite connection issue has been derived since
10 now in the Betic-Rif realm. The age of the anatexis products and melt mobilisates found within the
11 immediate envelope of the peridotite bodies is still the subject of debate, with Alpine and Hercynian
12 ages proposed so far (see Acosta Vigil et al., 2014 for a recent review). Granite magmatism in the
13 Ronda area (Betics) is commonly attributed to the early Miocene (Rb-Sr, whole-rock (Priem et al.,
14 1979); Ar-Ar on biotite (Monié et al., 1994); U-Pb zircon dating (Esteban et al., 2010)). However,
15 magmatic rocks of Hercynian age are also reported from the Betic Cordillera (Priem et al. 1966;
16 Platt and Whitehouse, 1999; Zeck and Williams, 1999). Recently, through SHRIMP U-Pb zircon
17 geochronology, Sanchez-Navas et al. (2014a) have documented Hercynian (286 ± 16 Ma) igneous
18 zircons and Alpine metamorphic resetting (early Miocene in age) in granitoid dykes intruded in the
19 Torrox unit of the Central Betics.

20 This duality of Hercynian and Alpine ages for the granite magmatism is also documented in
21 the immediate envelope of the Beni Bousera peridotites in the Rif (Fig. 1), where two generation of
22 peraluminous granites with distinct isotopic signatures are recognised (Rossetti et al., 2010; 2013):
23 (i) an early *HP*, garnet-kyanite-bearing, granitic suite with highly radiogenic Sr isotope ratios
24 ($0.736243\text{--}0.771449$) (the so-called "leptinites" Kornprobst (1974) of Hercynian age (Permo-
25 Carboniferous, 290-300 Ma; U-Pb zircon dating); and (ii) a subsequent *LP*, andalusite-bearing, sub-
26 vertical granite dyke swarm with lower Sr radiogenic ratios ($0.719753\text{--}0.722461$), dated by
27 coupled U-Pb zircon/monazite and $^{40}\text{Ar}/^{39}\text{Ar}$ muscovite/biotite geochronology to the early Miocene
28 (c. 22 Ma).

29 The Hercynian and Alpine ages are also systematically derived from the U-Th-Pb zircon and
30 monazite geochronology of the migmatitic sequences of the Alboran Domain, where a significant
31 inheritance from Cadomian-Pan African (560–640 Ma), Grevillian (940–1020Ma), to Early
32 Archean (2-2.5 Ga) crustal sources are also reported (Zeck and Whitehouse, 2002; Zeck and
33 Williams, 2001; Platt and Whitehouse, 1999; Acosta-Vigil et al., 2014; Montel et al., 2000; Rossetti
34 et al., 2010; Sanchez-Navas et al., 2014; Melchiorre et al., 2017).

1 Based on U-Pb SHRIMP dating on structureless zircon rims from both the migmatitic
2 dynamothermal sole and syn-tectonic intrusives from the Blanca unit of Central Betics, Esteban et
3 al. (2010) proposed an age of 22-21 Ma for the intracrustal emplacement of the Ronda peridotites.
4 Similarly, U-Pb zircon and Ar-Ar datings of syn-tectonic and post-tectonic intrusive granitic dykes
5 constrain the crust-mantle coupling in the Ronda area during the Early Miocene (22.5-20 Ma;
6 Frasca et al., 2017). However, based on integrated petrographic/textural and SHRIMP U-Pb dating
7 of magmatic zircons, Acosta-Vigil et al. (2014) have constrained the age of anatexis at the footwall
8 of the Ronda peridotite to the late stages of the Hercynian orogeny (280–290 Ma), and documented
9 an Alpine-aged recrystallisation and Pb loss event in the Hercynian zircons. These Hercynian ages
10 are in line with the U-Pb zircon dating results derived from (i) the migmatitic portions of the Torrox
11 basement units, which provided mean ages of 285 ± 5 Ma, 313 ± 7 Ma (Zeck and Whitehouse
12 (2002) and 286 ± 11 Ma (Sanchez Navas et al., 2017), and (ii) the migmatitic sequences of the
13 Jubrique zone (mean ages of 330 ± 9 and 265 ± 4 Ma) (Ruiz Cruz and Sainz de Galdeano, 2014),
14 both structurally overlying the Ronda peridotites.
15

16 Regarding the high-grade migmatitic crustal envelope of the Beni Bousera peridotites,
17 Montel et al. (2000), have documented late Hercynian (284 ± 27 Ma) granulite metamorphism, as
18 derived from U-Th-Pb dating of monazite inclusions in garnet. The intrusive relationships between
19 Permo-Carboniferous granitoid bodies and the host Beni-Bousera units, allowed Rossetti et al.
20 (2010) to propose a pre-Alpine age for the crustal envelope of the Beni Bousera peridotites. On the
21 other hand, Platt et al. (2003a) provided a lower Miocene (22.7 ± 0.3 Ma) U-Pb zircon age for the
22 peak of metamorphism in the Beni Bousera units that is referred to as the main stage of crustal
23 thinning and exhumation. Finally, Melchiorre et al. (2017) reported new zircon U-Pb ages from the
24 Beni Bousera granulites, which provided ages spanning from Paleoproterozoic (1508 ± 23 Ma) to
25 Miocene (22.9 ± 0.7 Ma). In particular, two main groups of ages at ca. 286-264 and ca. 23 Ma are
26 derived, interpreted as the timing of the prograde *HP* metamorphism and the *LT* exhumation of the
27 granulite envelope, respectively (Melchiorre et al., 2017).
28

29 As a final point, it is worth noting that the early Miocene granite magmatism overlaps in
30 time with the wealth of the available radiometric geochronological and low-temperature
31 thermochronological data (apatite and zircon fission tracks) from the Sebti-Alpujarride realm
32 that, regardless of the dating method, indicates a significant age clustering at 18-25 Ma, commonly
33 interpreted as the time of cooling and exhumation of the Alboran Domain (e.g., Michard et al.,
34 2006; Janots et al., 2007; Frasca et al., 2017; Gueydan et al., 2015; Homonnay et al., 2018;
35 Melchiorre et al., 2017; Monié et al., 1994; Platt et al., 1998; 2003b; Platt and Whitehouse, 1999;
36
37
38
39
40
41
42
43
44
45
46
47
48
49
50
51
52
53
54
55
56
57
58
59
60
61
62
63
64
65

1 Rossetti et al., 2010; Sanchez-Rodriguez and Gebauer, 2000; Zeck et al. , 1992; Azdimousa et al.,
2 2014; Sosson et al., 1998; Esteban et al., 2004; 2007; 2011; Andriessen and Zeck, 1996).
3
4
5
6

7 **3. The Study area**

8
9 The study area corresponds to the north-western, high-grade envelope of the Beni Bousera
10 peridotites, where the lower Sebtides are exposed. The lithological units grade from granulite
11 migmatites (kinzigites) at the contact with the peridotite (collectively named as the Beni Bousera
12 units) to gneisses and micaschists of the Filali unit (Figs. 2a-b). The regional metamorphic foliation
13 wraps around the Beni Bousera peridotites, showing a general domal attitude (Alvarez-Valero et al.,
14 2014; Bouybaouenne et al., 1998; El Maz and Guiraud, 2001; Gueydan et al., 2015; Kornprobst,
15 1974; Melchiorre et al., 2017; Michard et al., 2006; Negro et al., 2006) (Figs. 2b-c). As documented
16 by Raman spectroscopic analyses of graphitic material from the Filali unit (Negro et al., 2006), the
17 metamorphic grade increases down-section from subsolidus andalusite to kyanite zones, with
18 melting occurring at the transition from the Filali mica schists to the Filali gneiss in correspondence
19 of the sillimanite + alkali feldspar isograd (El Maz and Guiraud, 2001). The metamorphic signature
20 of the Filali unit is described as acquired during a polyphase clockwise P-T path in response to a
21 transition from a Hercynian Barrovian stage (peak conditions of 550-670 °C and 0.5-08 GPa)
22 metamorphic gradient of 20–26 °C/km), followed and overprinted by a *HT-LP* one (equilibrated at
23 550-750 °C and 0.3-06 GPa; metamorphic gradient of 45 °C/km), Alpine in age (at ca. 21 Ma;
24 Gueydan et al., 2015).
25
26
27
28
29
30
31
32
33
34
35
36
37
38

39 The granulite envelope is dominantly made of felsic (metapelite-derived) and minor mafic
40 protoliths, the latter occurring as intercalations and boudins close to the contact with the peridotites
41 (Bouybaouene et al., 1998; Haissen et al., 2004; Alvarez-Valero et al., 20014; Melchiorre et al.,
42 2014). The thermobaric evolution of the granulite rocks is similarly framed within a nearly
43 isothermal decompressional evolution, starting at *HP/HT* conditions of 1.2-1.5 GPa (up to 2.0 GPa
44 in the basic granulites; Bouybaouenne et al., 1998) at ca. 800 °C, with a final re-equilibration at 0.4-
45 0.5 GPa for *T* below ca. 600 °C (Bouybaouenne et al., 1998; Haissein et al., 2004; Alvarez-Valero
46 et al., 2014). Age of the climax of metamorphism is still debated, referred either to the Hercynian
47 (Michard et al., 1997; Bouybaouene et al., 1998; Montel et al. 2000; Rossetti et al., 2010;
48 Melchiorre et al., 2017) or the Alpine (Early Miocene; Platt et al., 2003; Gueydan et al. 2015)
49 tectono-metamorphic evolution. Available zircon and apatite zircon fission-track data constrain the
50 final exhumation of the Beni Bousera peridotite massif during Burdigalian-Langhian times (ca.
51 19.5-15.5 Ma; Azdimousa et al., 2014).
52
53
54
55
56
57
58
59
60
61
62
63
64
65

4. Materials and Methods

This study investigates a suite of migmatitic granulites in the immediate envelope of the Beni Boussera peridotites, exposed on a ca. 500 metre long, continuous outcrop (known as Playa Smeila) located along the sea side, 1 km south-east of the Bouh Ahmed village (Figs. 2b and 3a). Meso- and micro-scale studies were carried out in order to investigate the petrology and geochronology of rock anatexis and melt formation.

Selected rock samples, representative of the different textures recognised in the field, were chosen for petrographical investigation, mineral and whole-rock chemistry (major and trace elements). Sample selection was based on the structure at the outcrop scale and on meso- and micro-scale textural and mineralogical features. Samples are shown in their structural context in Fig. 3a and listed in Table 1, where their location, fabrics, and constituent mineralogy are detailed. Electron microprobe analyses (EMPA) were used to define compositions of the constituent mineral assemblages. Inverse and forward modelling techniques (Powell and Holland, 2008) were used to assess the thermo-baric conditions associated with anatexis, magma segregation and emplacement. The U-(Th)-Pb zircon geochronology was adopted to constrain the timing of crustal anatexis and magmatism in the metamorphic envelope. Trace and rare earth element (REE) compositions (both in situ and on separates) of zircon and garnet were also investigated to link the U-Pb ages to the reconstructed tectono-metamorphic history.

Details on the analytical methods and protocols adopted in this study are provided in the Supplementary Material#1. In the following, mineral abbreviations are after Whitney and Evans (2010).

5. Structure and petrography of the granulites

The granulites are characterised by a north-eastward dipping foliation that is sub-parallel to the one in the underlying peridotites. A major, NW-SE steeply-dipping extensional fault, marked by a ca. 20 wide damage zone, cuts across the granulite-peridotite contact. The whole outcrop is affected by intense jointing that defines NW-SE striking sub-vertical fracture arrays associated with rock alteration in both the footwall and hangingwall rocks. A sub-parallel pegmatitic dyke swarm is observed to intrude the granulite rocks (Fig. 3a).

The granulites are extensively migmatitic, with an overall stromatic texture, made of centimetre- to decimetre-scale lithological banding parallel to the dominant foliation at the outcrop scale, and defined by alternating leucocratic and melanocratic portions (Figs. 3b-e). The granulites host dm-scale metabasite boundins, typically surrounded by leucocratic layers and lenses, and with

boudin necks providing dilatational sites for accumulation of leucocratic material (Fig. 3b).

Following Sawyer (2008), the leucocratic portions consist of both in situ and in-source leucosome types (up to 30-40 % vol.), associated with leucocratic sills (up to 10% vol.) (Fig. 3a-e). The latter are typically extensively boundinaged and stretched along the main foliation (Fig. 3c). The melt structures (leucosomes and sills) invariably contain high proportions of garnet. The melanocratic portions are here almost entirely constituted by mm to cm-thick porphyroblastic aggregates of garnet and interpreted as a melt residuum (Taylor and Stevens, 2010). In particular, garnet porphyroblasts (up to 3 cm in diameter) are surrounded by and embedded within diffuse leucocratic patches and layers (Fig. 3d-e), suggestive of in situ melting, likely developed through incongruent melting reactions in which the garnets are formed as the solid peritectic products (e.g., Brown, 2013). Based on the overall rock texture, the Beni Bousera granulites can be classified as a metatexite migmatite (e.g., Brown, 1994; Sawyer, 1994).

The rock mineralogy is dominated by modally abundant Grt (locally up to 60 vol%) in an igneous matrix made of Qz-Pl-Kfsp-Ky+Gr, Rt (see Supplementary Material#2 for representative EMPA of the mineral constituents). Accessories include Zrn, Ap, and Mnz. The igneous assemblage in the melt segregates (leucosomes and sills) resembles peraluminous granites (e.g. Clark, 1981) (Figs. 3d-f and 4). Three main generations of garnets can be recognised based on textural evidence, with distinct inclusion assemblages and composition zoning (see below). An early garnet generation (Grt-1), occurring primarily in the melanosome portions, consists of coarse-grained (up to 1-3 cm in diameter), anhedral grains, usually with distinct core and rim structures. The inner Grt-1 cores are typically devoid of mineral inclusion, whereas the outer core and rim domains are poikilitic, hosting numerous (10–200 μm) xenomorphic and round to lobate mono- and poly-mineralic inclusions typically made of Qz-Kfs (Ab_{13-17})-Pl (An_{35-45}) aggregates, usually associated with Rt, Gr and Bt with high TiO_2 (up to 7.76 wt %) and high X_{Mg} ($[\text{Mg}/(\text{Mg}+\text{Fe})]\times 100 = 51-60$). Significantly, the outer core domains are also characterized by dense arrays of graphite-bearing fluid and solid inclusions, where usually Ky occurs embayed in multiphase Pl-Kfs-Qz aggregates (Figs. 4a-d). The presence of Sil inclusions is instead systematically observed in the rim domains of the largest Grt-1 grains (Fig. 4e). A second generation (Grt-2), occurring in leucosomes, consists of large (up to 1-2 cm in diameter), still poikilitic and anhedral grains hosting Qz-Kfs-Pl inclusion assemblages, usually associated with Sil in the core domains (Figs. 4f). Ky crystals either as single mineral inclusion or associated with Pl-Kfs-Qz aggregates are commonly observed at the Grt-2 rims (Fig. 4g). The third garnet generation (Grt-3) occurs again only in the leucosomes and typically show anhedral grain shapes with a nearly uniform grain size (ca. 50-250 μm), interstitially distributed along Qz-Fsp grains boundaries, indicating that Grt-3 directly crystallized from a melt

(Fig. 4h). Igneous textures are usually well preserved in the low strain domains, as documented by a well annealed polygonal texture made of inequigranular Qz-Fsp matrix, where Pl (An_{40-52}) and Kfs (Ab_{07-14}) form the framework microstructure (Figs. 4g-h).

Locally, an intense metamorphic overprint is documented in the melanosome portions and typified by symplectites of Crd-Sp-Pl-Qz \pm Ilm developed at the expenses of early Grt-Ky-Rt assemblages (Fig. 4i). A post-kynematic growth of Bt-Sil \pm Ms \pm late Chl aggregates also occurs in secondary foliation replacing the early Grt-Ky-bearing texture.

6. Chemical zoning in garnet

Garnet in both melanosomes and melt segregates is essentially a zoned almandine-pyrope-grossular solid solution with a minor content of spessartine. The zoning profiles are characterised by marked Ca and Mg compositional zoning as illustrated in Figure 5a. The Grt-1 grains are characterized by rather heterogeneous composition profiles, with a marked core-to-rim chemical zonation. When preserved, they show a broad core that is relatively homogeneous with respect to Fe and Mn ($Alm_{63-66}Pyr_{15-21}Grs_{15-17}Sps_{04-05}$), typically high in Ca and with the Mg content inversely correlated to the Ca content. In other cases, the Ca-rich core of Grt-1 is present only as relic (Fig. 5b) or completely lacking. The transition to the rim domains is characterized by a broad Ca-poor and Mg-rich domain ($Alm_{63-66}Pyr_{27-30}Grs_{05-07}Sps_{01-02}$), in conjunction with the transition from inclusion-free to inclusion-rich rim growth domains. The inclusion often contains a composite Qz-Fsp-Rt-Gr assemblage with Ky in addition. The occurrence of Sil is instead restricted to the outer rim zones of Grt-1 (Figs. 5a-b). The Grt-2 shows a nearly uniform core-to-rim composition with the core broadly corresponding to the Grt-1 outer rim compositions. Towards the rim, Ca increases at the expense of Mg and Fe. A variably developed (up to 50-70 μ m large) outer rim showing a strong decrease of Mg and Ca, concomitant with a slight increase in the Mn component ($Alm_{58-64}Pyr_{25-27}Grs_{15-17}Sps_{06-07}$) (Fig. 5c). The Grt-3 shows a contrasting zoning pattern being characterized by a large homogeneous core rich in Ca and Mg ($Pyr_{26}Grs_{15}$; similar to the composition of the Grt-2 rims) that grades into a relatively narrow rim with lower contents of Ca and Mg and higher Mn (Figs. 5d).

7. Whole-rock geochemistry

The chemical composition of four melanosome and five leucosome samples from the studied granulite migmatites (see Table 1 for sample location and constituent mineralogy) were analysed for major and trace element geochemistry. Data are reported in Table 2 and graphically shown in Fig. 6 for the leucosome compositions.

1 The leucosomes have acidic composition ($\text{SiO}_2 = 70.51\text{--}76.62$ wt%), associated with low
2 MgO (0.09-0.35 wt%), FeO_{TOT} (0.96-2.06 wt%), TiO_2 (0.01-0.14 wt%) and CaO (1.14-2.01 wt%)
3 contents. They are enriched in K_2O (5.29-5.57 wt%) with respect to Na_2O (1.7-2.78 wt%) and with
4 an Al_2O_3 content of 12.26-15.50 wt%. In the TAS (total alkali vs. silica) diagram, the leucosomes
5 fall in the granite field (Fig 6a). Significantly, the leucosome compositions fall within those derived
6 from experimental melts produced by biotite dehydration (Gao et al., 2016 and references therein)
7 (Fig. 6b). Leucosome compositions are however K-depleted and show higher $\text{Ca}/(\text{Ca} + \text{Na})$ ratios
8 than those of experimental and natural anatectic glasses (Fig. 6c-d; Taylor et al., 2014 and
9 references therein). Melanosomes show SiO_2 ranging 41-63 wt% with high Al_2O_3 (16.7-28.8 wt%)
10 and $\text{Fe}_2\text{O}_3^{\text{TOT}}$ (7.6-16.92 wt%) and low TiO_2 (1.0-1.4 wt%), associated with moderate MgO (2.1-4.2
11 wt%) and K_2O (2.1-3.1 wt%), variable CaO (0.8-4.1 wt%) and Na_2O (0.3-2.3 wt%). These
12 compositions are strongly Si and K depleted and strongly enriched in $\text{Ca}/(\text{Ca} + \text{Na})$ ratios and Fe +
13 Mg contents with respect to leucosomes (Fig. 6c-d).
14
15
16
17
18
19
20
21
22

23 The abundance of large-ion lithophile elements (LILEs, such as Ba, Rb, Sr) is positively
24 correlated with SiO_2 and it is higher in leucosomes. Conversely, high-field strength elements (such
25 as REE, Y, Nb and Zr) are negatively correlated with SiO_2 and their content is higher in
26 melanosomes. When normalized to chondrite (after Sun and McDonough, 1989), all samples are
27 generally enriched in light REE (LREE), with $(\text{La}/\text{Sm})_{\text{N}}$ and $(\text{La}/\text{Yb})_{\text{N}}$ ranging 3.09-7.40 and 1.73-
28 5.68 for the leucosomes and 3.87-4.33 and 6.35-12.57 for the melanosome, respectively. The Eu
29 anomaly ($\text{Eu}_{\text{N}}/[\text{Sm}_{\text{N}} \times \text{Gd}_{\text{N}}]^{1/2}$) is systematically positive for leucosomes (4.37-13.53), whereas in
30 melanosomes varies from positive (2.64) to slightly negative (0.47), when moving from
31 intermediate to low-silica compositions, respectively (Fig. 7).
32
33
34
35
36
37
38
39
40
41

42 8. U-Pb zircon geochronology

43 The zircon U-Pb geochronological study was carried out on zircon separates as obtained
44 from a melanosome-leucosome layering (sample K3L, representative of the in situ melt segregates)
45 and two leucosomes (sample Ma09/28L and Ma09/30L as representative of melt mobilisates).
46 Sample Ma09/28L is from an in situ melt segregation, while Ma09/30 is from a boudinated granite
47 (Fig. 3). Sample K3L is located within the alteration zone associated with dyke emplacement at the
48 base of the granulite exposure (Fig. 3).
49
50
51
52
53
54

55 Zircon grains were investigated through cathodoluminescence (CL) and back scattered
56 electron (BSE) imaging techniques and subsequently analysed in situ through a LA-ICP-MS system
57 at the Frankfurt Isotope and Element Research Center (FIERCE) of the Goethe University of
58
59
60
61
62
63
64
65

Frankfurt (see Supplementary Material#1). Analytical results are shown in Table 3a-c. Age calculations and graphical display were obtained through the ISOPLOT software (Ludwig, 2003).

8.1 Sample K3L

Zircons are generally euhedral to subhedral. Based on the BSE and CL imaging, two textural types are defined. The first and more abundant type consists of moderately luminescent, single-phase zircons with oscillatory zoning and planar growth banding (Fig. 8a). The second type comprises grains with distinct core and rim structures. The cores (inner and outer) show oscillatory and sector zoned growth zoning and are embayed by thin (10-30 μm wide), low-luminescent rims that commonly truncate the inner zoning (Fig. 8a). Minor metamict textures are also observed in some grains, documented by opaque, fractured domains. The Th/U values vary largely, with values significantly higher in the growth zoning domains (up to 0.70) with respect to the low-luminescent rims (<0.01) (Table 3a; Fig. 9).

The range of analytical zircon ages is very large, with apparent $^{206}\text{Pb}/^{238}\text{U}$ ages spanning from the Late Archean (ca. 2.5 Ga) in the cores to Cenozoic (ca. 22 Ma) in the structureless rim domains. However, a significant age cluster from the oscillatory growth domains is observed at c. 300 Ma (Table 3a; Fig. 8a). Taking into account the age population younger than 300 Ma, data array defines a Discordia with an upper intercept at 297 (+16/-17) Ma and a lower intercept of early Miocene age, at 20.0 (+4.4/-4.8) Ma. Eight analyses from the low-luminescent structureless rims form a nearly concordant age cluster at the lower end of the Discordia, yielding a weighted mean $^{206}\text{Pb}/^{238}\text{U}$ age of 22.1 ± 0.4 (Fig. 8a).

8.2 Sample Ma09/30L

Zircons are generally euhedral to subhedral. Most zircon grains show short to long prismatic habits (usually $>250 \mu\text{m}$), with length/width ratios up to 5:1. They appear as nearly homogeneous in BSE images. In CL images, zircons are weakly luminescent and show oscillatory to sector (soccer ball) growth zoning (Fig. 8b), typical of igneous zircons (Corfu et al., 2003; Harley et al. 2007). No inherited cores are present. The U content of these growth domains is moderate to high (330–1340 ppm) and the Th/U is generally low (0.02–0.01) (Table 3b; Fig. 9). The probability distribution plot of the cumulative eighty-six spots provides a mean cluster of $^{206}\text{Pb}/^{238}\text{U}$ ages at 294 ± 1 Ma (2σ ; 79% of the data). Thirty-three spots define a near concordant group, intercepting the Concordia curve at 301 ± 2 Ma (2σ , MSWD = 4.4) (Fig. 8b).

8.3 Sample Ma09/28L

Zircons are typically long prismatic in shape and euhedral. A minor aliquot shows a pyramidal shape. They are homogeneous in BSE and the CL images reveal dominant oscillatory to sector growth zoning (Fig. 8c), typical of igneous zircons. Also in this case, no inherited cores are present. The Th/U values range 0.01–0.22 (Table 3c; Fig. 9). The probability distribution plot of the cumulative thirty-two spots provides a mean cluster of $^{206}\text{Pb}/^{238}\text{U}$ ages at 290 ± 1 Ma (2σ ; 81% of the data). Twenty-nine spots define a Concordia age at 291 ± 1 Ma (2σ , MSWD = 1.3) (Fig. 8c).

9. Zircon and garnet REE chemistry

Zircon and garnet crystals from the same samples used for U-Pb zircon geochronology (Table 1), were analyzed both on mineral separates and in thin sections for REE and trace element determination by LA-ICP-MS at the Institut für Mineralogie, Universität Stuttgart (see Supplementary Material#1). The analyzed spots in zircons correspond to the oscillatory or sector growth zoning domains analysed for the U-Pb geochronology. The different garnet growth domains in igneous Grt-2 (core and rims) and Grt-3 (cores) grains were analysed. The results are presented in Fig. 10 and Table 4.

9.1 Zircon

The analysed spots areas correspond to the same sector-zoned or oscillatory growth domains investigated for the U-Pb geochronology. Irrespective of the sample, all the analysed zircon domains (22 spots) are characterized by low LREE (ΣLREE of 0.74–6.9 ppm, with a mean value of 2.4 ppm) and high HREE (ΣHREE ranging 335–1264 ppm, average value: 894 ppm) contents, respectively. They show chondrite-normalised (Sun and McDonough, 1989) depleted LREE (average $\text{La}_N = 0.40$ and $\text{La}_N/\text{Sm}_N < 0.15$) and enriched HREE (average $\text{Yb}_N = 21745$ and Dy_N/Yb_N values of 0.19–0.38) patterns. All analyzed zircons show a systematic negative Eu anomaly (0.05–0.11). The observed REE patterns are fully compatible with those presented in Melchiorre et al. (2017) (Fig. 10a).

The Ti contents of the zircons were also analysed in order to constrain the temperature at which the zircons grew using the Ti-in-zircon thermometer (Watson and Harrison, 2005; Watson et al., 2006). The measured Ti values range between 3.4 and 13.8 ppm, corresponding to a temperature estimate of 654–770 °C (Table 4), provided that rutile was present at the time of zircon crystallization.

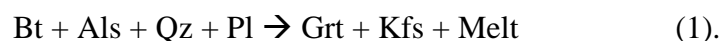
9.2 Garnet

1 The Grt-2 cores (6 spots) are characterized by low LREE (Σ LREE ranging 0.54-8.2 ppm,
2 average value of 2.8 ppm) and elevated HREE (Σ HREE ranging 552-1366 ppm) contents. They are
3 characterised by extremely depleted chondrite-normalised LREE ($La_N/Sm_N < 0.002$) and enriched
4 HREE patterns (Yb_N/Gd_N : 8-38) (Fig. 10b). The Grt-2 rims (9 spots) show comparable low LREE
5 (Σ LREE: 3.0-9.8 ppm) but lower HREE (Σ HREE of 81-219 ppm) contents. They show similar
6 LREE ($La_N/Sm_N < 0.007$) depletion, together with a less evident HREE enrichment (Yb_N/Gd_N :
7 0.42-2.9). Both the Grt-2 cores and rims show a systematic negative Eu/Eu* anomaly (0.17 and
8 0.19, average value of cores and rims, respectively) (Fig. 10b).

9 The Grt-3 garnets (cores, 22 spots) are characterised by moderate LREE (Σ LREE of 1.8-12
10 ppm) and elevated HREE (Σ HREE of 53-181 ppm) contents, with depleted chondrite-normalized
11 LREE ($La_N/Sm_N < 0.1$) and HREE ($Yb_N/Gd_N < 0.9$) patterns and negative Eu/Eu* anomaly (0.08-
12 0.37).

13 10. Discussion

14 The structures in the field and the petrographic evidence presented in this study provide
15 evidence of granulite-facies migmatitisation of the immediate crustal envelope of the Beni Bousera
16 peridotites. The presence of modally abundant garnet invariably characterises the mineral textures
17 of both the melt segregates and melanosomes. In particular, the systematic spatial association of
18 restitic garnet with leucosome segregations (Figs. 3e-f and 4a) is suggestive of incongruent melting
19 and peritectic garnet growth during crustal (Brown, 2013) anatexis in the immediate envelope of the
20 Beni Bousera peridotites. This is compatible with the presence of multiphase mineral inclusions of
21 overall granitic compositions (Qz-Pl-Kfs \pm Als) with lobate shapes and low-angle termination
22 hosted in Grt-1 and Grt-2 grains (Figs. 4a-d), which can be interpreted as melt inclusions (Cesare et
23 al., 2015), similarly to what already recognised for the migmatitic granulites of the Jubrique unit in
24 the envelope of the Ronda peridotites of the Betic Cordillera (Barich et al., 2014; Acosta-Vigil et
25 al., 2016). The evidence of high Ti^{4+} and high Mg# Bt inclusion in Grt-1 outer rims surrounded by
26 Pl-Kfsp-Qz aggregates supports a scenario of in situ dehydration melting of biotite and garnet
27 growth according to the following general reaction (Patiño Douce and Johnston, 1991; Vielzeuf and
28 Montel, 1994):



30 Accordingly, the peak metamorphic assemblage is assumed to be constituted by the anhydrous
31 assemblage made of Grt + Fsp + Qz + Rt \pm Als that was associated with melt. The pre-melting
32 metamorphic evolution in the crustal envelope of the Beni Bousera peridotites is dominantly
33 recorded by the Ca-rich and Mg-poor Grt-1 inner cores that are surrounded by the low (patchy
34
35
36
37
38
39
40
41
42
43
44
45
46
47
48
49
50
51
52
53
54
55
56
57
58
59
60
61
62
63
64
65

1 zoned) Ca- and Mg-rich rim domains. Remnants of the melt(s) produced at the peak stage are
2 preserved in the Grt-1 rim and Grt-2 growth domains as composite mineral/melt inclusions (Qz-
3 Fsp-Als), which document prograde melting, started within the Ky stability field and continued to
4 the Sil stability as recorded by the inner-to-outer rim inclusion assemblages in Grt-1. The Ca-poor
5 and Mg-rich growth domains of Grt-1 rim compositions are thus interpreted as peritectic
6
7 crystallisation products of prograde incongruent melting. Incipient crystallisation of the melt in the
8
9 stability field of sillimanite is documented by Grt-2 cores. (Figs. 11a-b) Progressive crystallisation
10
11 and cooling of the melt resulted in the formation of Ca-rich, Mg-poorer Grt-2 outer rims and Grt-3
12
13 grains during continuous cooling within the Ky stability field (Fig. 11c).
14
15

16 The post-peak retrograde evolution is attested by garnet resorption, Mn increase in garnet,
17
18 and complex symplectic intergrown of Crd-Qz-Pl-Sp (Fig. 4i). The symplectite formation can be
19
20 framed in a scenario of retrograde melt consuming reactions (e.g., White and Powell, 2002),
21
22 controlled by reactions such as (e.g., Cai et al., 2017):
23



25 The formation of texturally late Bt-Sil ± Ms aggregates around garnet can be explained as a
26
27 consequence of the reversal of reaction (1).
28

29 The almost complete preservation of the garnet porphyroblasts in the leucosomes and the
30
31 relatively minor replacement of garnet in the melanosome, also suggests that significant hydrous
32
33 melt extraction occurred after rocks anatexis in the envelope of the Beni Bousera peridotites. In
34
35 fact, in migmatitic granulites where no melt loss occurred, the replacement of the anhydrous
36
37 peritectic assemblage by hydrous phases (such as muscovite and biotite) in consequence of
38
39 retrograde melt-residuum chemical interactions is expected (White and Powell, 2002). In this view,
40
41 the melanosome is interpreted as the residuum produced by the passive accumulation of garnet after
42
43 partial melting and extraction of a significant amount of melt.
44

45 **10.1 Crustal anatexis: Inverse thermobarometry**

46 The *P-T* conditions attained during crustal anatexis are constrained through inverse
47
48 thermobarometry as derived from the inclusion assemblages hosted in the peritectic Grt-1 rim and
49
50 Grt-2 core growth domains, by coupling (i) the *P*-dependent Zr-in-rutile thermometry of Tomkins et
51
52 al. (2007), combined with (ii) the Grt-Pl-Qz-Als (GASP) barometry (Ghent, 1976) as calculated
53
54 with the THERMOCALC software v.3.33 (Powell et al., 1998).
55

56 The composition of the Rt grains found in different textural positions (as inclusion in Grt-1
57
58 (rims) and Grt-2 (cores and rims) and in the Qz-Fsp leucosome portions, respectively) were
59
60 investigated through EMPA. The Rt inclusions in garnet yielded Zr contents ranging 1975-8827
61
62
63
64
65

1 ppm ($n = 29$), which provided temperatures ranging $776-1015 \pm 40$ °C (analytical uncertainty) at
2 0.8 GPa and $826-1076 \pm 40$ °C at 1.7 GPa, respectively. The corresponding lower and upper limits
3 of the interquartile range values (Tomkins et al., 2007; Taylor Jones et al., 2015) are 799-887 and
4 850-921°C with a median value of 844 ± 40 °C and 898 ± 42 °C, respectively (see Supplementary
5 Material#3). The Rt grains in the leucosome portions provided lower Zr contents, ranging 888-2053
6 ppm ($n = 64$), resulting in temperature estimates of $741-833 \pm 40$ °C at 0.8 GPa and $789-886 \pm 40$
7 °C at 1.7 GPa. The corresponding lower and upper limits of the interquartile range values are 774-
8 812 and 823-863 with a median value of 794 ± 19 and 845 ± 19 °C, respectively (see
9 Supplementary Material#3).

10 The GASP equilibria were calculated using the Grt-1 rim (Grt-2 core) composition
11 ($X_{\text{Grs}}=0.07-0.09$), combined with the Pl ($X_{\text{An}}=35-45\%$) inclusion, setting the Qz and Sil (stable at
12 the Grt-1 rim) activity to unit. The GASP barometry provided pressure estimates ranging from ca.
13 1.0 ± 0.1 GPa at 800 °C to 1.3 ± 0.1 GPa at 1000 °C.

14 The results from inverse thermo-barometry show that the minimum peak P-T conditions
15 associated with melt segregation in the granulite envelope of the Beni Bousera peridotites are ca.
16 900-950 °C at 1.1-1.3 GPa, across the transition from the Ky (Grt-1 core) to the Sil (Grt-1 rim)
17 stability (Fig. 12). These estimates are compatible with the results of melting experiments on pelitic
18 compositions, which indicate that biotite is fully consumed by reaction (1) at temperature in the
19 range 850–870 °C and garnet is the Fe-Mg peritectic phase produced at high-pressure (≥ 1.0 GPa)
20 conditions (see reviews in Weinberg and Hasalová, 2015; Gao et al., 2016). The post-peak,
21 retrograde assemblage made of Crd-Qz-Pl-Sp-Bt-Sil \pm Ms indicates decompressional cooling and
22 constrains the final retrograde re-equilibration within the Crd stability field, below to ca. 0.5 GPa
23 (e.g. White and Powell, 2011) (Fig. 12).

24 **10.2 The path to crustal anatexis: forward modelling**

25 To refine the thermobaric evolution leading to crustal anatexis and magma production in the
26 granulite envelope of the Beni Bousera peridotites, we adopted a single-step melt re-integration
27 approach (e.g. Bartoli et al., 2017) by (i) estimating the relative fraction (vol%) of melt and residue
28 at the outcrop scale (see Supplementary Material#4); and (ii) re-integrating the measured bulk
29 average composition of leucosomes to that of a representative melanosome residue (Table 2). The
30 resulting bulk composition as derived by using a 45 vol% of melt composition is assumed as the
31 pre-melt bulk composition that is used for forward modelling thermobarometry using the software
32 program PERPLEX (Connolly, 2005). The model system MnNCaKFMASHTH (MnO–Na₂O–CaO–
33 K₂O–FeO–MgO–Al₂O₃–SiO₂–TiO₂–H₂O) was chosen. The Fe₂O₃ was not considered in the model
34
35
36
37
38
39
40
41
42
43
44
45
46
47
48
49
50
51
52
53
54
55
56
57
58
59
60
61
62
63
64
65

1 system, due to the presence of graphite in the mineral assemblage that is indicative of a reducing
2 environment. The analysed loss of ignition (LOI) was assumed as H₂O. The following solid-
3 solution models were used (details in the file solution.dat enclosed in the Perple_X package;
4 database: hp04ver.dat, an updated version of the Holland and Powell (1998) thermodynamic
5 dataset; Perple_X_6.8.7 version, downloaded July 27 2019): Grt(WPH) for garnet, Mica (CGH) for
6 white mica, Bio(TCC) for biotite, Omph(GHP) for clinopyroxene, Pl (h) for plagioclase, San for K-
7 feldspar and melt (HP) for the melt phase. Additional end-member phases considered in the
8 calculations comprise quartz, rutile, ilmenite, kyanite and sillimanite. The pseudosections were
9 constructed between 0.8 and 1.7 GPa and from 500 to 1100 °C.
10
11
12
13
14
15

16 These calculations are to be considered as tentative, for the uncertainty on (i) the starting
17 bulk composition and proportion of melt loss, and (ii) the water content during progress of the
18 metamorphism and crustal melting. Moreover, since the modal content of retrogressive biotite in the
19 melt products is very limited (ca 1% vol.), escape of water-rich melt has likely occurred, with a
20 consequent bias in the melt re-integration procedure (e.g. Bartoli et al., 2017).
21
22
23
24

25 The output of the pseudosection modelling is shown in Fig. 13. The isopleth plots of the
26 core-to-rim compositions as measured from garnet grains in the melanosome (Grt-1), combined
27 with the hosted inclusion assemblages are used as a proxy of the thermobaric evolution during
28 granulitisation and anatexis. Using the relevant Ca zoning in conjunction with the Mg content, the
29 Grt-1 core compositions ($X_{\text{Grs}} = 0.15-0.16$, $X_{\text{Py}} = 0.15-0.16$) constrains the pre-melting prograde
30 metamorphic evolution at ca. 550-600 °C and 1.3 GPa. These thermobaric estimates are well below
31 the temperature conditions compatible with muscovite- and/or biotite-dehydration melting (800-850
32 °C in the relevant pressure range) and compatible with the biotite stability field, which limits peak
33 pressure to 1.5-1.6 GPa (Fig. 13). Taking into account the abrupt rimward X_{Grs} decrease and X_{Py}
34 increase (to 0.05-0.06 and to 0.30-0.31, respectively), combined with the evidence of transition from
35 Ky to Sil inclusion from outer core to rim in Grt-1 (Figs. 4g), a nearly isothermal heating path is
36 proposed. Peak conditions are therefore attained within the Sil stability field for temperatures of
37 950-1000 °C (Fig. 13). The transition to Ca-richer (up to 0.10) outer rim domains in some Grt-2
38 garnets, coupled with the leucosome mineralogy documenting Ky as the stable Al₂SiO₅ polymorph
39 in melt segregates (Qz-Fsp-Grt-Ky + Rt + Gr), provide evidence of nearly isothermal cooling within
40 the Ky stability field during progressive crystallisation of the melt as monitored by the GASP
41 reaction $\text{An} = \text{Grs} + \text{Ky} + \text{Qz}$. The absence of retrograde Bt in most of the leucosomes constrains
42 the minimum P-T conditions of final melt crystallisation at ca. 1.1-1.2 GPa and 850-900 °C. The
43 presence of lately formed Sil after Ky in the leucosomes, coupled with the Ca-poor rim composition
44
45
46
47
48
49
50
51
52
53
54
55
56
57
58
59
60
61
62
63
64
65

1 of Grt-3 at a constant or even slightly increasing Mg content (Fig. 5d) impose a nearly isothermal
2 exhumation path at a temperature of ca. 800 °C (Fig. 13).

3 To sum up, integration of inverse and forward modelling thermobarometry (Figs. 12-13)
4 suggests that melt production in the envelope of the Beni Bousera peridotites occurred at HP-(U)HT
5 conditions with peak temperatures > 950° C and crustal depths of ca. 50 km (assuming a rock
6 density of 2800 kg/m³ at 1.3 GPa), followed by a nearly isobaric cooling at HP conditions (ca. 1.1-
7 1.2 GPa and 800-850 °C). Despite the different peak temperature conditions, this scenario confirms
8 what proposed for the granulites from Jubrique in the Betics, where the presence of melt at peak HP
9 conditions has been also documented (Barich et al., 2014), but contrasts with the scenario of
10 decompressional melting as earlier proposed both for the Ronda (Argles et al., 1999; Platt et al.
11 (2003a) and the Beni Bousera (Alvarez Valero et al. 2014) envelopes.

12 It is worth noting that the peak temperatures reconstructed in this study as derived from both
13 inverse (Zr-in-Rt thermometry) and forward thermobarometry (likely > 900-950 °C) are not
14 compatible with the Ti-in-zircon thermometry, which provided lower temperatures (ca. 654–770
15 °C ; Table 4). This is in accordance with the previous studies of HT and UHT migmatites, where
16 the Zr-in-Rt thermometry has been documented to be more robust than the Ti-in-zircon in retaining
17 the peak metamorphic conditions (Bin Fu et al., 2008; Clark et al., 2009; Ewing et al., 2013). The
18 convergence of the two thermometers requires the buffering assemblage of zircon-rutile-quartz
19 (Watson et al., 2006; Taylor Jones et al., 2015). In our samples, (i) the rutile grains found in the
20 inclusion assemblage of the peritectic and igneous garnets (Grt-1 and Grt-2) only occur in
21 equilibrium with quartz and not with zircon; (ii) zircon is instead dominantly observed in the matrix
22 assemblages representing the final melt crystallization. However, as discussed below, there are
23 good arguments suggesting that zircon was present at peak temperature as represented by the Grt-1
24 outer rim/Gtr-2 core domains crystallization.

25 ***10.3 Zircon-garnet-melt equilibria and the age of crustal anatexis***

26 In high-grade environments as the one documented in this study, garnet and zircon are the
27 primary competitors in controlling the MREE and HREE (from Sm to Lu) budget. In particular, the
28 REE partitioning between zircon and garnet has become an essential tool to decipher the history of
29 crustal anatexis and to link the U-Pb geochronology to the metamorphic evolution (e.g., Hokada
30 and Harley, 2004; Clark et al., 2009; Herman and Rubatto, 2003; Rocha et al., 2017; Rubatto, 2002;
31 Rubatto and Hermann, 2007; Taylor et al., 2015, 2017; Villaros et al., 2009; Whitehouse and Platt,
32 2003).

1 The REE contents of the different garnet growth domains during melt crystallisation (Grt-2
2 and Grt-3) can be thus compared to those of the zircon and the melts products in order to better
3 elucidate a possible timing of zircon growth with respect to the leucosome production,
4 crystallisation and cooling.
5
6

7 In order to verify equilibria between zircon and the two different suprasolidus (igneous)
8 garnet populations, zircon/garnet ($D_{\text{REE}}^{\text{Zrn/Grt}}$) REEs distribution coefficients were calculated from
9 the analyzed material. Due to the homogeneous REE abundances in zircons (Fig. 10a), an average
10 zircon composition was compared to those of the different garnet generations. Results are reported
11 in Table 4 and shown in Fig. 14, where $D_{\text{REE}}^{\text{Zrn/Grt}}$ are compared with those experimentally
12 determined for silicate melts at 900–1000 °C and 0.7 GPa (Taylor et al., 2015) and 800-1000 °C
13 and 2.0 GPa (Rubatto and Herman, 2007), conditions that are relevant for this study.
14
15
16
17
18
19

20 The elevated negative Eu anomalies in both zircon and garnet (Figs. 10) is mirrored by a
21 strong positive Eu anomaly in the leucosomes (Fig. 7), which together indicate that zircons and
22 garnet crystallised in equilibrium with plagioclase-bearing melts (e.g., Rubatto, 2002; Hoskin and
23 Schaltegger, 2003). Significantly, the melanosomes show neutral to negative Eu anomaly,
24 suggesting a fractionation process involving extraction of the Eu-rich phases from melanosome to
25 leucosome (Fig. 7). This is in line with the major element composition of the in situ melt segregates
26 (leucosomes), which are slightly K-depleted and enriched in Ca/(Ca + Na) with respect to
27 experimental melts (Figs. 6c-d), suggesting disequilibrium melting of plagioclase in the source and
28 melt loss from the sites of melt accumulation (Sanchez-Navas, 2014; Taylor et al., 2014).
29
30
31
32
33
34
35

36 Significantly, the $D_{\text{REE}}^{\text{Zrn/Grt}}$ for the Grt-2 cores show nearly flat patterns for the HREE (from
37 Dy to Lu), with the $D_{\text{REE}}^{\text{Zrn/Grt}}$ values varying close to the unity (Fig. 14; Table 4). These patterns
38 are overlapping with the experimental data of Taylor et al. (2015) and Rubatto and Herman (2007)
39 at HT (1000 °C) (Fig. 14). In contrast, Grt-2 rims and Grt-3 show a significant increase of the
40 HREE partitioning to zircon (Fig. 14; Table 4), essentially resulting from the HREE poor Grt-2 rim
41 and Grt-3 compositions (Fig. 10b). This suggests an impoverishment of HREE in the remaining
42 melt after major zircon crystallization simultaneously or shortly after Grt-2 core growth. It is
43 therefore suggested that the analysed zircons crystallised at nearly equilibrium conditions with the
44 Grt-2 core throughout the cooling history of the segregated melts. We can thus propose an origin
45 from the same melt/silicate system for both zircon and garnet sampled in the melt segregates from
46 the inner granulite envelope of the Beni Bousera peridotites, in a scenario of prograde incongruent
47 melting at high-pressure, melt production, extraction, crystallisation and cooling.
48
49
50
51
52
53
54
55
56
57

58 The internal structures (Fig. 8), together with the steep HREE patterns (Fig. 10a) of the
59 zircons recovered from the leucosomes are compatible with this reconstruction, being indicative of
60
61
62
63
64
65

1 crystallisation from a melt (e.g. Harley et al., 2007). The U-Pb geochronology on euhedral and
2 oscillatory to sector zoned growth domains constrains the partial melting event to Hercynian times
3 (300-290 Ma) (Fig. 8). The low Th/U values obtained from the Hercynian igneous domains of the
4 studied samples (Fig. 9) is compatible with the presence of monazite (Th-rich phase; e.g. Rubatto et
5 al., 2013) during zircon growth and progress of rock anatexis in the crustal envelope of the Beni
6 Bousera peridotites (Montel et al., 2000).
7
8
9

10 The few Cenozoic (ca. 20 Ma) U-Pb zircon ages derived from the low Th/U (typically
11 <0.01), structureless rims in zircons from the sample K3L (Fig. 8a) are instead compatible with
12 metamorphic overgrowth. We refer this overgrowth stage to the low-pressure Alpine
13 metamorphic/metasomatic event already documented in the inner envelope of the Beni Bousera
14 peridotites, associated with a renewed episode of crustal anatexis and acidic magmatism, early
15 Miocene in age (Rossetti et al., 2010; 2013). Similarly, an Alpine-aged recrystallisation and Pb loss
16 event in the Hercynian zircons has been proposed for the polymetamorphic high-grade basement
17 units of the Alpujarride complex in the Betics (Acosta Vigil et al., 2014; Sanchez-Navas et al.,
18 2014; 2017).
19
20
21
22
23
24
25
26
27

28 **10.4 A Hercynian granulite-granite suite: implications at regional scale**

29
30
31
32
33 When integrated at the regional scale, the field, textural and geochronological data set
34 discussed above may contribute to elucidate the *P-T-t* conditions and the petrological/geodynamic
35 issues involved in the granulite-granite connection in the crustal section of the Alboran Domain.
36
37

38 The first significant result of our study is Hercynian *HP/(U)HT* granulite-facies migmatitic
39 event is preserved in the core of the Alboran Domain of the Rif chain. Significantly, the
40 crystallisation ages obtained from the melt segregates investigated in this study are, within error, the
41 same as those obtained from the peraluminous *HP* (Grt-Ky-bearing) Hercynian granitoids
42 (leptinites) that intrude the metamorphic core of the Alboran Domain of the Rif chain (Rossetti et
43 al., 2010) (Fig. 9a). This evidence supports a scenario of *HP/(U)HT* Hercynian anatexis in the Beni
44 Bousera envelope, synchronous with the segregation, crystallisation and emplacement of a suite of
45 leucogranitic bodies in the supracrustal metamorphic sequence of the Filali unit. We therefore
46 propose that a Hercynian granulite–granite suite is preserved in the Lower Sebtides nappe stack of
47 the Moroccan Rif. In particular, the documented Hercynian granulite–granite suite can be
48 coherently explained by a single metamorphic loop involving isobaric heating and cooling,
49 followed by decompression, without the need to introduce a second (Alpine) major anatectic event
50 in the high-grade basement of the Alboran Domain. This reconstruction is coherent with the isotopic
51
52
53
54
55
56
57
58
59
60
61
62
63
64
65

1 data (Sr and Nd) available from both the Hercynian granitoids and the hosting granulite envelope of
2 the Beni Bousera peridotites (Rossetti et al., 2013). The Hercynian granitoids show a relatively high
3 $^{143}\text{Nd}/^{144}\text{Nd}$ values comparable with those of the coeval Iberian-French crustal magmas formed by
4 the partial melting of metasedimentary protoliths that experienced a significant juvenile addition
5 during the Cadomian events. Their origin by partial melting of the associated high-grade
6 metamorphic rocks of the Beni Bousera units is thus isotopically consistent. The Alpine (early
7 Miocene) crustal magmatism, being characterised by low $^{143}\text{Nd}/^{144}\text{Nd}$ values, is instead isotopically
8 distinct from both the Hercynian granitoids and the granulite host rocks (Rossetti et al., 2013), thus
9 attesting for a different metasedimentary source that is possibly identifiable in the metapelitic
10 sequences drilled in the Alboran Basin (Comas et al., 1992).

11
12
13
14
15
16
17
18 Similar Hercynian ages are also derived from partial melting products in migmatitic units
19 both at the footwall (Acosta Vigil et al., 2014) and hanging wall (Ruiz Cruz and Sains de Galdeano,
20 2014; Zeck and Williams, 2001; Zeck and Whitehouse, 2002; Sanchez Navas et al., 2014; 2017;
21 Gómez-Pugnaire, 2019) of the Ronda peridotites. Significant on this regard is the fact that the
22 crustal melting from the granulite envelope of the Beni Bousera peridotites as reconstructed in this
23 study is fully compatible, in terms of both textures and peak thermo-baric environments, with the
24 HP anatectic history of the Jubrique unit at the hanging-wall of the Ronda peridotites (Barich et al.,
25 2014; Acosta Vigil et al., 2016). This evidence further confirms that partial melting in the envelope
26 of the Alboran peridotites has occurred before the early Miocene Alpine decompressional evolution
27 (e.g. Argles et al., 1999; Platt et al., 2003a). Moreover, the pre-Hercynian U-Pb zircon ages derived
28 in this study from the high Th/U growth zoning domains (Fig. 9b-c) are also in agreement with
29 those recovered from the high-grade migmatitic units of the Alpujarride-Septide realm (Acosta-
30 Vigil et al., 2014; Melchiorre et al., 2017; Platt and Whitehouse, 1999; Rossetti et al., 2010;
31 Sanchez-Navas et al., 2014; Zeck and Whitehouse, 2002; Zeck and Williams, 2001), suggesting a
32 common crustal inheritance from wall-rock incorporation during the Hercynian anatectic event.
33 This reconstruction supports the presence of a Hercynian migmatized crustal domain in the
34 metamorphic core of the Alboran Domain, structurally associated with the intracrustal emplacement
35 of the Ronda and Beni Bousera peridotite bodies.

36
37
38
39
40
41
42
43
44
45
46
47
48
49
50
51 The *P-T* evolution reconstructed for the migmatitic granulite envelope of the Beni Bousera
52 peridotite documents a significant isobaric temperature increase (ca. 400 °C, from ca. 600 to ca.
53 1000 °C) and anatectic melt production at deep crustal conditions (ca. 1.3 GPa), during the Permo-
54 Carboniferous transition from a subduction- (ca. 12 °C/km) to a Barrovian-type metamorphic
55 gradient. This is followed by nearly isobaric cooling (ca. 150 °C) and a major isothermal
56 decompression path (ca. 0.5 GPa at ca. 800 °C) during the final crystallisation history of the melt
57
58
59
60
61
62
63
64
65

1 segregates (Fig. 13). This thermo-baric evolution implies a transient thermal input, followed by
2 cooling and exhumation, compatible with a geodynamic scenario dominated by the convective
3 removal of the deep roots of a mature orogen in a collisional setting (e.g., Dewey, 1988; Platt and
4 England, 1994). The Beni Bousera units can be thus tentatively interpreted as fossil zone of crust-
5 mantle coupling, developed after crustal thickening and intracrustal emplacement of hot peridotites
6 bodies at convergent plate margins. Significantly, the late Carboniferous-early Permian ages
7 documented in this study well fit with the late Carboniferous-early Permian tectono-magmatic
8 events framed within the orogenic collapse stage of the Hercynian chain (e.g. Burg et al., 1994;
9 Matte et al., 2001; Franke, 2015; Petri et al., 2017 and references therein). We can thus propose
10 that the transition from the isobaric prograde/retrograde metamorphism to the isothermal
11 exhumation in the Beni Bousera records the thermo-mechanical evolution of the deep roots of the
12 Hercynian orogeny during the shift from crustal thickening to crustal thinning and collapse of the
13 thermally-weakened orogen (Molnar and Lyon Caen, 1998; Platt and England, 1994;
14 Vanderhaeghe, 2012).

15
16
17
18
19
20
21
22
23
24
25
26
27
28
29
30
31
32
33
34
35
36
37
38
39
40
41
42
43
44
45
46
47
48
49
50
51
52
53
54
55
56
57
58
59
60
61
62
63
64
65
Despite still debated are the peak pressure conditions attained by the high-grade crustal
basement of the Alboran Domain (see Massonne et al., 2014), our results confirm previous
estimates pointing to *HP* conditions for the metamorphic climax (Haissein et al., 2004;
Bouybaouene et al., 1998) that we interpret as the evidence of a pre-Alpine (likely Hercynian in
age) crustal thickening event preserved in the Lower Sebtides units of the Rif (e.g., Michard et al.,
1997). Still unclear, however, is the linkage (if any) with the Hercynian UHP conditions proposed
by Ruiz Cruz and Sains de Galdeano (2012; 2013) for the metamorphic evolution of the Lower
Sebtides (Monte Hacho gneiss) exposed in the Ceuta region (Fig. 1).

The post-peak near-isothermal decompression led to the growth of a sequence of
symplectitic reaction textures that record exhumation to higher crustal levels of the Beni Bousera
units (within the cordierite stability field; below ca. 0.5 GPa; see also Alvarez Valero et al., 2014).
This final exhumation stage is geochronologically constrained during the Early Miocene (Rossetti et
al., 2010; Melchiorre et al., 2017; this study), which corresponds to the main stage of the Alboran
basin back-arc extension (Comas et al., 1999). Significantly, Early Miocene andalusite-bearing
dyke swarms are intruded in the Beni-Bousera units, indicating the exhumation of the high-grade
basement was almost already completed at that time (Rossetti et al., 2010; 2013).

Noteworthy are the implications of the above reconstruction for what concerns the impact of
the Late Paleozoic template into the Alpine orogeny at a regional scale. First of all, the definitive
demonstration of a polymetamorphic evolution of the high-grade basement of the Alboran Domain
of the Western Mediterranean region is given (see also Acosta Vigil et al., 2014; Sanchez-Navas et

al., 2017), providing evidence that an important Hercynian tectono-metamorphic inheritance contributed to the structuration of the metamorphic core of the Betic-Rif orogen. In such a scenario, taking into account and re-interpreting the existing *P-T-t* data and tectonic/geodynamic reconstructions for the crust-mantle tectonic coupling in the Betic-Rif realm (e.g., Melchiorre et al., 2017; Hidas et al., 2013; Gueydan et al., 2015; 2019; Mazzoli and Martin Algarra, 2011; Hidas et al., 2013; Frasca et al., 2016; 2017; Platt et al., 2003a, b; Platt and Vissers, 1989; Garrido et al., 2011), it is possible to propose a tentative re-appraisal of the tectono-metamorphic evolution of the high-grade basement the Betic-Rif realm from Late Paleozoic onward, including insights on the intracrustal emplacement of the Ronda and Beni-Bousera mantle bodies. In particular, two main stages of crust-mantle coupling can be recognised in the region, that can be framed in Permo-Carboniferous and Neogene times, at deep and shallow crustal conditions, respectively. The early stage occurred in the deep crust at the waning stage of the Hercynian orogeny, associated with diffuse crustal anatexis and associated granite magmatism (Fig. 15a-b). The Hercynian crust-mantle tectonic boundary then resided in the middle to shallow crustal conditions during the subsequent Early Mesozoic rifting phase associated with the formation of the oceanic Tethyan realm (Melchiorre et al., 2017; Gimeno Vives et al., 2019). During the Tertiary (Eocene), Alpine subduction and associated *HP/LT* metamorphism affected the Permo-Triassic supracrustal crustal rock units (upper Sebtides and Alpujarride complexes; Azanon et al. 1997, Bouybaouene et al., 1998; Michard et al., 2006), whereas the Hercynian basement largely escaped subduction and burial, being likely at the footwall of the main Alpine deformation front (Fig. 15c). Starting from the Neogene onward, the westward retreat of the Tethyan subduction caused back-arc extension, asthenosphere upwelling, lithosphere delamination and diffuse magmatism in the inner sectors of the chain, concurrently with the westward migration of the compressional fronts, thrusting the early structured and exhumed belt onto the external flysch domains (Royden et al., 1993; Frasca et al., 2016; 2017; Faccenna et al., 2004; Michard et al., 2006; Rossetti et al., 2013; Auguier et al., 2005; Platt et al., 2013; Van Hinsbergen et al., 2014) (Fig. 15d). This corresponds to the final stage of intracrustal emplacement of the Ronda peridotites, commonly framed in a scenario of hot thrusting/transpression at shallow crustal conditions during switching from crustal extension to shortening in the upper plate domain of the Tethyan subduction (Pregicout et al., 2013; Garrido et al., 2011; Hidas et al., 2011; Frasca et al., 2017; Gueydan et al., 2019; Mazzoli and Martin Algarra, 2011). The hypothesis of the two-stage (pre-Alpine and Alpine) crust-mantle coupling at different crustal depths in the Betic-Rif realm should be further validated through focused structural, petrological and geochronological investigations of the metamorphic envelopes of the Ronda and Beni Bousera peridotites.

1 On a wider scale, it is worth noting that the Hercynian (Permo-Carboniferous) signature
2 detected from the granulite facies migmatitic envelopes of the Alboran peridotites is a common
3 character of the pre-Alpine basement sections tectonically interleaved within the orogenic structure
4 of the Alpine chain. In particular, similar temporal relationships between the Permo-Carboniferous
5 granulite metamorphism and magmatism and are derived from the deep-crust/mantle transitions as
6 exposed in the Ulten (Del Moro et al., 1999; Tumiati et al., 2003; Langone et al., 2011) and Ivrea-
7 Verbano (e.g., Quick et al., 1995; Klötzli et al., 2014; Kunz et al., 2019; Guergouuz et al., 2018)
8 zones, Val Malenco (Herman et al., 1997; Herman and Rubatto, 2003), Calabria (Graessner and
9 Schenk, 2001) and the Northern Pyrenean Zone (Choukroune, 1992). This evidence is indicative of
10 the complex growth of the continental crust across the Alpine realm through the multiple
11 collisional-rifting events suffered by these basements since they were detached from northern
12 Gondwana paleo-margin (Early Palaeozoic), assembled along the Hercynian belt, then
13 fragmented/dispersed again during the Mesozoic and finally assembled and exhumed during the
14 Alpine orogenic cycle (e.g. Stampfli and Borel, 2002). The serendipitous spatial association of
15 Hercynian and Alpine migmatitic complexes and crustal-derived granites across the Alpine orogen is
16 indicative of this story and stresses the importance of detailed petrographic, geochronological,
17 geochemical and isotopic studies of the exposed high-grade basement section for the formulation of
18 a consistent geodynamic-petrologic interpretation.

11. Conclusion

The main results that can be extracted from this study are as follow:

- (i) A major Hercynian *HP/(U)HT* granulite-facies anatexis event associated with the intracrustal emplacement of the Beni Bousera peridotites is documented;
- (ii) A Hercynian granulite–granite suite is preserved in the Lower Sebtides nappe stack of the Alboran Domain of the Moroccan Rif;
- (iii) A fossil Hercynian crust-mantle coupling zone is preserved at the core of the Alboran Domain, recording transition from orogenic construction to collapse;
- (iv) The polymetamorphic nature of the high-grade basement of the Alboran Domain is confirmed, imposing the need to investigate further the *P-T-t*-deformation history associated with the crust-mantle coupling in the region;
- (v) The crustal envelopes of the Alboran peridotites can be correlated to the pre-Alpine Permian-Carboniferous lower crustal exposures exposed within the Alpine orogen of the Mediterranean region.

1 Results of this study impose a re-assessment of the metamorphic gradients, exhumation rates
2 and thermo-baric environments associated with the Alpine construction of the Betic-Rif orogeny.
3 In particular, when integrated with the available data from the Alboran Domain of the Betic chain
4 our reconstruction fosters to re-consider the geodynamic significance of the Alpine high-grade
5 tectono-metamorphic event in the Betic-Rif realm, including the models of the intracrustal
6 emplacement of the Beni-Bousera and Ronda peridotites.
7
8
9

10 11 12 13 **Acknowledgements**

14 C. Faccenna, F. Tecce, D. Cozzupoli participated to the field work and are thanked for
15 fruitful discussion and advice. N. Zaghoul is acknowledged for discussion and advice. H-J
16 Massonne is thanked for discussion and for allowing access to the analytical facilities at the Institut
17 für Mineralogie and Cristalchemie, Universität Stuttgart. M. Schmeltz is thanked for sample
18 preparation. The Grant to Department of Science, Roma Tre University (MIUR-Italy Dipartimenti
19 di Eccellenza, ARTICOLO 958 1, COMMI 314-337 LEGGE 232/2016) is gratefully
20 acknowledged. This is FIERCE contribution No. XX. The constructive revision of L. Jolivet and A.
21 Acosta Vigil contributed to improve significantly the manuscript.
22
23
24
25
26
27
28
29
30

31
32
33 **Supplementary Material#1:** Analytical methods and protocols.
34
35

36
37 **Supplementary Material#2:** Representative EMPA and structural formulae of garnet, feldspar and
38 biotite.
39
40

41
42 **Supplementary Material#3:** Temperature estimates as derived from the Zr-in-rutile thermometer of
43 Tomkins et al. (2007). The results are presented in the form of box-plots showing the interquartile
44 range of the data for each textural setting (calculated @ 1.7 and 0.8 GPa): (a), (b), Rutile inclusion
45 in garnet; (c), (d) Rutile in the matrix. Data statistics obtained through Kirkman, T.W. (1996)
46 Statistics to Use; <http://www.physics.csbsju.edu/stats/> (16 Sept 2019).
47
48
49
50

51
52
53 **Supplementary Material#4:** Estimate of melt (leucosome)/restite (melanosome) proportions (vol%)
54 from outcrop observation
55
56
57

58 59 **References**

60
61
62
63
64
65

- 1 Acosta-Vigil, A., Rubatto, D., Bartoli, O., Cesare, B., Meli, S., Pedrera, A. Azor, A., Tajčmanová,
2 L., 2014. Age of anatexis in the crustal footwall of the Ronda peridotites, S Spain. *Lithos*
3 210–211, 147–167, doi:10.1016/j.lithos.2014.08.018.
4
- 5 Acosta-Vigil, A., Barich, A., Bartoli, O. Garrido, C. J., Cesare, B., Remusat, L., Poli, S., Raepsaet,
6 C., 2016. The composition of nanogranitoids in migmatites overlying the Ronda peridotites
7 (Betic Cordillera, S Spain): the anatectic history of a polymetamorphic basement. *Contrib*
8 *Mineral Petrol* 171, doi: 10.1007/s00410-016-1230-3.
9
- 10 Álvarez-Valero, A. M., Jagoutz, O., Stanley, J., Manthei, C., El Maz, A., Moukadiri, A., Piasecki,
11 A., 2014. Crustal attenuation as a tracer for the emplacement of the Beni Bousera ultramafic
12 massif (Bético-Rifean belt). *Geol. Soc. Am Bulletin* 126, 1614–1624, doi: 10.1130/B31040.1.
13
- 14 Andriessen, P.A.M., Zeck, H.P., 1996. Fission-track constraints on timing of Alpine Nappe
15 emplacement and rates of cooling and exhumation, Torrox area, Betic Cordilleras, S. Spain.
16 *Chem Geol* 131, 199–206.
17
- 18 Andrieux, J., Fontbote, J. M. Mattauer, M., 1971. Sur un modèle explicatif de l'arc de Gibraltar.
19 *Earth Planet. Sci. Lett.* 12, 191–198.
20
- 21 Argles, T. W., Platt, J. P., Waters, D. J., 1999. Attenuation and excision of a crustal section during
22 extensional exhumation: The Carratraca massif, Betic Cordillera, southern Spain. *J. Geol. Soc.*
23 *London* 156, 149–162, doi:10.1144/gsjgs.156.1.0149.
24
- 25 Augier, R., Agard, P., Moni[, P., Jolivet, L., Robin, C., and Booth-Rea, G., 2005. Exhumation,
26 doming and slab retreat in the Betic Cordillera (SE Spain): In situ $^{40}\text{Ar}/^{39}\text{Ar}$ ages and P–T–d–t
27 paths for the Nevado-Filabride complex. *Journal of Metamorphic Geology* 23, 357–381, doi:
28 10.1111/j.1525-1314.2005.00581.x.
29
- 30 Azañón, J.M., Crespo-Blanc, A., Garcíá-Dueñas, V., 1997. Continental collision, crustal thinning
31 and nappe-forming during the pre-Miocene evolution of the Alpujarride Complex (Alboran
32 Domain, Betics). *Journal of Structural Geology* 19, 1055–1071.
33
- 34 Azdimousa, A., Bourgois, J., Poupeau, G., Vazquez, M., Asebriy, L., Labrin, E., 2014. Fission track
35 thermochronology of the Beni Bousera peridotite massif (Internal Rif, Morocco) and the
36 exhumation of ultramafic rocks in the Gibraltar Arc. *Arabian Journal of Geosciences* 7, 1993–
37 2005.
38
- 39 Balanyá, J.C., Garcíá-Dueñas, V., Azañón, J.M., Sánchez-Gómez, M., 1997. Alternating
40 contractional and extensional events in the Alpujarride nappes of the Alboran Domain (Betics,
41 Gibraltar Arc). *Tectonics* 16, 226–238.
42
43
44
45
46
47
48
49
50
51
52
53
54
55
56
57
58
59
60
61
62
63
64
65

- 1 Barich, A., Acosta-Vigil, A., Garrido, C. J., Cesare, B., Tajčmanová, L., Bartoli,
2 2014. Microstructures and petrology of melt inclusions in the anatectic sequence of Jubrique
3 (Betic Cordillera, S Spain): implications for crustal anatexis. *Lithos* 206–207, 303–320.
4
5 Bartoli, O., 2017. Phase equilibria modelling of residual migmatites and granulites: An evaluation
6 of the melt-reintegration approach. *J Metamorph Geol.* 2017 35, 919–942, doi:
7 10.1111/jmg.12261
8
9 Booth-Rea, G., Ranero, C.R., Martínez-Martínez, J.M., Grevemeyer, I., 2007. Crustal types and
10 Tertiary tectonic evolution of the Alboran sea, westernMediterranean. *Geochem. Geophys.*
11 *Geosyst.* 8, doi: 10.1029/2007GC001639.
12
13 Bouybaouene, M.L., Michard, A., Goffé, B., 1998. High-pressure granulites on top of the Beni
14 Bousera peridotites, Rif Belt, Morocco: a record of an ancient thickened crust in the Alboran
15 domain. *Bull. Soc. Géol. Fr.* 169, 153–162.
16
17 Brown, M., 2013. Granite: From genesis to emplacement. *Geological Society of America Bulletin*
18 125, 1079-1113
19
20 Brown, M., 1994. The generation, segregation, ascent and emplacement of granite magma: the
21 migmatite-to-crustally-derived granite connection in thickened orogens. *Earth Science*
22 *Reviews* 36, 83-130.
23
24 Burg J-P, Van Den Drissche J, Brun J-P, 1994. Syn- to post-thickening extension in the Variscan
25 Belt of Western Europe: modes and structural consequences. *Geologie de la France* 3,33-51.
26
27 Cai, J., Liu, F., Liu, P., Wang, F., Liu, C., Shi, J., 2017. Anatectic record and P–T path evolution of
28 metapelites from the Wulashan Complex, Khondalite Belt, North China Craton. *Precambrian*
29 *Research* 303, 10–29.
30
31 Casciello, E., Fernández, M., Vergés, J., Montserrat, T., 2015. The Alboran Domain in the Western
32 Mediterranean evolution: the birth of a concept. *Bulletin de la Societe Geologique de France*
33 186, doi: 10.2113/gssgfbull.186.4-5.371
34
35 Cesare, B., Acosta-Vigil, A., Bartoli, O., Ferrero, S., 2015. What can we learn from melt
36 inclusions in migmatites and granulites?. *Lithos* 239, 186–216.
37
38 Choukroune, P., 1992. tectonic evolution of the Pyrenees. *Annual Review of Earth and Planetary*
39 *Sciences* 20, 143-158.
40
41 Clark, C., Collins, A. S., Santosh, M., Taylor, R., Wade, B. P., 2009. The P-T-t architecture of a
42 Gondwanan suture: REE, U–Pb and Ti-in-zircon thermometric constraints from the Palghat
43 Cauvery shear system, South India. *Precambrian Research* 174, 129–144.
44
45
46
47
48
49
50
51
52
53
54
55
56
57
58
59
60
61
62
63
64
65

- 1 Comas, M. C., Platt, J. P., Soto, J. I., Watts. A. B., 1999. The origin and tectonic history of the
2 Alboran Basin: insights from Leg 161 results. *Proc. Ocean Drill. Proj. Sci. Results* 161, 555–
3 79.
4
- 5 Connolly J.A.D., 2005. Computation of phase equilibria by linear programming: A tool for
6 geodynamic modeling and its application to subduction zone decarbonation. *Earth and*
7 *Planetary Science Letters* 236, 524-541.
8
- 9 Corfu, F., Hanchar, J.M., Hoskin, P.W.O., Kinny, P., 2003. Atlas of Zircon Textures. *Reviews in*
10 *Mineralogy and Geochemistry* 53, 469-500.
11
- 12 Del Moro, A., Martin, S., Prosser, G., 1999. Migmatites of the Ulten zone (NE Italy), a record of
13 melt transfer in deep crust. *Journal of Petrology* 40, 1803–1826.
14
- 15 Dewey, J. F., 1988. Extensional collapse of orogens, *Tectonics* 7 , 1123–1139, doi:
16 10.1029/TC007i006p01123.
17
- 18 Dewey, J. F., Helman M. L., Turco E., Hutton D. H. W., Knott S. D., 1989. Kinematics of the
19 western Mediterranean, In: *Alpine Tectonics*, edited by M. P. Coward, D. Dietrich, and R. G.
20 Park, *Geol. Soc. Spec. Publ.*, 45, 421–443.
21
- 22 El Maz, A., Guiraud, M., 2001. Paragenese à faible variance dans les métapelites de la sèrie de
23 Filali (Rif interne marocain): description, interpretation et conséquences géodynamiques.
24 *Bulletin de la Société Géologique de France* 172, 469–485.
25
- 26 Esteban, J. J., Sánchez-Rodríguez, L., Seward, D., Cuevas, J., Tubía, J.M., 2004. Late thermal
27 history of the Ronda area, southern Spain. *Tectonophysics* 398, 81–92.
28
- 29 Esteban, J.J., Cuevas, J., Tubía, J.M., Sergeev, S., Larionov, A., 2010. A revised Aquitanian age for
30 the emplacement of the Ronda peridotites (Betic Cordilleras, southern Spain). *Geol. Mag.*
31 147, doi:10.1017/S0016756810000737.
32
- 33 Esteban, J.J., Sánchez-Rodríguez, L., Seward, D., Cuevas, J. and Tubía, J.M., 2004. The late
34 thermal history of the Ronda area, southern Spain. *Tectonophysics* 389, 81–92.
35
- 36 Esteban, J. J., Cuevas, J., Tubía, J. M., Liati, A., Seward, D., Gebauer, D. 2007. Timing and origin
37 of zircon-bearing chlorite schists in the Ronda peridotites (Betic Cordilleras, Southern Spain).
38 *Lithos* 99, 121–135.
39
- 40 Ewing, T.A., Hermann, J., Rubatto, D., 2013. The robustness of the Zr-in-rutile and Ti-in-zircon
41 thermometers during high-temperature metamorphism (Ivrea-Verbano Zone, northern Italy).
42 *Contributions to Mineralogy and Petrology* 165, 757–779.
43
- 44 Faccenna, C., Becker, T.W., Lucente, F.P., Rossetti, F., 2001. History of Subduction and Back-arc
45 Extension in the Central Mediterranean. *Geophysical Journal International* 145, 1–21.
46
47
48
49
50
51
52
53
54
55
56
57
58
59
60
61
62
63
64
65

- 1 Faccenna, C., Piromallo, C., Crespo-Blanc, A., Jolivet, L., Rossetti, F., 2004. Lateral slab
2 deformation and the origin of the western Mediterranean arcs. *Tectonics* 23:TC1012
- 3 Franke, W., 2006. The Variscan orogen in Central Europe: construction and collapse. In: Gee, D.
4 G., Stephenson, R. A. (eds). *European Lithosphere Dynamics*. Geological Society, London,
5 Memoirs, 32, 333-343.
- 6
7
8
9 Frasca, G., Gueydan, F., Pujol, M., Brun, J.-P., Parat, F., Monié, P., et al., 2017. Fast switch from
10 extensional exhumation to thrusting of the Ronda Peridotites (South Spain). *Terra Nova* 29,
11 117–126, doi:10.1111/ter.12255.
- 12
13
14 Bin Fu, F., Page, Z., Cavosie, A. J., Fournelle, J., Kita, N. T., Lackey, J. S., Wilde, S. A., Valley, J.
15 W., 2008. Ti-in-zircon thermometry: applications and limitations. *Contrib Mineral Petrol* 156,
16 197–215.
- 17
18
19
20 Gao, P., Zheng, Y-F, Zhao, Z-F., 2016. Experimental melts from crustal rocks: A lithochemical
21 constraint on granite petrogenesis. *Lithos* 266–267, 133–157.
- 22
23
24 García-Dueñas, V., Balanyá J. C., Martínez-Martínez J. M., 1992. Miocene extensional
25 detachments in the outcropping basement of the northern Alboran Basin and their tectonic
26 implications, *Geo-Mar. Lett.*, 12, 88–95, doi:10.1007/BF02084917.
- 27
28
29 García-Casco, A., Torres-Roldán, R. L., 1999. Natural metastable reactions involving garnet,
30 staurolite and cordierite: Implications for petrogenetic grids and the extensional collapse of
31 the Betic-Rif Belt. *Contributions to Mineralogy and Petrology* 136, 131-153, doi:
32 10.1007/s004100050528.
- 33
34
35
36 Garrido, C.J., Gueydan, F., Booth-Rea, G., Precigout, J., Hidas, K., Padron-Navarta, J.A., Marchesi,
37 C., 2011. Garnet lherzolite and garnet-spinel mylonite in the Ronda peridotite: Vestiges of
38 Oligocene backarc mantle lithospheric extension in the western Mediterranean. *Geology* 39,
39 927-930. 10.1130/G31760.1.
- 40
41
42
43 Graessner, T., Schenk, V., 2001. An exposed Hercynian deep crustal Section in the Sila Massif of
44 northern Calabria: mineral chemistry, petrology and a P–T path of granulite-facies metapelitic
45 migmatites and metabasites. *Journal of Petrology* 42, 931-961.
- 46
47
48
49 Ghent, E.D., 1976. Plagioclase-garnet- Al_2SiO_5 -Quartz: A potential geobarometer-geothermometer.
50 *American Mineralogist* 61, 710-714.
- 51
52
53 Gimeno-Vives, O., Mohn, G., Bosse, V., Haissen, F., Zaghloul, M. N., Atouabat, A., Frizon de
54 Lamotte, D., 2019. The Mesozoic margin of the Maghrebian Tethys in the Rif belt (Morocco):
55 Evidence for polyphase rifting and related magmatic activity. *Tectonics* 38, 2894–
56 2918. <https://doi.org/10.1029/2019TC005508>
- 57
58
59
60
61
62
63
64
65

- 1 Gómez-Pugnaire, M.T., Nieto, F., Abad, I., Velilla, N., Garrido, C.J., Acosta-Vigil, A., Barich, A.,
2 Hidas, K., Lopez Sanchez-Vizcaino, V., 2019. Alpine Metamorphism in the Betic Internal
3 Zones. In: C. Quesada, J.T. Oliveira (eds.), *The Geology of Iberia: A Geodynamic Approach*,
4 pp. 519-554, Springer Nature, Switzerland, https://doi.org/10.1007/978-3-030-11295-0_13.
5
6 Guergouz, C, Martin, L., Vanderhaeghe, O., Thébaud, N., Fiorentini, M. 2018. Zircon and monazite
7 petrochronologic record of prolonged amphibolite to granulite facies metamorphism in the
8 Ivrea-Verbano and Strona-Ceneri Zones, NW Italy. *Lithos* 308–309, 1–18.
9
10 Guerrera, F., Martín-Martín, M., Tramontana, M., 2019. Evolutionary geological models of the
11 central-western peri-Mediterranean chains: a review, *International Geology Review*, doi:
12 10.1080/00206814.2019.1706056
13
14 Gueydan, F., Mazzotti, S., Tiberi, C., Cavin, R., and Villasenor, A., 2019. Western Mediterranean
15 sub-continental mantle emplacement by continental margin obduction. *Tectonics*,
16 doi:10.1029/2018TC005058.
17
18 Gueydan, F., Pitra, P., Afiri, A., Poujol, M., Essaifi, A., Paquette, J.-L., 2015. Oligo-Miocene
19 thinning of the Beni Bousera peridotites and their Variscan crustal host rocks, Internal Rif,
20 Morocco. *Tectonics* 34, 1244–1268, doi:10.1002/2014TC003769.
21
22 Harley, S. L., Kelly, N. M., Möller, A., 2007. Zircon behaviour and the thermal histories of
23 mountain chains, *Elements*, 3, 25–30, doi:10.2113/gselements.3.1.25.
24
25 Hermann, J., Rubatto, D., 2003. Relating zircon and monazite domains to garnet growth zones: age
26 and duration of granulite facies metamorphism in the Val Malenco lower crust. *Journal of*
27 *Metamorphic Geology* 21, 833–852.
28
29 Hidas, K., Booth-Rea, G., Garrido, C.J., Martínez-Martínez, J.M., Padrón-Navarta, J.A., Konc, Z.,
30 Giaconia, F., Frets, E., Marchesi, C., 2013. Backarc basin inversion and subcontinental mantle
31 emplacement in the crust: kilometre-scale folding and shearing at the base of the proto-
32 Alborán lithospheric mantle (Betic Cordillera, southern Spain). *Journal of the Geological*
33 *Society* 170, 47-55, doi: 10.1144/jgs2011-151.
34
35 Hokada, T., Harley, S.L., 2004. Zircon growth in UHT leucosome: constraints from zircon–garnet
36 rare earth elements (REE) relations in Napier Complex, East Antarctica. *Journal of*
37 *Mineralogical and Petrological Sciences* 99, 180–190.
38
39 Holland, T.J.B., Powell, R., 1998. An internally consistent thermodynamic data set for phases of
40 petrological interest. *Journal of Metamorphic Geology* 16, 309–343.
41
42 Homonnay, E., Corsini, M., Lardeaux, J-M, Romagny, A., Münch, P. Bosch D., Cenki-Tok, B.,
43 Ouazzani-Touhami, M., 2018. Miocene crustal extension following thrust tectonic in the
44 Lower Sebtides units (internal Rif, Ceuta Peninsula, Spain): Implication for the geodynamic
45
46
47
48
49
50
51
52
53
54
55
56
57
58
59
60
61
62
63
64
65

1 evolution of the Alboran domain, *Tectonophysics* 722, 507-535, doi:

2 10.1016/j.tecto.2017.11.028.

3 Hoskin, P.W.O., Schaltegger, U., 2003. The composition of zircon and igneous and metamorphic
4 petrogenesis. In: Hanchar, J.M., Hoskin, P.W.O. (Eds.), *Zircon*, 53. Mineralogical Society of
5 America, *Reviews in Mineralogy & Geochemistry*, Washington, DC, pp. 27–62.

6 Jolivet, L., Augier, R., Faccenna, C., Negro, F., Rimmelé, G., Agard, P., Robin, C., Rossetti, F.,
7 Crespo-Blanc, A., 2008. Subduction, convergence and the mode of backarc extension in the
8 Mediterranean region. *Bull. Soc. Géol. Fr.* 179, 525–550.

9 Jolivet, L., Faccenna, C. 2000. Mediterranean extension and the Africa-Eurasia collision.
10 *Tectonics*, 19, 1095-1106, doi:10.1029/2000TC900018.

11 Janots, E., Negro, F., Brunet, F., Goffè, B., Engi, M., Bouybaouene, M. L., 2006. Evolution of the
12 REE mineralogy in HP-LT metapelites of the Sebides complex, Rif, Morocco: Monazite
13 stability and geochronology. *Lithos* 87, 214–234.

14 Kotková, J., Harley, S. L., 2010. Anatexis during highpressure crustal metamorphism: evidence
15 from garnet–whole-rock REE relationships and zircon–rutile Ti–Zr thermometry in
16 leucogranulites from the Bohemian Massif. *Journal of Petrology* 51, 1967–2001

17 Kornprobst, J., 1974. Contribution à l'étude pétrographique et structurale de la zone interne du Rif
18 (Maroc septentrional); Petrography and structure of the Rif inner area, northern Morocco.
19 Notes Mèm. Serv. Géol. Rabat, 251, 256 pp.

20 Kunz BE, White RW. Phase equilibrium modelling of the amphibolite to granulite facies transition
21 in metabasic rocks (Ivrea Zone, NW Italy). *J Metamorph Geol.* 37, 935–950.

22 Klötzli, U.S., Sinigoi, S., Quick, J.E., Demarchi, G., Tassinari, C.C., Sato, K., Günes, Z., 2014.
23 Duration of igneous activity in the Sesia Magmatic System and implications for high-
24 temperature metamorphism in the Ivrea–Verbano deep crust. *Lithos* 206, 19–33.

25 Kunz, B. E., Manzotti, P., von Niederhäusern, B., Engi, M., Darling, J. R., Giuntoli, F., Lanari, P.,
26 2018. Permian high-temperature metamorphism in the Western Alps (NW Italy). *Int J Earth
27 Sci* 107, 203–229, doi:10.1007/s00531-017-1485-6.

28 Langone, A, Braga, R., Massonne H. J., Tiepolo, M., 2011. Preservation of old (prograde
29 metamorphic) U–Th–Pb ages in unshielded monazite from the high-pressure paragneisses of
30 the Variscan Ulten Zone (Italy). *Lithos* 127, 68–85.

31 Lonergan L., White N., 1997. Origin of the Betic-Rif mountain belt, *Tectonics* 16, 504–22

32 Ludwig, K. (2003), User's manual for Isoplot/Ex v3.0, a geochronological toolkit for Microsoft
33 Excel, Spec. Publ. 4, 25–31 Berkeley Geochronological Center, Berkeley, California

- 1
2
3
4
5
6
7
8
9
10
11
12
13
14
15
16
17
18
19
20
21
22
23
24
25
26
27
28
29
30
31
32
33
34
35
36
37
38
39
40
41
42
43
44
45
46
47
48
49
50
51
52
53
54
55
56
57
58
59
60
61
62
63
64
65
- Matte, P., 2001. The Variscan collage and orogeny (480-290 Ma) and the tectonic definition of the Armorica microplate: a review, *Terra Nova* 13, 122-128.
- Mazzoli, S., Martín-Algarra, A., 2011. Deformation partitioning during transpressional emplacement of a 'mantle extrusion wedge': The Ronda peridotites, western Betic Cordillera. Spain, *Journal of the Geological Society, London* 168, 373–382.
- Melchiorre, M., Álvarez-Valero, A.M., Vergés, J., Fernández, M., Belousova, E.A., El Maz, A., and Moukadiri, A., 2017. In situ U-Pb zircon geochronology on metapelitic granulites of Beni Bousera (Betic-Rif system, N Morocco), in Bianchini, G., Bodinier, J.-L., Braga, R., and Wilson, M., eds., *The Crust-Mantle and Lithosphere-Asthenosphere Boundaries: Insights from Xenoliths, Orogenic Deep Sections, and Geophysical Studies: Geological Society of America Special Paper 526*, 151–171, doi:10.1130/2017.2526(08).
- Michard, A., Goffé B., Bouybaouene M. L., Saddiqi O., 1997. Late Hercynian-Mesozoic thinning in the Alboran domain; metamorphic data from the northern Rif, Morocco, *Terra Nova*, 9, 171–174, doi:10.1046/j.1365-3121.1997.d01-24.x.
- Michard, A., Negro F., Saddiqi O., Bouybaouene M. L., Chalouan A., Montigny R., Goffé B., 2006. Pressure-temperature-time constraints on the Maghrebide mountain building: Evidence from the Rif-Betic transect (Morocco, Spain), Algerian correlations, and geodynamic implications, *C. R. Acad. Sci., Ser. II*, 338, 92–114.
- Molnar, P., Lyon-Caen, H., 1988. Some Physical Aspects of the Support, Structure, and Evolution of Mountain Belts, vol. 218. *Special Papers of the Geological Society of America*, pp. 179–207.
- Monié, P., Torres Roldan, R.L., García Casco, A., 1994. Cooling and exhumation of the Western Betic Cordilleras, $40\text{Ar}/39\text{Ar}$ thermochronological constraints on a collapsed terrane. *Tectonophysics* 238, 353–379.
- Montel, J.M., Kornprobst, J., Vielzeuf, D., 2000. Preservation of old U–Th–Pb ages in shielded monazite; example from the Beni Bousera Hercynian kinzigites (Morocco). *J. Metamorph. Geol.* 18, 335–342.
- Negro, F., Beyssac, O., Goffé, B., Saddiqi, O., Bouybaouene, M.L., 2006. Thermal structure of the Alboran Domain in the Rif (northern Morocco) and the Western Betics (southern Spain) constraints from Raman spectroscopy of carbonaceous material. *J. Metamorph. Geol.* 24, 309–327.
- Petri, B., Mohn, G., Skrzypek, E., Mateeva, T., Galster, F., Manatschal, G., 2017. U–Pb geochronology of the Sondalo gabbroic complex (Central Alps) and its position within the Permian post-Variscan extension. *International Journal of Earth Sciences* 106, 2873–2893.

- 1 Patiño Douce, A.E., Johnston, A.D., 1991. Phase equilibria and melt productivity in the pelitic
2 system: implications for the origin of peraluminous granitoids and aluminous granulites.
3 Contrib. Miner. Petrol. 107, 202–218.
4
- 5 Platt, J.P., England, P.C., 1994. Convective removal of lithosphere beneath mountain belts: thermal
6 and mechanical consequences. American Journal of Science 294, 307–336.
7
- 8 Platt, J. P. , Behr, W. M., Johanesen K., Williams J. R, 2013. The Betic-Rif Arc and Its Orogenic
9 Hinterland: A Review. Annu. Rev. Earth Planet. Sci., 2013, 41, 14.1–14.45, doi:
10 10.1146/annurev-earth-050212-123951
11
- 12 Platt, J.P., Vissers, R.L.M., 1989. Extensional collapse of thickened continental lithosphere: a
13 working hypothesis for the Alboran Sea and Gibraltar Arc. Geology 17, 540–543.
14
- 15 Platt, J.P., Whitehouse, M.J., 1999. Early Miocene high-temperature metamorphism and rapid
16 exhumation in the Betic Cordillera (Spain): evidence from U–Pb zircon ages. Earth Planet.
17 Sci. Lett. 171, 591–605.
18
- 19 Platt, J.P., Soto, J.I., Whitehouse, M.J., Hurford, A.J., Kelley, S.P., 1998. Thermal evolution, rate of
20 exhumation, and tectonic significance of metamorphic rocks from the floor of the Alboran
21 extensional basin, western Mediterranean. Tectonics 17, 671–689.
22
- 23 Platt, J.P., Argles, T.W., Carter, A., Kelley, S.P., Whitehouse, M.J., Lonergan, L., 2003a.
24 Exhumation of the Ronda peridotite and its crustal envelope: constraints from thermal
25 modelling of a P–T–time array. J. Geol. Soc. Lond. 160, 655–676.
26
- 27 Platt, J.P., Whitehouse, M.J., Kelley, S.P., Carter, A., Hollick, L., 2003b. Simultaneous extensional
28 exhumation across the Alboran Basin: implications for the causes of late orogenic extension.
29 Geology 31, 251–254.
30
- 31 Platt, J.P., Kelley, S.P., Carter, A., Orozco, M., 2005. Timing of tectonic events in the Alpujarride
32 Complex, Betic Cordillera, southern Spain. Journal of the Geological Society of London 162,
33 451–462.
34
- 35 Powell, R., Holland, T.J.B., 2008. On thermobarometry. Journal of Metamorphic Geology 26, 155-
36 179.
37
- 38 Powell, R., Holland, T.J.B., Worley, B, 1998. Calculating phase diagrams involving solid solutions
39 via non-linear equations, with examples using THERMOCALC. Journal of Metamorphic
40 Geology 16, 577–588.
41
- 42 Priem, H.N.A., Boelrijk, N.A.I.M., Hebeda, E.H., Oen, I.S., Verdurmen, E.A.Th., Verschure, R.H.,
43 1979. Isotopic dating of the emplacement of the ultramafic masses in the Serranía de Ronda,
44 Southern Spain. Contributions to Mineralogy and Petrology 70, 103–109
45
46
47
48
49
50
51
52
53
54
55
56
57
58
59
60
61
62
63
64
65

- 1
2
3
4
5
6
7
8
9
10
11
12
13
14
15
16
17
18
19
20
21
22
23
24
25
26
27
28
29
30
31
32
33
34
35
36
37
38
39
40
41
42
43
44
45
46
47
48
49
50
51
52
53
54
55
56
57
58
59
60
61
62
63
64
65
- Priem, H.N.A., Boelrijk, N.A.I.M., Hebeda, E.H., Verschure, R.H., 1966. Isotopic age determinations on tourmaline granite-gneisses and a metagranite in the eastern Betic Cordilleras (southeastern Sierra de los Filabres), SE Spain. *Geol. Mijnbouw* 45, 184-187.
- Puga, E., Nieto, J.M., Diaz de Federico, A., Bodinier, J.L., and Morten, L., 1999. Petrology and metamorphic evolution of ultramafic rocks and dolerite dykes of the Betic Ophiolite Association (Mulhacen Complex, SE Spain): Evidence of eo-Alpine subduction following an ocean-floor metasomatic process. *Lithos* 49, 23–56.
- Quick, J. E., Sinigoi, S., A., Mayer, 1995 Emplacement of mantle peridotite in the lower continental crust, Ivrea-Verbano zone, northwest Italy. *Geology* 23, 739–742.
- Rocha, B.C., Moraes, R., Möller, A., Cioffi, C.R., Jercinovic, M.J., 2017. Timing of anatexis and melt crystallization in the Socorro–Guaxupé Nappe, SE Brazil: Insights from trace element composition of zircon, monazite and garnet coupled to U—Pb geochronology. *Lithos* 277, 337–355.
- Rossetti, F., Theye, T., Lucci, F., Bouybaouene, M.L., Dini, A., Gerdes, A., Phillips, D., Cozzupoli, D. 2010. Timing and modes of granites magmatism in the core of the Alboran Domain, Rif Chain, northern Morocco: Implications for the Alpine evolution of the Western Mediterranean. *Tectonics* 29,TC2017, doi:10.1029/2009TC002487.
- Rossetti, F., Faccenna, C., Crespo-Blanc, A. 2005. Structural and kinematic constraints to the exhumation of the Alpujarride Complex (Central Betic Cordillera, Spain). *J. Struct. Geol.*, 27, 199–216,.doi:10.1016/j.jsg.2004.10.008.
- Rossetti, F., Dini, A., Lucci, F., Bouybaouene, M. L., Faccenna, C., 2013. Early Miocene strike-slip tectonics and granite emplacement in the Alboran Domain (Rif chain, Morocco): significance for the geodynamic evolution of westernMediterranean. *Tectonophysics* 608, 774–791.
- Royden, L.H., 1993. Evolution of retreating subduction boundaries formed during continental collision. *Tectonics* 12, 629–38.
- Rubatto, D., 2002. Zircon trace element geochemistry: distribution coefficients and the link between U–Pb ages and metamorphism. *Chemical Geology* 184, 123–138.
- Rubatto, D., Hermann, J., 2007. Experimental zircon/melt and zircon/garnet trace element partitioning and implications for the geochronology of crustal rocks. *Chemical Geology* 241, 38–61.
- Rubatto, D., Chakraborty, S., Dasgupta, S., 2013. Timescales of crustal melting in the Higher Himalayan Crystallines (Sikkim, Eastern Himalaya) inferred from trace element constrained monazite and zircon chronology. *Contributions to Mineralogy and Petrology* 165, 349–372.

- 1 Ruiz Cruz, M. D., Sanz de Galdeano, C., 2014. Garnet variety and zircon ages in UHP meta-
2 sedimentary rocks from the Jubrique zone (Alpujarride Complex, Betic Cordillera, Spain):
3 Evidence for a pre-Alpine emplacement of the Ronda peridotite. *International Geology*
4 *Reviews* 56, 845–868.
5
6
7 Ruiz-Cruz, M.D., Sanz de Galdeano, C., 2012. Diamond and coesite in the ultrahigh-pressure–
8 ultrahigh-temperature granulites from Ceuta, Northern Rif, Northwest Africa *Mineralogical*
9 *Magazine*, 76 (2012), pp. 683-705
10
11
12 Ruiz-Cruz, M.D., Sanz de Galdeano, C., 2013. Coesite and diamond inclusions, exsolutions
13 microstructures and chemical patterns in ultrahigh-pressure garnet from Ceuta (Northern Rif,
14 Spain). *Lithos* 177, 184-206.
15
16
17 Sánchez-Navas, A., García-Casco, A., Martín-Algarra, A., 2014. Pre-Alpine discordant granitic
18 dikes in the metamorphic core of the Betic Cordillera: tectonic implications. *Terra Nova* 26,
19 477–486.
20
21
22 Sánchez-Navas, A., García-Casco, A., Mazzoli, S., Martín-Algarra, A., 2017. Polymetamorphism in
23 the Alpujarride Complex, Betic Cordillera, South Spain. *The Journal of Geology*, 125,
24 doi:10.1086/693862
25
26
27 Sánchez-Rodríguez, L., Gebauer, D., 2000. Mesozoic formation of pyroxenites and gabbros in the
28 Ronda area (southern Spain), followed by Early Miocene subduction metamorphism and
29 emplacement into the middle crust: U-Pb sensitive high-resolution ion microprobe dating of
30 zircon. *Tectonophysics* 316, 19–44.
31
32
33 Sawyer, E. W., 1994. Melt segregation in the continental crust. *Geology* 22, 1019- 1022.
34
35
36 Sawyer, E.W., 2008. Atlas of migmatites. The Canadian Mineralogist. In: Special Publication, vol.
37 9. NRC Research Press, Ottawa, Ontario, p. 371.
38
39
40 Schmid, S.M., Fügenschuh, B., Kissling, E., Schuster, R., 2004. Tectonic map and overall
41 architecture of the Alpine orogen. *Eclogae Geol Helv* 97, 93–117.
42
43
44 Sosson, M., Morrillon, A.-C., Bourgois, J., Feraud, G., Poupeau, G., Saint-Marc, P., 1998. Late
45 exhumation stages of the Alpujarride complex (western Betic Cordilleras, Spain): new
46 thermochronological and structural data on Los Reales and Ojen nappes. *Tectonophysics* 285,
47 253–273.
48
49
50 Soto, J.I., Platt, J.P., 1999. Petrological and structural evolution of high-grade metamorphic rocks
51 from the floor of the Alboran Sea basin, Western Mediterranean. *J. Petrol.* 40, 21–60.
52
53
54 Spear F. S., Daniel C. G., 2001. Diffusion control of garnet growth, Harpswell Neck, Maine, USA.
55
56
57 J. *Metamorphic Geol.* 19, 179-195.
58
59
60
61
62
63
64
65

- Stampfli, G.M., Borel, G.D., 2002. A plate tectonic model for the Paleozoic and Mesozoic constrained by dynamic plate boundaries and restored synthetic oceanic isochrones. *Earth and Planetary Science Letters* 196, 17-33, doi:10.1016/S0012-821X(01)00588-X
- Sun, S.S., McDonough, W.S., 1989. Chemical and Isotopic Systematics of Oceanic Basalts: Implications for Mantle Composition and Processes. Geological Society, London, Special Publications 42, pp. 313-345.
- Taylor, J. ., Nicoli, G., Stevens, G., Frei, D. Moyen, J.F., 2014. The processes that control leucosome compositions in metasedimentary granulites: perspectives from the Southern Marginal Zone migmatites, Limpopo Belt, South Africa. *Journal of Metamorphic Geology* 32, 713–742.
- Taylor, R. J. M., Harley, S. L., Hinton, R. W., Elphick, S., Clark, C., Kelly, N. M., 2015. Experimental determination of REE partition coefficients between zircon, garnet and melt: A key to understanding high-T crustal processes. *Journal of Metamorphic Geology* 33, 231–248.
- Taylor, R. J. M., Clark, C., Harley, S. L., Kylander-Clark, A. R. C., Hacker, B. R., Kinny, P. D., 2017. Interpreting granulite facies events through rare earth element partitioning arrays. *Journal of Metamorphic Geology* 35, 759–775, doi:10.1111/jmg.12254.
- Taylor-Jones, Powell, R., 2015. Interpreting zirconium-in-rutile thermometric results. *Journal of Metamorphic Geol.* 33, 115–122.
- Tomkins, H.S., Powell, R., Ellis, D.J., 2007. The pressure dependence of the zirconium-in-rutile thermometer. *Journal of Metamorphic Geology* 25, 703–713.
- Torres-Roldán, R.L., 1983. Fractionated melting of metapelite and further crystal-melt equilibria. The example of the Blanca Unit migmatite complex, north of Estepona (southern Spain). *Tectonophysics* 96, 95–123.
- Tubía, J., Cuevas, J., Ibarra, J. G., 1997. Sequential development of the metamorphic aureole beneath the Ronda Peridotites and its bearing on the tectonic evolution of the Betic Cordillera. *Tectonophysics* 279, 227 -252.
- Tubía, J., Cuevas, J., 1986. High-temperature emplacement of the Los Reales Peridotite nappe (Betic Cordillera, Spain). *Journal of Structural Geology* 8, 473–482.
- Tumiati, S., Thöni, M., Nimis, P., Martin, S., Mair, V., 2003. Mantle–crust interactions during Variscan subduction in the Eastern Alps (Nonsberg–Ulten zone): geochronology and new petrological constraints. *Earth and Planetary Science Letters* 210, 509–526.
- Vanderhaeghe, O., 1999. Pervasive melt migration from migmatites to leucogranite in the Shuswap metamorphic core complex, Canada: control of regional deformation. *Tectonophysics* 312, 35–55.

- 1
2
3
4
5
6
7
8
9
10
11
12
13
14
15
16
17
18
19
20
21
22
23
24
25
26
27
28
29
30
31
32
33
34
35
36
37
38
39
40
41
42
43
44
45
46
47
48
49
50
51
52
53
54
55
56
57
58
59
60
61
62
63
64
65
- Vanderhaeghe, O., 2009. Migmatites, granites and orogeny: flow modes of partially molten rocks and magmas associated with melt/solid segregation in orogenic belts. *Tectonophysics* 477, 119–134.
- Vanderhaeghe, O., 2012. The thermal–mechanical evolution of crustal orogenic belts at convergent plate boundaries: A reappraisal of the orogenic cycle. *Journal of Geodynamics* 56– 57, 124–145.
- Van Hinsbergen, D.J.J., Vissers, R.L.M., Spakman, W., 2014. Origin and consequences of Western Mediterranean subduction, rollback, and slab segmentation. *Tectonics* 33, 393–419.
- von Raumer, J.F., Bussy, F., Schaltegger, U., Schulz, B., Stampfli, G.M., 2013. Pre-Mesozoic Alpine basements—their place in the European Paleozoic framework. *Geol Soc Am Bull* 125:89–108.
- Vérges, J, Fernández, M., 2012. Tethys-Atlantic interaction along the Iberia-Africa plate boundary: the Betic-Rif orogenic system. *Tectonophysics* 579,144–72.
- Vielzeuf, D. , Clemens, J.D., Pin, C., Moinet, E., 1990. Granites, granulites and crustal differentiation In: Vielzeuf, D, Vidal, P. (eds) *Granulites and crustal evolution*. Kluwer Academic Publishers, Dordrecht, 59-85.
- Vielzeuf, D., Montel, J.M., 1994. Partial melting of metagreywackes part I. Fluid-absent experiments and phase relationships. *Contrib. Miner. Petrol.* 117, 375–393.
- Villaros, A., Stevens, G. Buick, I. S., 2009. Tracking S-type granite from source to emplacement: Clues from garnet in the Cape Granite Suite. *Lithos* 112,217–235
- Watson, E.B., Harrison, T.M., 1983. Zircon saturation revisited: temperature and composition effects in a variety of crustal magma types. *Earth Planet. Sci. Lett.*, 295-304.
- Watson, E.B., Wark, D.A., Thomas, J.B., 2006. Crystallization thermometers for zircon and rutile. *Contrib. Mineral. Petrol.* 151, 413.
- Weinberg, R. F., Hasalová, P., 2015. Water-fluxed melting of the continental crust: A review. *Lithos* 212–215, 158–188.
- White, R.W. & Powell, R., 2002. Melt loss and the preservation of granulite facies mineral assemblages. *Journal of Metamorphic Geology* 20, 621–632.
- White, R. W., Powell, R., 2011. On the interpretation of retrograde reaction textures in granulite facies rocks. *Journal of Metamorphic Geology* 29, 131-149, doi:10.1111/j.1525-1314.2010.00905.x
- Whitehouse, M. J., Platt, J. P., 2003. Dating high-grade metamorphism - Constraints from rare-earth elements in zircon and garnet. *Contributions to Mineralogy and Petrology* 145, 61-74.

- 1
2 Whitney, D.L., Evans, B.W., 2010. Abbreviations for Names of Rock-Forming Minerals. *American Mineralogist*, 95, 185-187, doi:10.2138/am.2010.3371.
- 3
4 Zeck, H.P., Monié, P., Villa, I.M., Hansen, B.T., 1992. Very high rates of cooling and uplift in the
5 Alpine belt of the Betic Cordilleras, southern Spain. *Geology* 20, 79–82.
- 6
7 Zeck, H. P., Whitehouse, M. J., 2002. Repeated age resetting in zircons from Hercynian–Alpine
8 polymetamorphic schists (Betic–Rif tectonic belt, S. Spain)—a U–Th–Pb ion microprobe
9 study. *Chemical Geology* 182, 275–292.
- 10
11
12 Zeck, H.P., Williams, I. S., 2001. Hercynian Metamorphism in Nappe Core Complexes of the
13 Alpine Betic–Rif Belt, Western Mediterranean—a SHRIMP Zircon Study. *Journal of*
14
15 *Petrology* 42, 1373-1385, doi: 10.1093/petrology/42.7.1373.
- 16
17
18 Zeck, H. P., Whitehouse, M.,J., 2002. Repeated age resetting in zircons from Hercynian–Alpine
19 polymetamorphic schists (Betic–Rif tectonic belt, S. Spain)—a U–Th–Pb ion microprobe
20 study, *Chemical Geology* 182, 275-292,doi: 10.1016/S0009-2541(01)00296-0.
- 21
22
23
24
25
26
27
28
29
30
31
32
33
34
35
36
37
38
39
40
41
42
43
44
45
46
47
48
49
50
51
52
53
54
55
56
57
58
59
60
61
62
63
64
65

Figure captions

1
2
3 Figure 1 – (a) The Mediterranean region with location of the Betic-Rif orogen. (b) Regional
4 geology of the western Mediterranean region and crustal-scale geological cross section across the
5 Rif chain (modified and re-adapted after Michard et al., 2002 and references therein). The study
6 area (Fig. 2) is also indicated.
7
8
9

10
11
12 Figure 2 - (a) Tectono-stratigraphic column of the Alboran Domain Complex in the Moroccan Rif ,
13 with indication of the migmatitic granulites (Mg) that are the focus of this study. (b) The geology
14 of the study area (modified after Kronmpbst, 1975). (c) General structural architecture across the
15 Beni Bousera peridotite bodies (geological cross-section A-B).
16
17
18
19
20

21 Figure 3 – Outcrop-scale rock textures in the field. (a) Geological sketch showing the across-strike
22 structure of the peridotite (β)-migmatitic granulites (Mg) contact (Beni Bousera units), showing
23 representative lithologies and the structural significance of the studied samples (see also Table 1).
24 (b) Stromatic leucosome layering within the granulites enveloping metabasite boudins. (c)
25 Coexistence of deformed (early segregated) leucosomes and stromatic leucosome layering within
26 the granulite foliation. (d) Coarse-grained garnet-bearing (Grt-1) residua (melanosome) hosting
27 stromatic and nebulitic leucosomes (stromatic metatexite). (e) Detail shown in (d) showing the
28 intimate relationships between garnet (Grt-1) and leucosomes. (f) The melanosome-leucosome
29 contact showing enclaves of grt-bearing melanosome portions and the two igneous garnet types
30 (Grt-2 and Grt-3, sample). Mineral abbreviations follow Whitney and Evans (2010).
31
32
33
34
35
36
37
38
39
40

41 Figure 4 - Microtextures and mineral assemblages. (a) Scanned thin section of a melanosome-
42 leucosome layering, showing the textural characteristics and arrangement of the Grt-1 types (sample
43 K3). (b) Enlargement of the garnet core shown in Fig. 4a, showing the inclusion assemblages
44 hosted at the garnet core. Plane polarised light. (c) Back-scattered electron (BSE) image showing of
45 the area indicated in (b) showing the polymineralic and single-phase inclusion assemblage made of
46 Rt, Qz, Kfs, Pl, Ky, Gr. (d) High-Ti Bt crystals hosted in poikiloblastic Grt-1 inner rim domain
47 (area indicated in Fig. 4a). Bt inclusions occur together with rounded, single-phase, Qz inclusions.
48 Plane polarised light. (e) Detail of a Grt-1 outer rim domain (area indicated in Fig. 4a), showing
49 sillimanite inclusion. Plane polarised light. (f) Grt-2 in leucosome. The enlargement shows the
50 sillimanite inclusion at the garnet core (sample Ma48). Plane polarised light. (g) The mineral
51 assemblage in leucosomes, showing a well annealed Qz-Fsp-Qz matrix showing equilibrium
52 textures with Ky and garnet (Grt-3; sample K3L). Crossed polarised light. (H) BSE image to
53
54
55
56
57
58
59
60
61
62
63
64
65

1 illustrate the leucosomes microtexture (sample Ma09/28L). Note the crystal framework made by
2 plagioclase, with K-feldspar, quartz. Garnet (Grt-3) occurs as an interstitial phase with subhedral
3 habit (sample Ma09/30L). (h) BSE image showing evidence of the retrograde metamorphism, as
4 documented by spinel–cordierite symplectic intergrowths that replaces early garnet-kyanite
5 assemblages (sample K3M). Mineral abbreviations follow Whitney and Evans (2010).
6
7
8
9

10 Figure 5 – Representative qualitative compositional maps and quantitative EMPA profiles showing
11 variation in cations (Mn, Mg, Fe, Ca) distribution in garnet grains from the Beni Bousera granulite
12 units. (a)-(b) Grt-1. (c) Grt-2. (c) Grt-3.
13
14
15
16

17 Figure 6 – Whole-rock major element composition of the studied samples. (a) Total alkali vs. silica
18 (TAS) chemical classification diagram (LeMaitre et al. 2002) for the melt products interlayered
19 within the Beni Bousera granulites. (b) The same samples plotted in the CaO–Na₂O–K₂O ternary
20 diagram and compared to experimental melts produced through fluid-absent biotite-dehydration
21 melting. (c)-(d) The major element compositions (100 wt% normalized) plotted as atomic K vs. Si
22 and Ca/(Ca + Na) and vs. Fe + Mg (after Taylor et al. 2014).
23
24
25
26
27
28
29
30

31 Figure 7: Chondrite-normalized (after Sun and McDonough, 1989) REE patterns of the studied
32 leucosome samples compared to the experimental S-type melts (after Taylor et al. 2014).
33
34
35

36 Figure 8 – (a)-(c) Cathodoluminescence images with location of the LA-ICPMS laser spots (white
37 circles) indicated (all ages are ²⁰⁶Pb/²³⁸U ages in Ma, with errors quoted at 2σ level) and
38 conventional Concordia diagrams of the analysed zircon grains from the studied samples (see Table
39 3). The inset in (a) shows the weighted average of ²⁰⁶Pb/²³⁸U ages for the data population at the
40 lower end of the Discordia.
41
42
43
44
45

46 Figure 9 – (a) Probability age distribution plot as obtained from the cumulative ²⁰⁶Pb/²³⁸U zircon
47 age data. (b)-(c) ²⁰⁶Pb/²³⁸U ages vs. U/Th diagram values for the analysed zircon ages. Data are
48 compared with those available from the Hercynian leptinites intruded into the Lower Sebtides units
49 (after Rossetti et al., 2010)
50
51
52
53
54
55

56 Figure 10: Chondrite-normalized (Sun and McDonough, 1989) REE pattern of the (a) analysed
57 zircons and (b) garnets.
58
59
60
61
62
63
64
65

1
2 Figure 11 – Conceptual evolutionary model for the textural and compositional characteristics of the
3 different garnet types recognised in the Beni Bousera migmatitic granulites.
4

5 Figure 12 –Pressure-Temperature diagram showing the thermo-baric conditions attained during
6 crustal anatexis in the Beni Bousera granulites as derived from inverse thermobarometry. The P-T
7 grid and the relevant mineral and melting reactions are after Kotková and Harley (2010) and
8 references therein.
9
10
11

12
13 Figure 13 - Representative P-T pseudosection calculated for the reconstructed bulk rock
14 composition (pre-melting) assuming a 45 vol% of melt loss in the system MnNKCFMASHT (MnO-
15 Na₂O-K₂O-CaO-FeO-MgO-Al₂O₃-SiO₂-H₂O-TiO₂) with a bulk composition (wt%) MnO = 0.27,
16 Na₂O = 1.54, K₂O = 4.19, FeO = 9.15, MgO = 2.44, Al₂O₃ = 22.98, SiO₂ = 55.43, H₂O = 1.46, TiO₂
17 = 0.86, using the Perple_X software. The dashed lines and arrows depict the inferred P-T path to
18 Biotite dehydration melting as as constrained from the X_{Grt} and X_{Pyr} isopleths in Grt-1 (core and rim
19 domains) and Grt-2 (core domains) garnets. The colored ellipses indicate the pre-melting and the
20 climax of metamorphism attained by the inner crustal envelope of the Beni Bousera peridotites.
21
22
23
24
25
26
27
28
29

30 Figure 14 - Calculated zircon/garnets REE partitioning coefficients for the different samples
31 compared with experimental data. The coloured fields display the whole range of values, the
32 coloured continuous lines are the corresponding average values (see Table 4).
33
34
35
36
37

38 Figure 15 - Conceptual evolutionary model for the Beni Bousera Hercynian migmatitic granulites in
39 the framework of the Betic-Rif tectonics. A two-stage (Permo-Carboniferous and Early Miocene)
40 crust-mantle coupling is tentatively proposed.
41
42
43
44
45
46

47 **Table captions**

48
49
50
51 Table 1 - Localisation of the samples, constituent mineralogy and analytical methods
52
53

54
55 Table 2 – Whole-rock chemical compositions
56
57

58
59 Table 3 - Results of U-Th-Pb LA-ICP-MS analyses and calculated ages for zircon separates from
60 the migmatitic granulites of the Beni Bousera unit
61
62
63
64
65

1
2
3
4
5
6
7
8
9
10
11
12
13
14
15
16
17
18
19
20
21
22
23
24
25
26
27
28
29
30
31
32
33
34
35
36
37
38
39
40
41
42
43
44
45
46
47
48
49
50
51
52
53
54
55
56
57
58
59
60
61
62
63
64
65

Table 4: Representative REE compositions of zircon and garnet with the corresponding $D_{\text{REE}}^{\text{Zrn/Grt}}$ coefficients.

Supplementary Material#1

[Click here to download e-component: Supplementary#1_ANALYTICAL METHODS & PROTOCOLS.docx](#)

Supplementary Material#2

[Click here to download e-component: Supplementary#2-EMPA.xls](#)

Supplementary Material#3

[Click here to download e-component: Supplementary#3_Zr-in-Rt-Thermometry.docx](#)

Supplementary Material#4

[Click here to download e-component: Supplementary#4_melt-restite proportions.docx](#)

Figure 1
[Click here to download high resolution image](#)

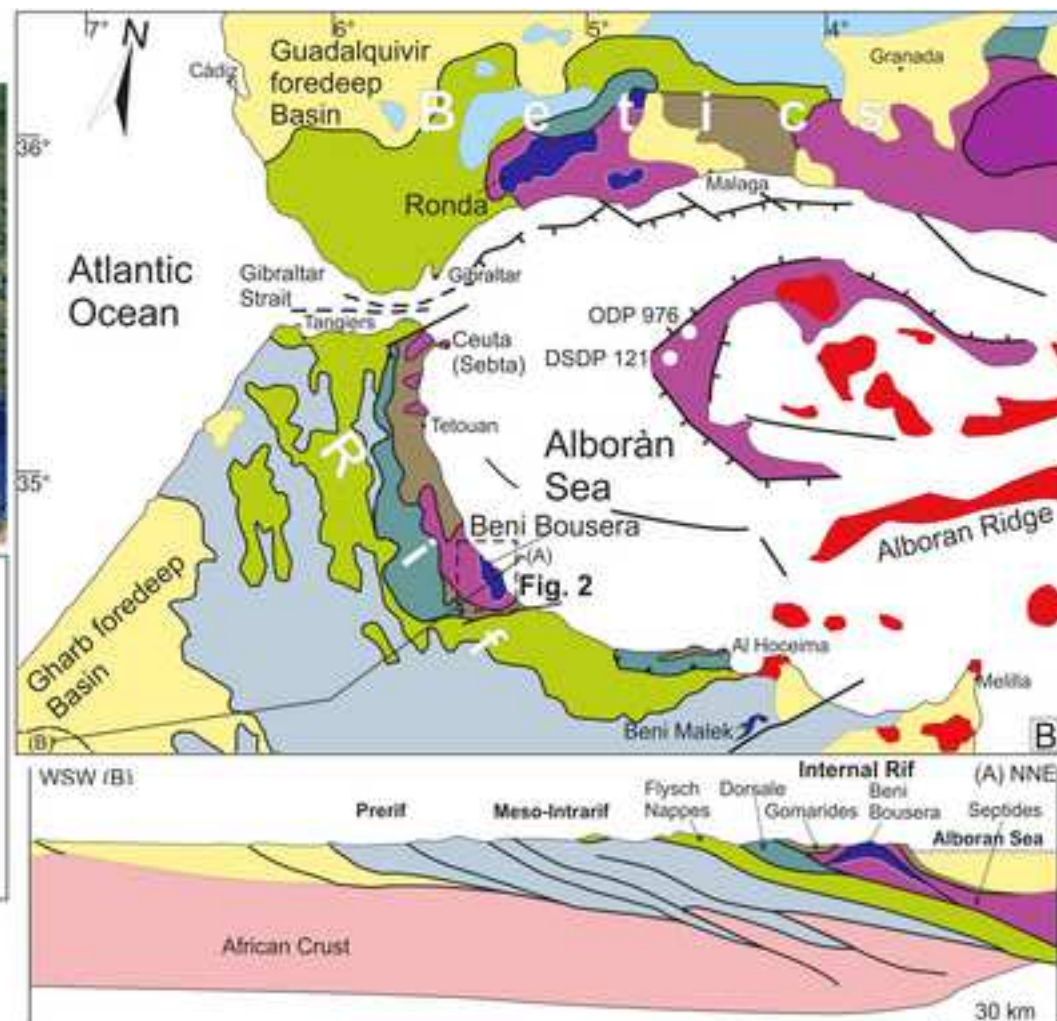


Figure 2

[Click here to download high resolution image](#)

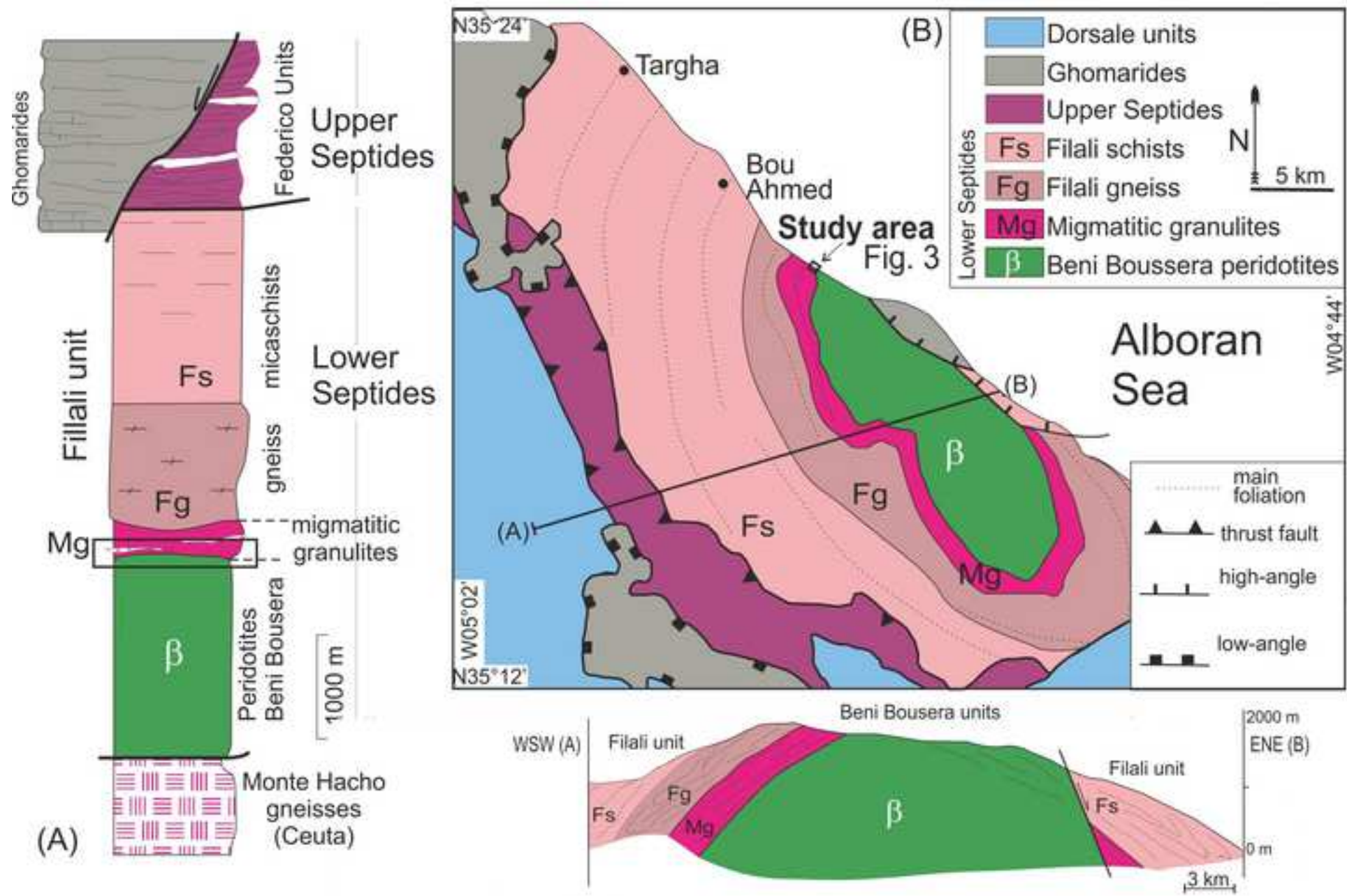


Figure 3
[Click here to download high resolution image](#)

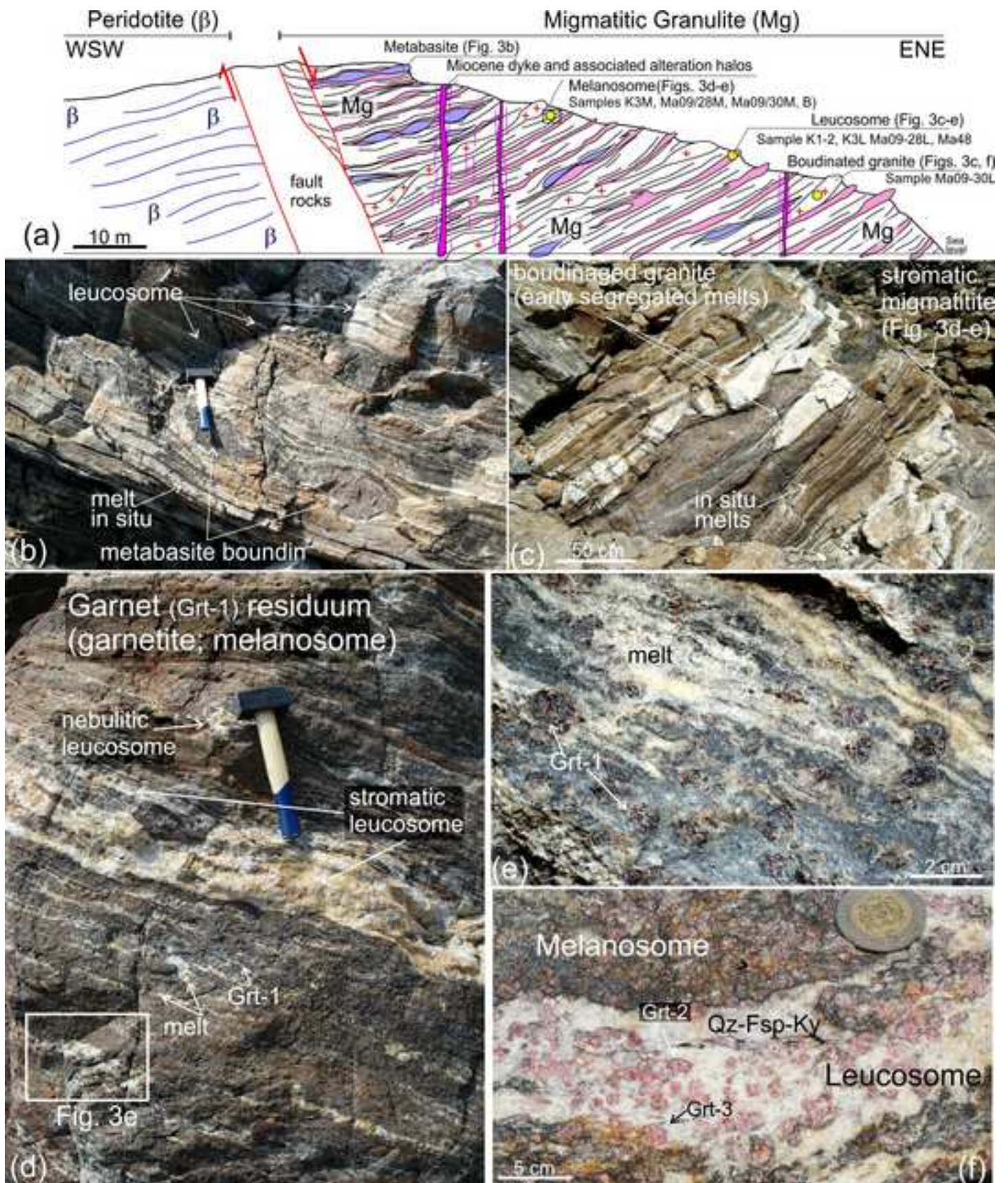


Figure 4
[Click here to download high resolution image](#)

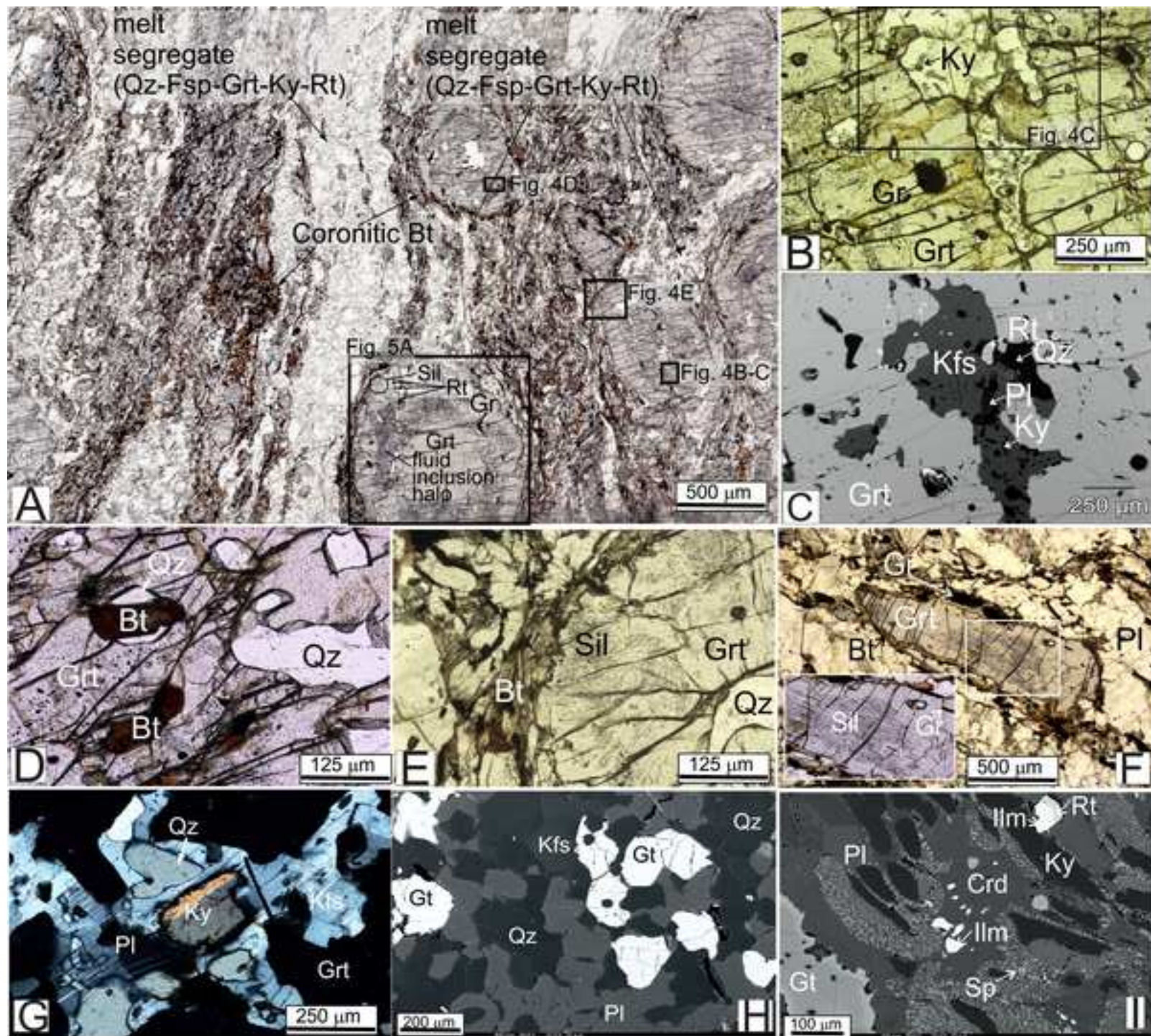


Figure 5
[Click here to download high resolution image](#)

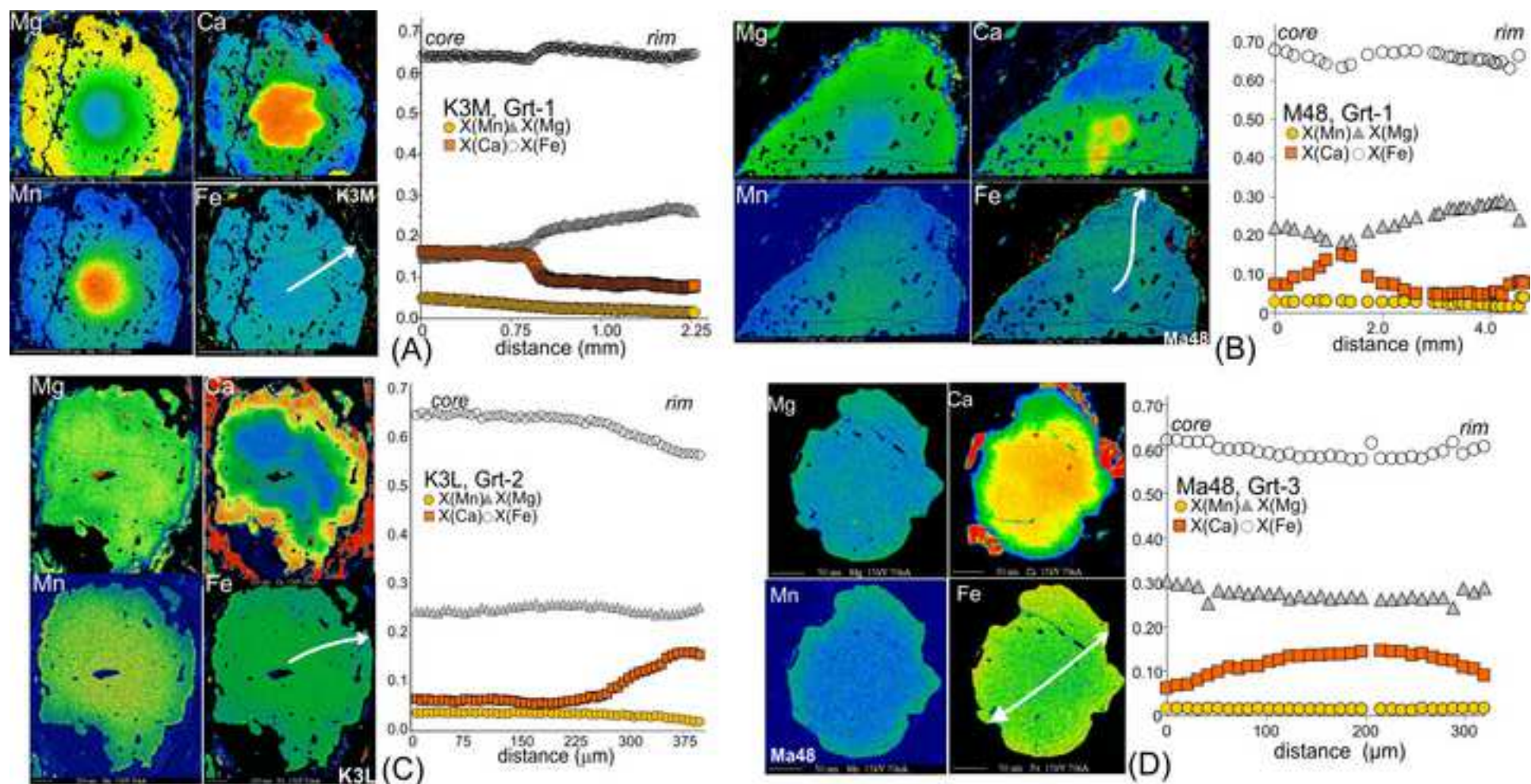


Figure 6
[Click here to download high resolution image](#)

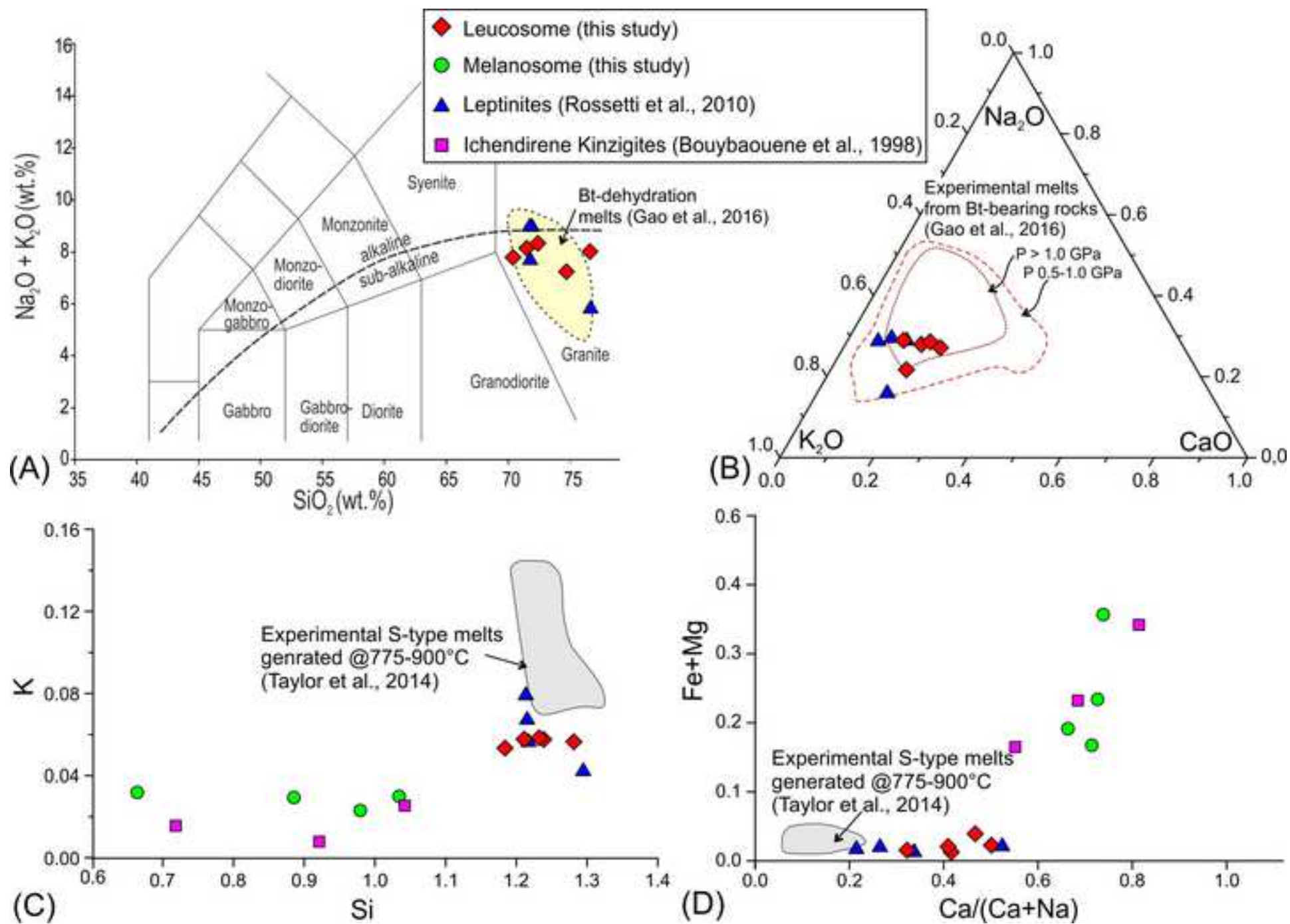


Figure 7
[Click here to download high resolution image](#)

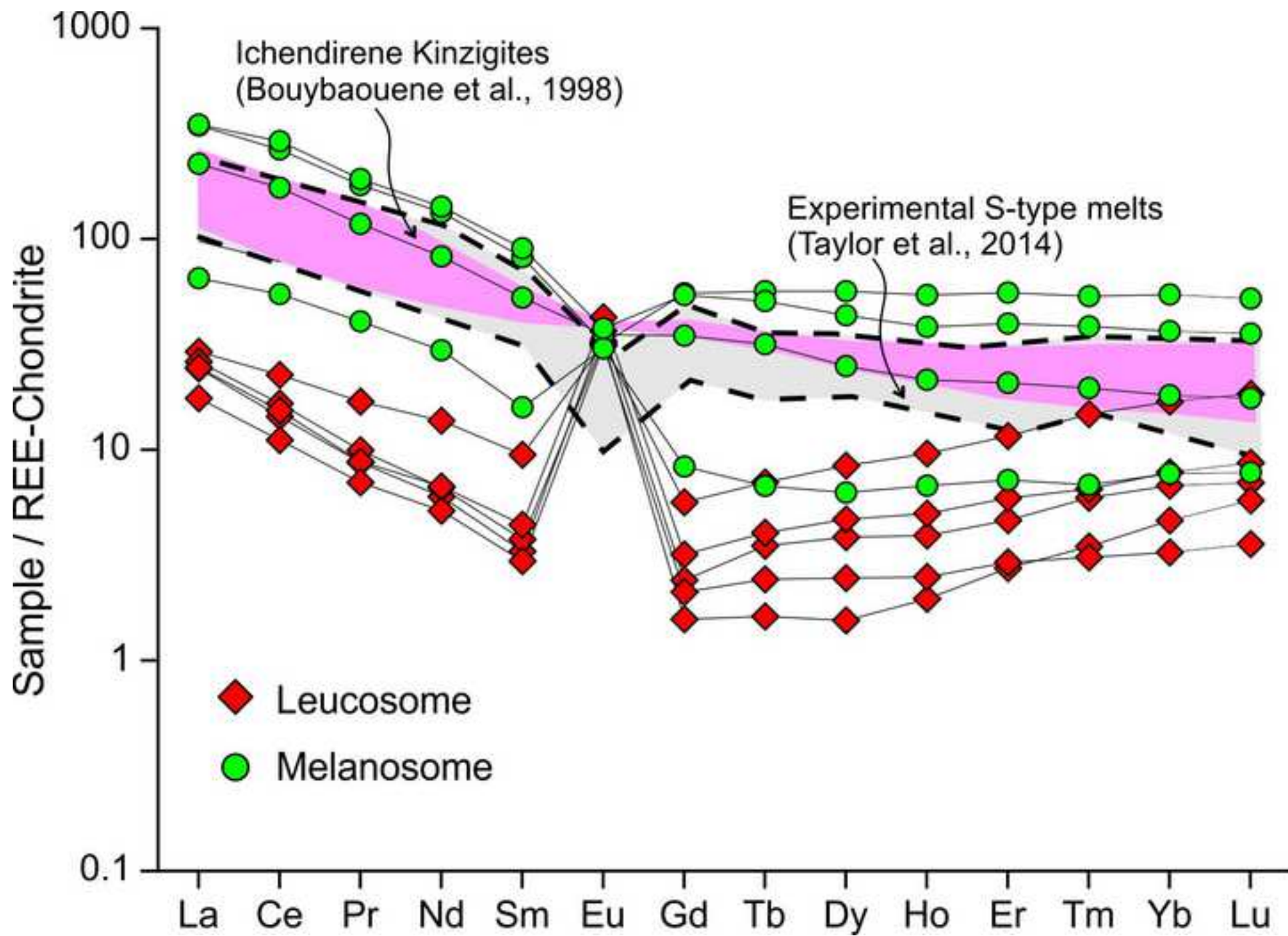
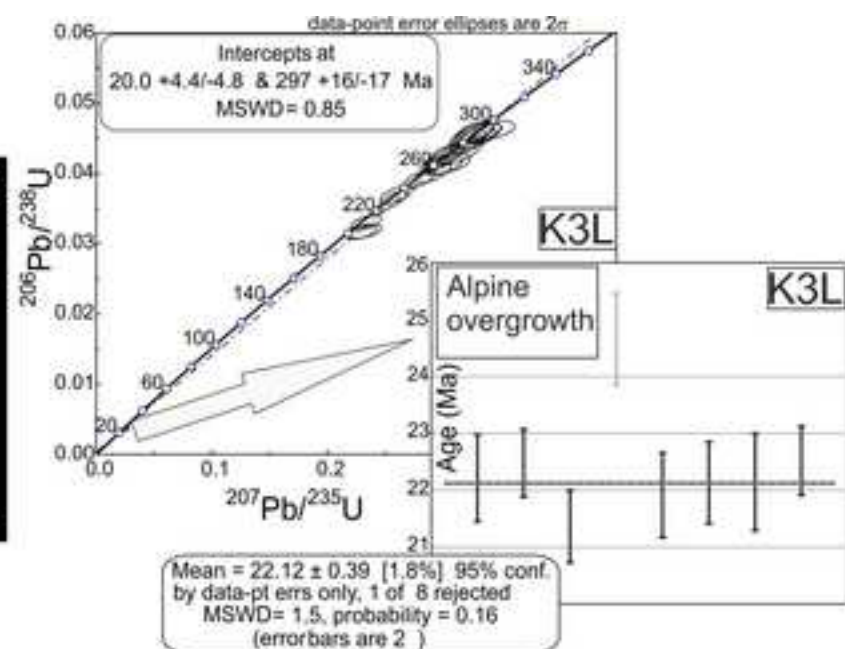
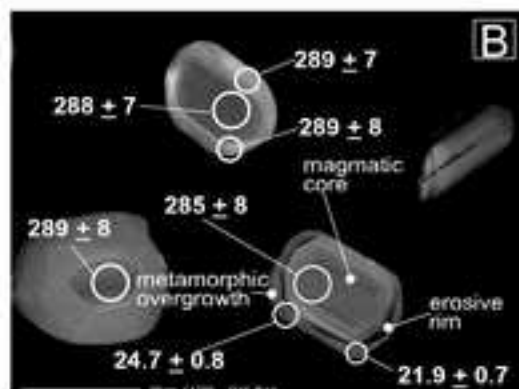
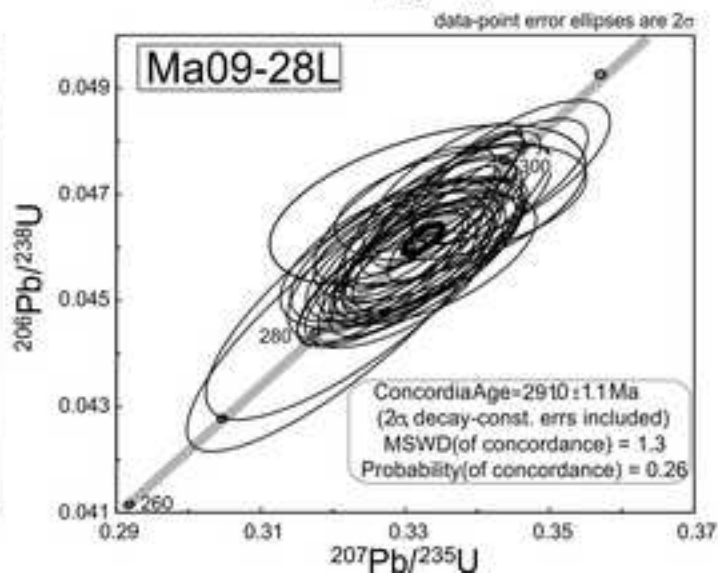
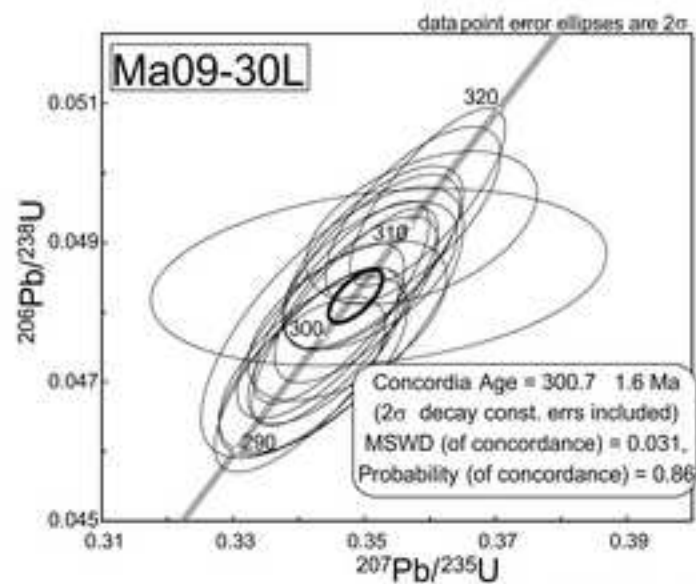
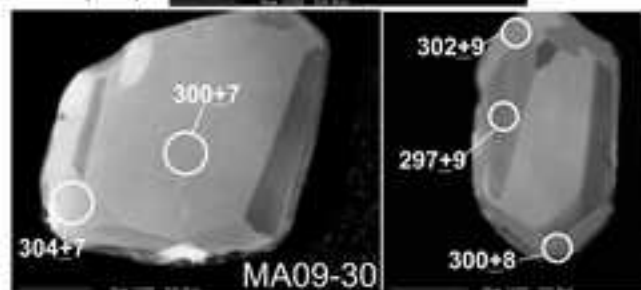
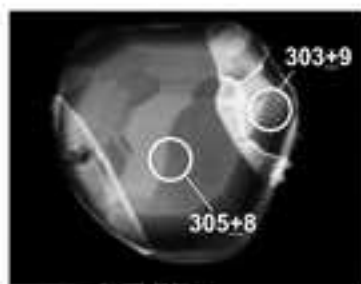


Figure 8

[Click here to download high resolution image](#)



(B)



(C)

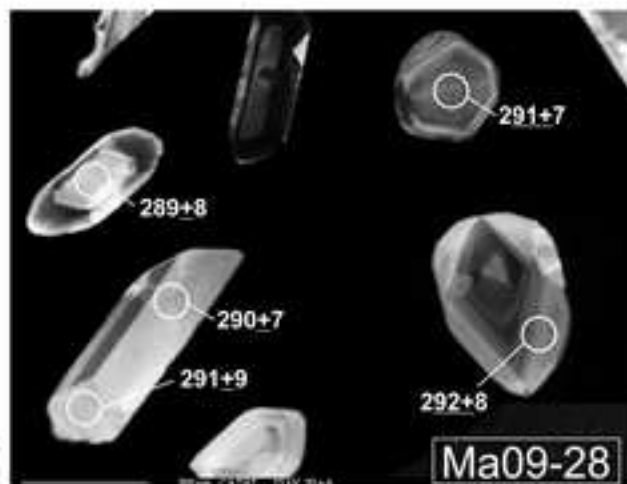


Figure 9
[Click here to download high resolution image](#)

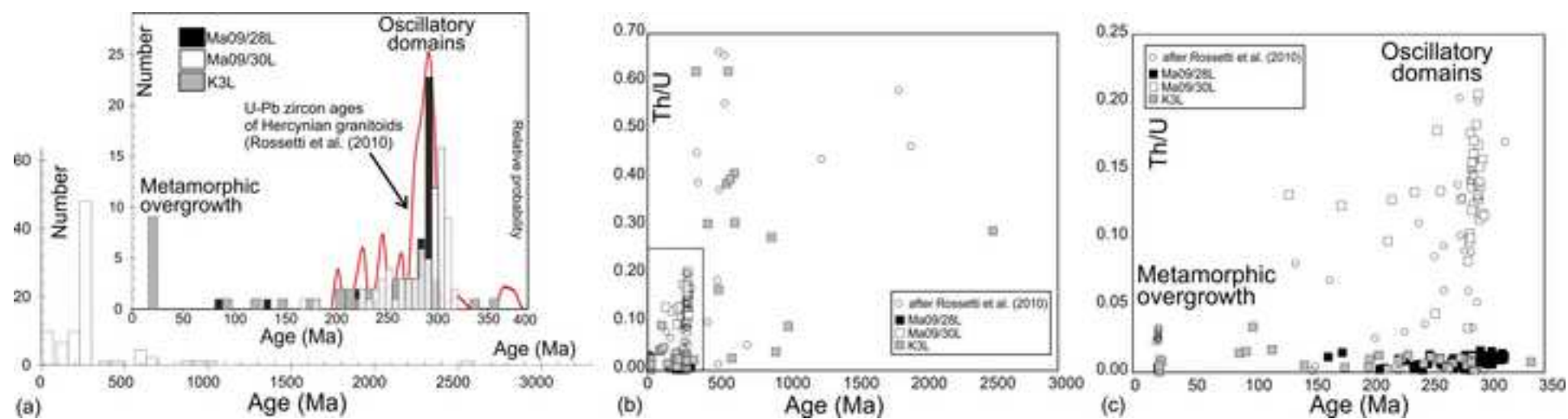
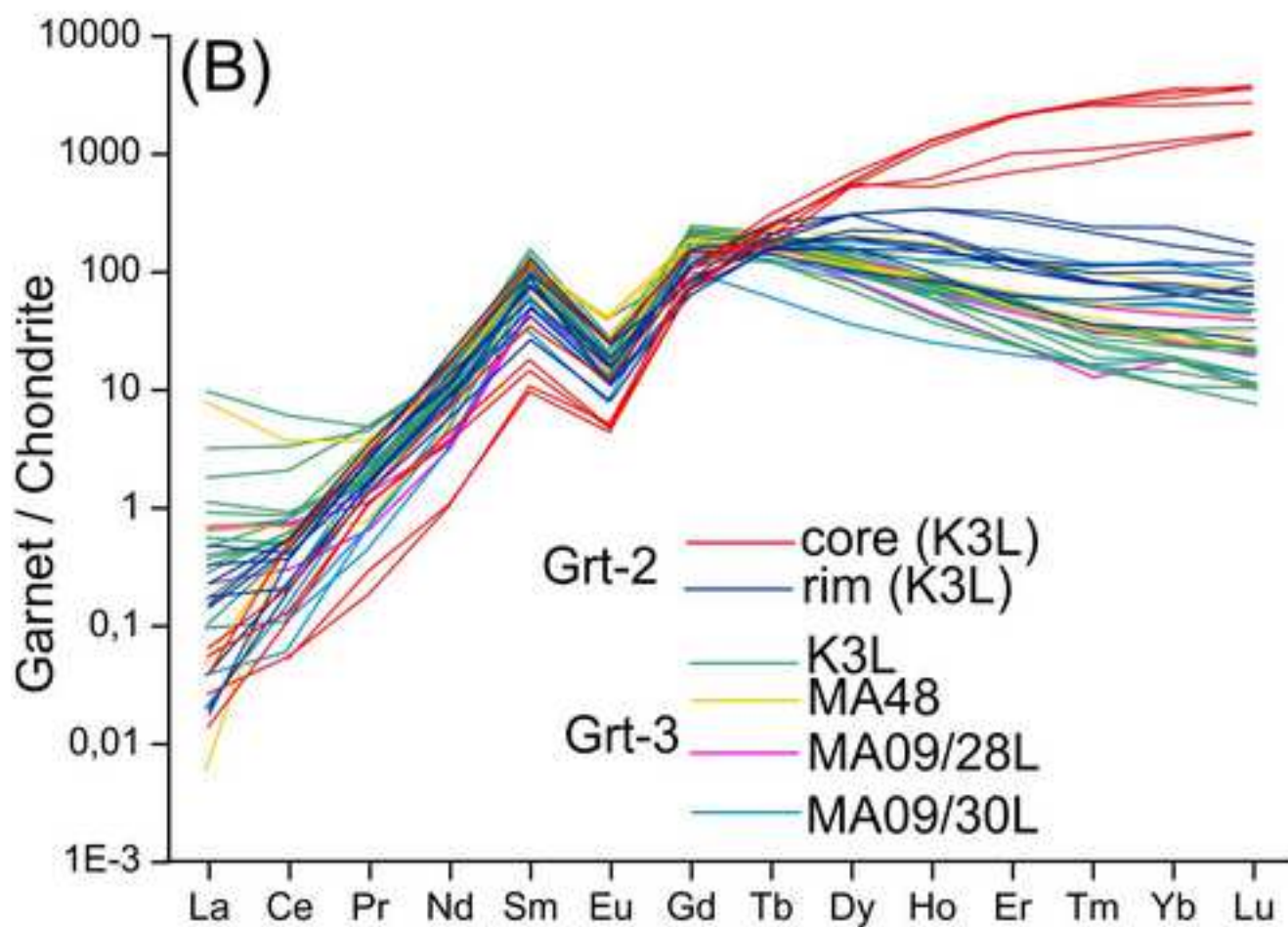
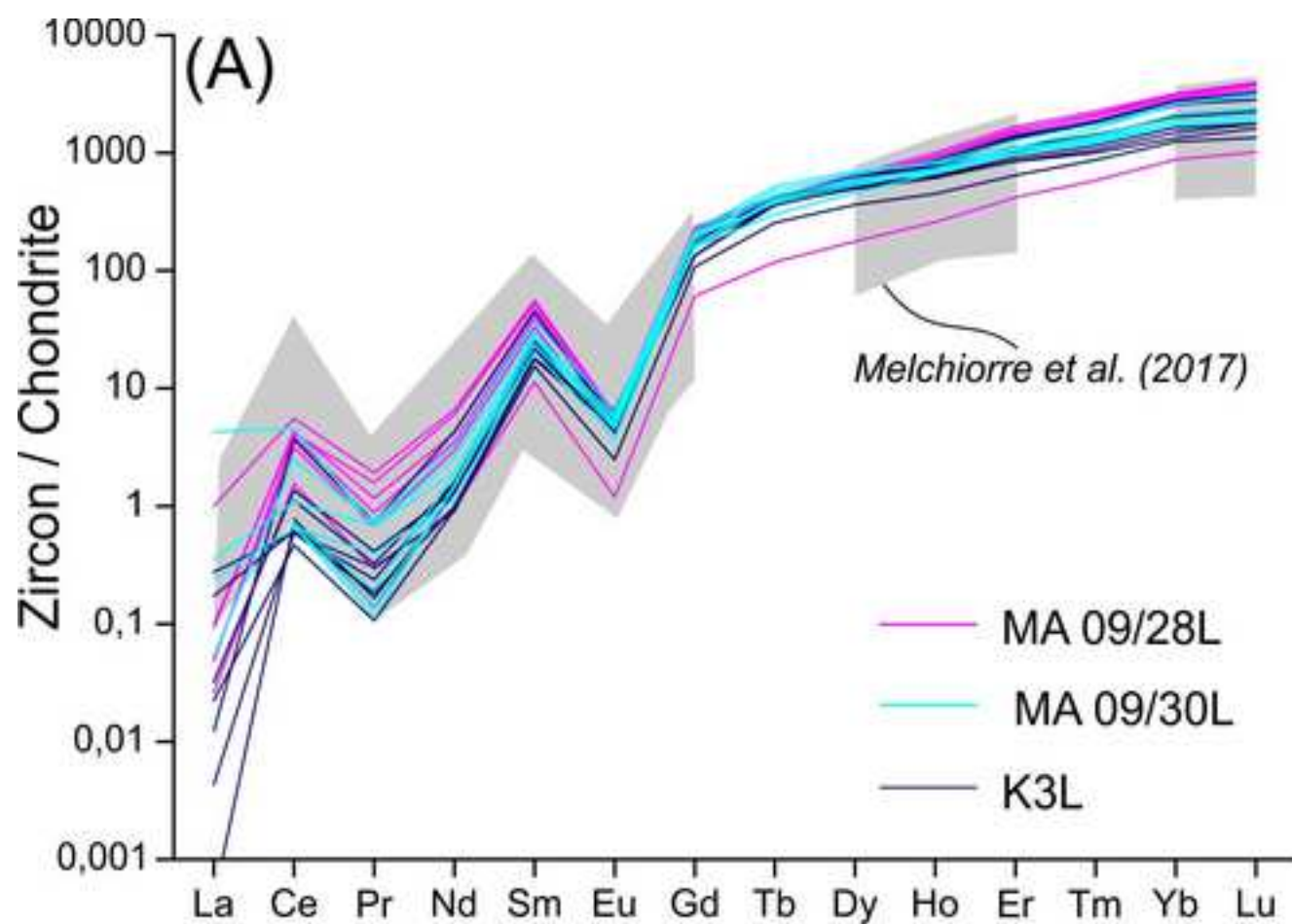
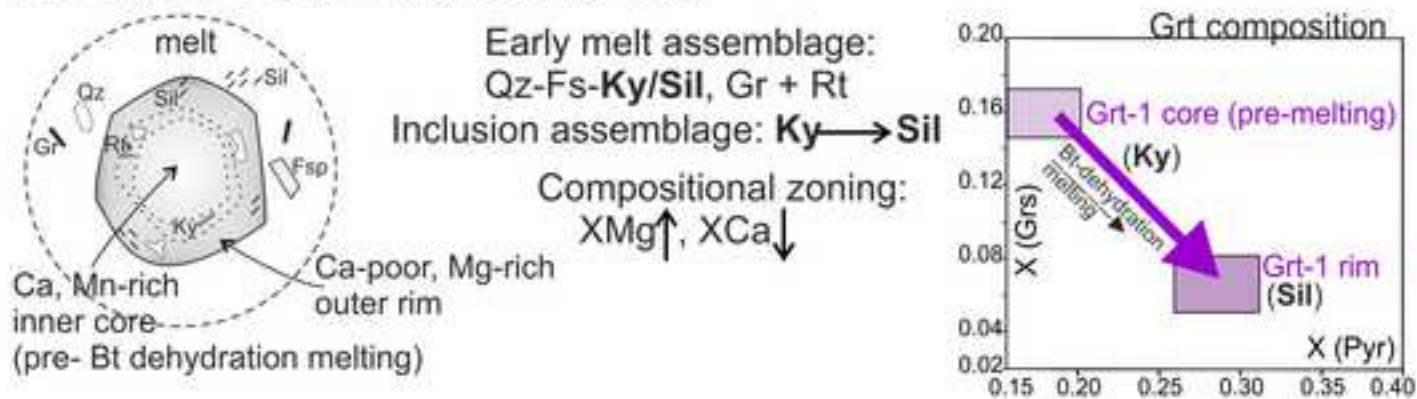


Figure 10

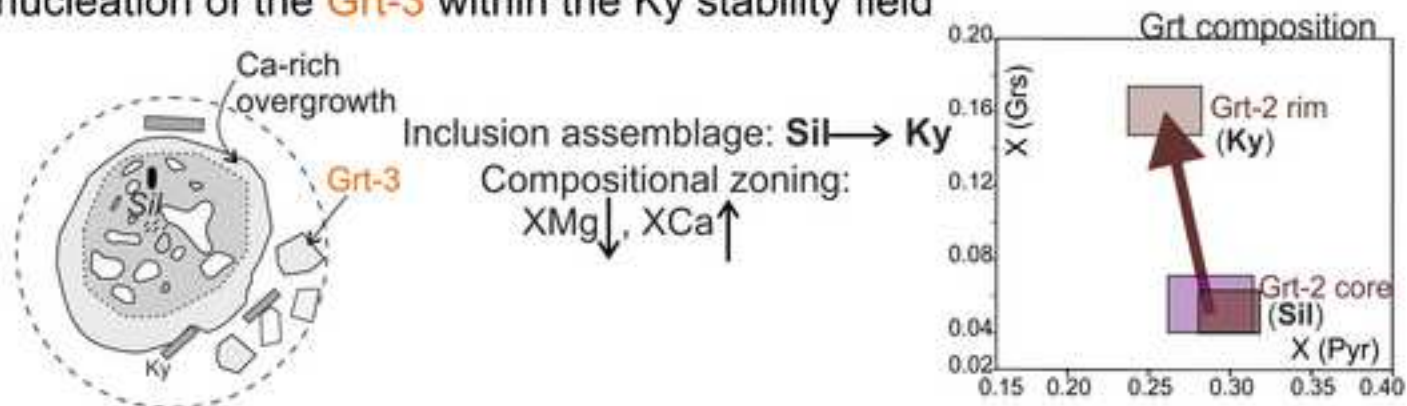
[Click here to download high resolution image](#)



(A) Peritectic garnet overgrowth onto a pre-existing generation (Grt-1 inner core) during prograde incongruent melting: from the Ky (Grt-1 inner rim) to the Sil (Grt-1 outer rim) stability field



(B) Grt-2 core nucleation in melt within the Sil stability field, major element re-equilibration at HT, continuous equilibration with melt (Grt-2 rim) and nucleation of the Grt-3 within the Ky stability field



(D) Final re-equilibration with the igneous matrix: Grt-3 rim



Figure 12
[Click here to download high resolution image](#)

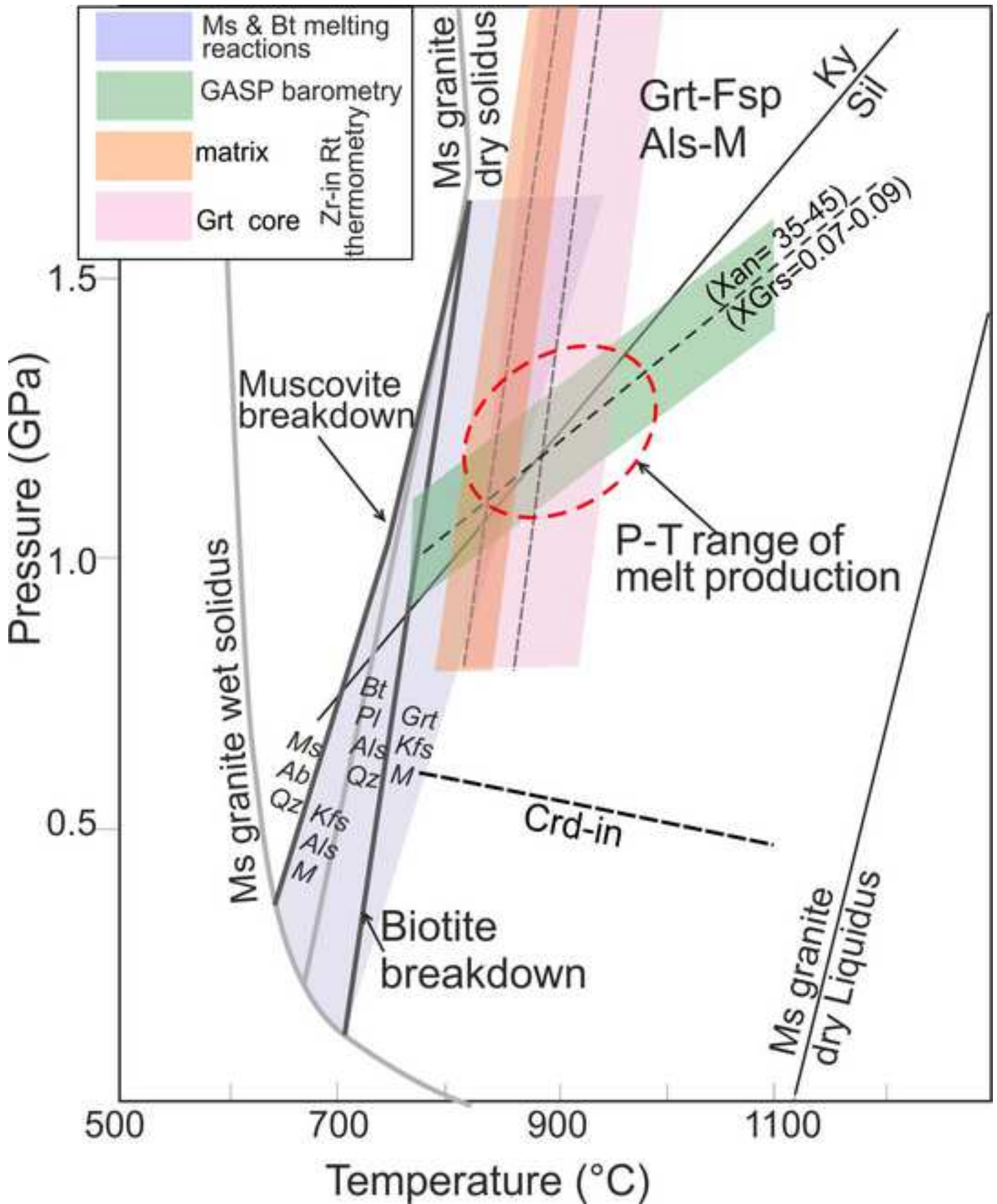


Figure 13
[Click here to download high resolution image](#)

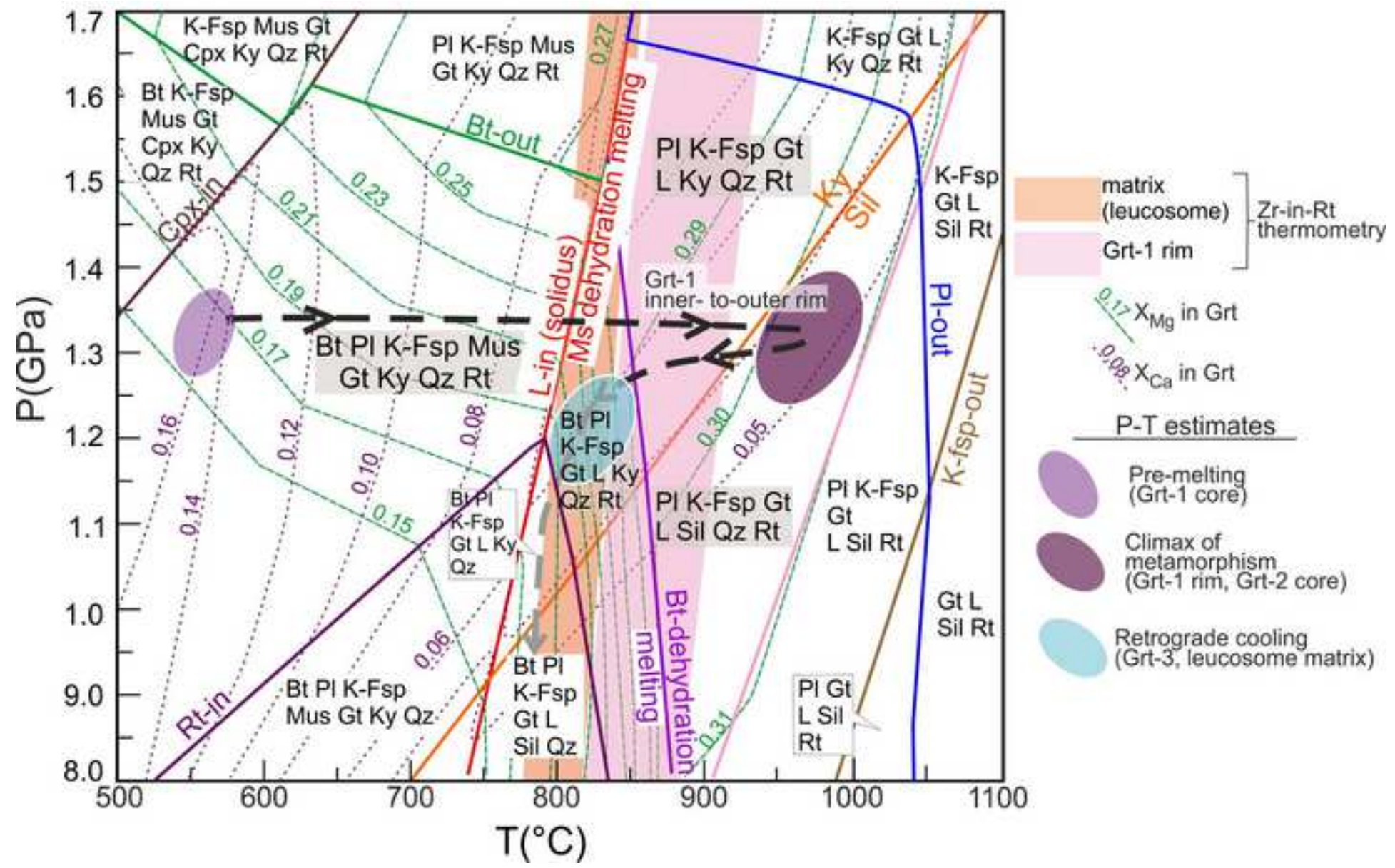
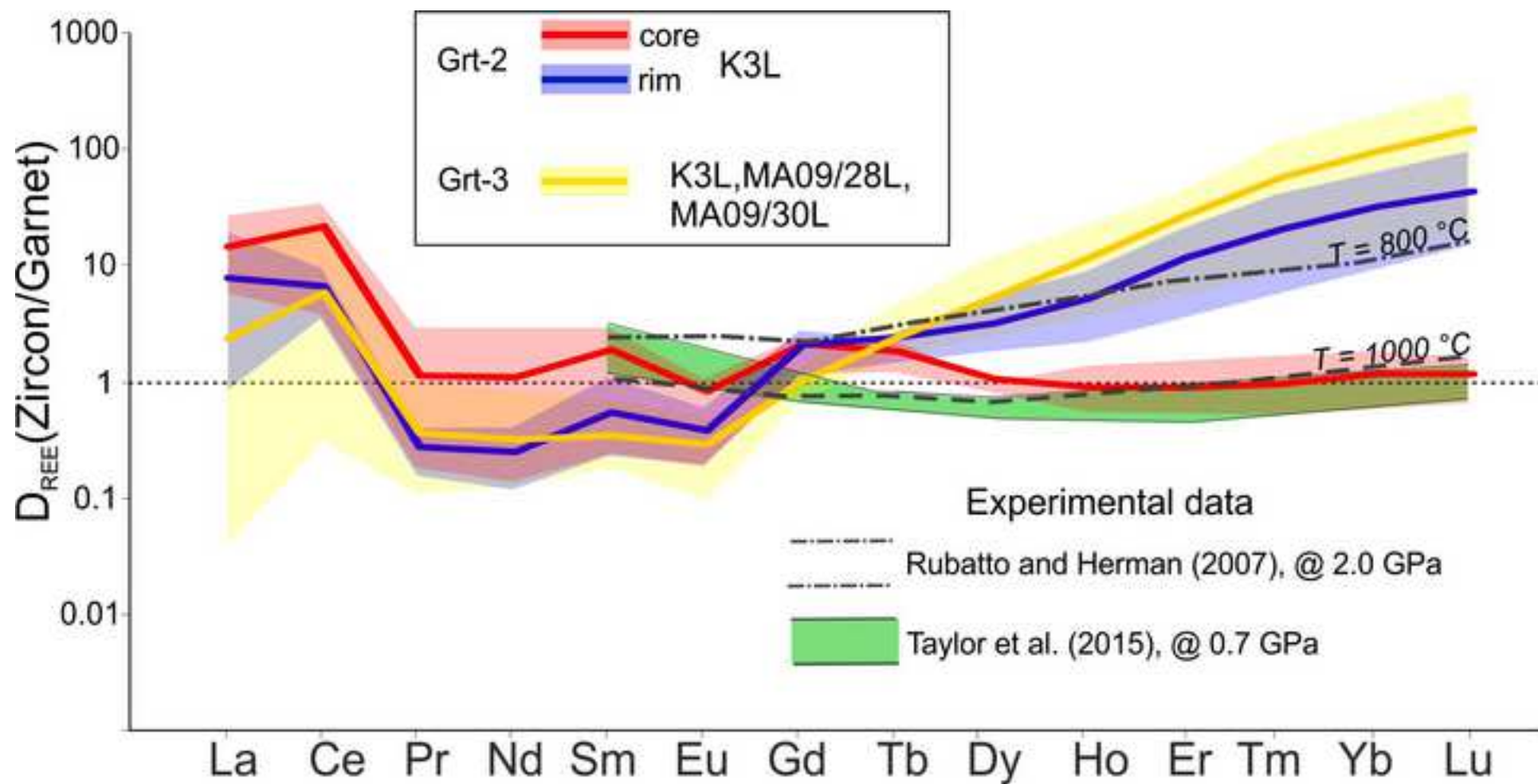
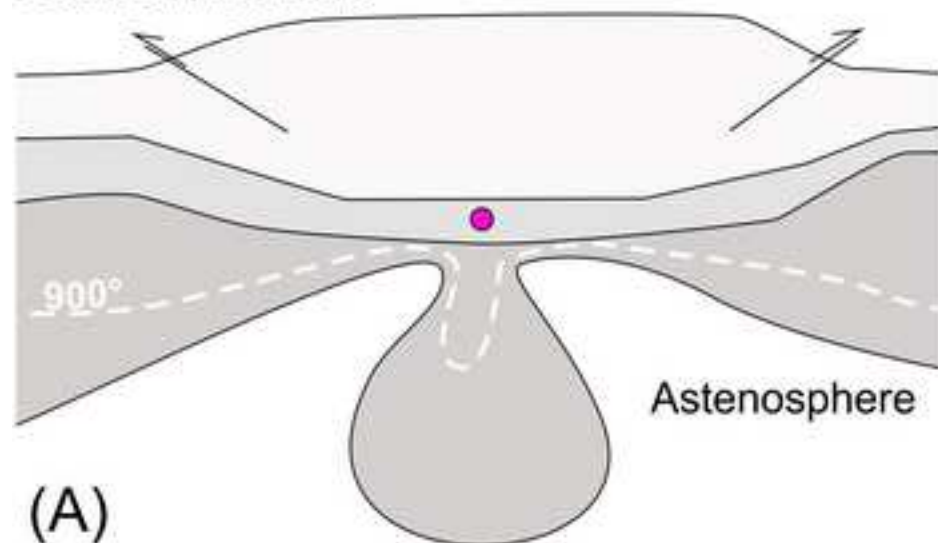


Figure 14
[Click here to download high resolution image](#)

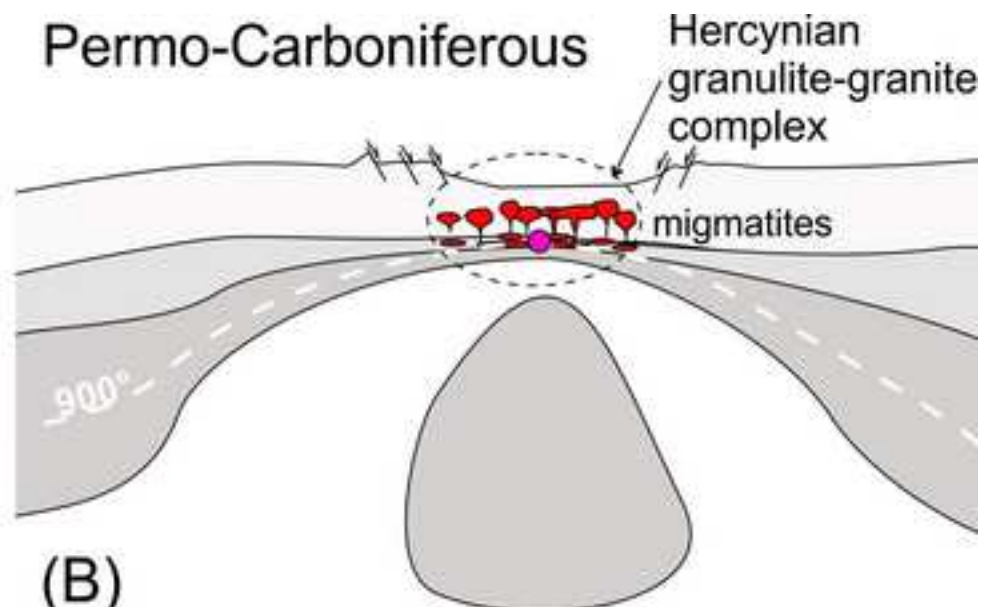


Carboniferous



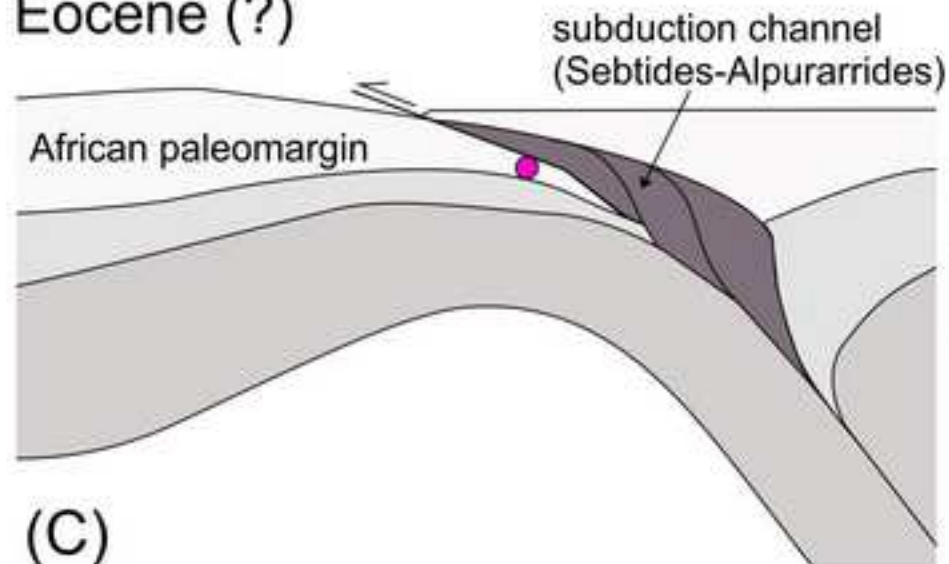
(A)

Permo-Carboniferous



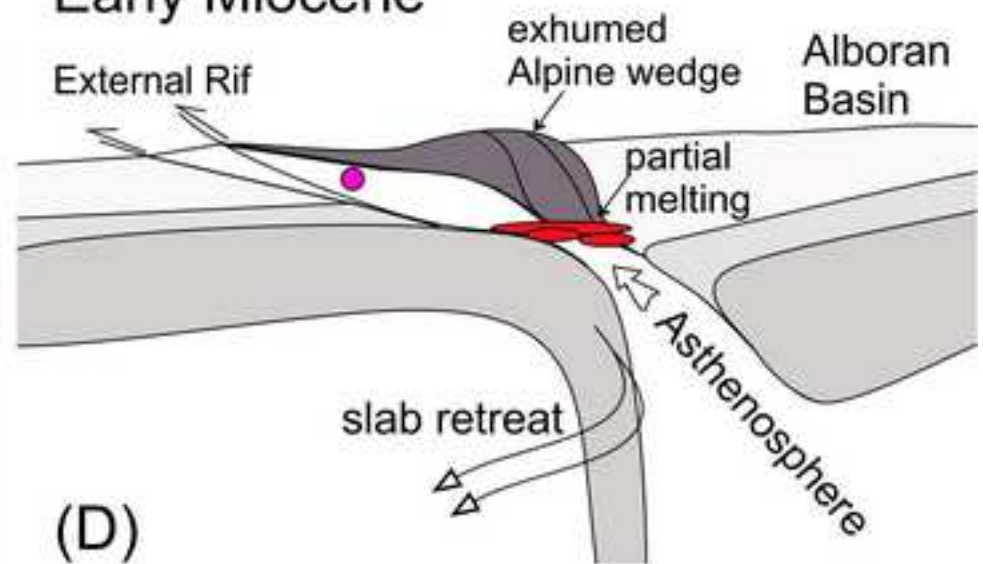
(B)

Eocene (?)



(C)

Early Miocene



(D)

● Beni Bousera units
● Crustal anatexis

□ Upper crust
□ Lower crust
□ Mantle lithosphere

Table 1

Table 1 - Location of analysed samples with constituent mineralogy and analytical techniques

Sample	Latitude	Longitude	Rock type	Mineral assemblage	EMPA	U-(Th)-Pb geochronology	whole rock geochemistry	in situ LA-ICPMS analysis
K3M	N35°19'19.6"	W004°55'51.2"	Melanosome	Qz-Kfs-Pl-Gt-Bt-Ky/Sil-Rt +Crd +Ap +Zrc +Mnz	X		X	
K3L	N35°19'19.6"	W004°55'51.2"	Leucosome	Qz-Kfs-Pl-Gt-Bt-Ky-Rt +Sil +Ap +Zrc	X	X	X	X
K1	N35°19'19.6"	W004°55'51.2"	Leucosome	Qz-Kfs-Pl-Gt-Bt-Ky-Rt +Sil +Ap +Zrc	X		X	
K2	N35°19'19.6"	W004°55'51.2"	Leucosome	Qz-Kfs-Pl-Gt-Bt-Ky/Sil-Rt +Sil +Ap +Zrc	X		X	
Ma09/28M	N35°19'19.6"	W004°55'51.2"	Melanosome/Leucosome layering	Qz-Kfs-Pl-Gt-Bt-Ky/Sil-Rt +Crd + Ap + Zrc +Mnz	X		X	
Ma09/28L	N35°19'19.6"	W004°55'51.2"	Leucosome	Qz-Kfs-Pl-Gt-Bt-Ky-Rt +Sil +Ap +Zrc		X	X	X
B	N35°19'20.1"	W004°55'41.8"	Melanosome/Leucosome layering	Qz-Kfs-Pl-Gt-Bt-Ky/Sil-Rt +Crd + Ap + Zrc +Mnz	X		X	
Ma09/30L	N35°19'20.1"	W004°55'41.8"	Leucosome	Qz-Kfs-Pl-Gt-Bt-Ky-Rt +Sil +Ap +Zrc	X	X	X	X
Ma09/30M	N35°19'20.1"	W004°55'41.8"	Melanosome/Leucosome layering	Qz-Kfs-Pl-Gt-Bt-Ky/Sil-Rt +Crd + Ap + Zrc +Mnz	X		X	
Ma48	N35°19'20.1"	W004°55'41.8"	Melanosome/Leucosome layering	Qz-Kfs-Pl-Gt-Bt-Ky/Sil-Rt +Crd + Ap + Zrc +Mnz	X			

Table 2

Table 2 - Whole rock chemical compositions

(wt%)	Leucosome ⁽¹⁾						Melanosome ⁽¹⁾	Melanosome-leucosome Layering		
	Ma09/28L	Ma09/30	K1	K2	K3L	Av(K1-K2-K3L) ⁽⁵⁾	K3M	MA09/28M	MA09/32	B
SiO ₂	76.62	74.72	71.98	70.51	71.51	71.33	41.01	58.19	52.28	63.08
Al ₂ O ₃	12.26	14.42	14.84	15.41	15.50	15.25	28.82	16.7	23.81	18.36
Fe ₂ O _{3(T)}	0.96	1.29	1.26	2.06	1.58	1.63	16.92	8.2	12.41	7.66
MnO	0.024	0.027	0.06	0.09	0.04	0.06	0.429	0.072	0.294	0.13
MgO	0.09	0.33	0.16	0.35	0.24	0.25	4.18	3.52	3.02	2.11
CaO	1.14	1.56	1.88	2.01	1.76	1.88	1.47	4.13	0.85	2.1
Na ₂ O	2.62	1.7	2.78	2.57	2.67	2.67	0.57	2.29	0.35	0.92
K ₂ O	5.42	5.57	5.48	5.29	5.43	5.40	3.09	2.16	2.73	2.88
TiO ₂	0.016	0.141	0.02	0.01	0.02	0.01	1.437	1.463	1.427	1.001
P ₂ O ₅	0.1	0.14	0.12	0.18	0.13	0.14	0.07	0.03	0.1	0.19
LOI	0.24	0.68	0.12	0.09	0.23	0.15	2.54	2.89	2.1	2.18
Total	99.49	100.58	98.70	98.57	99.11	98.79	100.54	99.65	99.37	100.61
A/CNK	1.00	1.24	1.07	1.13	1.15	1.12	4.14	1.23	4.69	2.17
(ppm)										
Sc	1	1	3	6	3		54	17	32	18
Be	< 1	< 1	< 1	4	< 1		2	1	1	1
V	< 5	< 5	< 5	< 5	< 5		358	269	264	167
Cr	< 20	< 20	< 20	< 20	< 20		270	220	180	110
Co	< 1	< 1	< 1	1	< 1		39	32	33	19
Ni	< 20	< 20	< 20	< 20	< 20		90	60	70	50
Cu	< 10	< 10	< 10	< 10	< 10		30	100	40	40
Zn	< 30	< 30	< 30	< 30	< 30		190	160	180	110
Ga	10	10	11	17	14		34	23	42	23
Ge	2.2	1.5	2.5	2.7	1.6		4.1	0.5	3.1	1.7
As	< 5	< 5	< 5	< 5	< 5		< 5	< 5	5	< 5
Rb	148	10	134	124	158		120	97	118	113
Sr	239	215	268	335	261		119	195	89	167
Y	4.2	3.6	6.9	16.2	7.1		84.6	10	57.3	36.3
Zr	9	72	4	3	5		398	248	291	235
Nb	< 0.2	< 0.2	< 0.2	< 0.2	0.3		21.4	19.9	20.1	15.8
Mo	< 2	< 2	< 2	< 2	< 2		< 2	3	3	< 2
Ag	< 0.5	3.9	< 0.5	< 0.5	< 0.5		1.5	< 0.5	< 0.5	< 0.5
In	< 0.1	< 0.1	< 0.1	< 0.1	< 0.1		0.1	< 0.1	< 0.1	< 0.1
Sn	< 1	< 1	< 1	< 1	< 1		< 1	< 1	< 1	1
Sb	< 0.2	< 0.2	< 0.2	< 0.2	1.6		< 0.2	< 0.2	1.6	< 0.2
Cs	2.1	0.2	1.2	0.5	1.6		1.1	0.5	1.3	0.6
Ba	676	41	736	822	722		770	389	598	752
La	4.14	6.18	5.73	6.89	5.79		81.9	15.4	82.8	53.8
Ce	6.76	10.1	8.76	13.8	9.35		163	33.4	178	107
Pr	0.66	0.94	0.82	1.6	0.83		17.1	3.84	18.3	11.2
Nd	2.38	3.07	2.78	6.38	3.11		62.5	13.8	66.5	38.5
Sm	0.45	0.57	0.5	1.44	0.67		12.5	2.42	13.8	8.03
Eu	1.8	1.89	2.11	1.84	2.46		1.84	1.75	2.18	2.03
Gd	0.43	0.32	0.49	1.15	0.65		11.3	1.7	11.1	7.13
Tb	0.09	0.06	0.13	0.26	0.15		2.11	0.25	1.89	1.18
Dy	0.62	0.39	0.97	2.12	1.18		14.3	1.58	11	6.31
Ho	0.14	0.11	0.22	0.54	0.28		3.06	0.38	2.16	1.21
Er	0.48	0.45	0.76	1.91	0.97		9.19	1.18	6.54	3.42
Tm	0.078	0.088	0.15	0.374	0.165		1.36	0.173	0.978	0.498
Yb	0.55	0.78	1.14	2.86	1.32		9.25	1.3	6.18	3.07
Lu	0.09	0.145	0.176	0.466	0.219		1.32	0.197	0.902	0.444
Hf	0.2	23.5	< 0.1	< 0.1	0.2		10.2	6.1	7.8	5.7
Ta	0.08	< 0.01	0.02	0.02	0.03		1.42	1.23	1.17	1.08
W	1.1	< 0.5	< 0.5	< 0.5	0.5		< 0.5	< 0.5	< 0.5	0.9
Tl	0.61	0.13	0.67	0.61	0.85		0.5	0.28	0.88	0.71
Pb	39	10	64	39	89		18	< 5	17	17
Bi	< 0.1	< 0.1	< 0.1	< 0.1	< 0.1		< 0.1	< 0.1	0.1	8.9
Th	0.11	0.34	0.41	0.11	0.45		22.6	2.52	31.2	17
U	0.15	2.61	0.25	0.15	0.36		1.86	0.99	2.03	1.38
(La/Sm) _N	5.94	7.00	7.40	3.09	5.58		4.23	4.11	3.87	4.33
(La/Yb) _N	5.40	5.68	3.61	1.73	3.15		6.35	8.50	9.61	12.57
Eu/Eu*	12.51	13.53	13.03	4.37	11.40		0.47	2.64	0.54	0.82
^(a) T _{Zr} (°C)	585	738	541	529	557					

⁽¹⁾ Grey shaded whole rock compositions are used for the pseudosection modelling

⁽⁵⁾ Average whole rock compositions used for the pseudosection modelling

^(a) T_{Zr} (°C) = Zircon saturation thermometry (Watson and Harrison, 1983)

Table 3 - Results of U-Th-Pb LA-ICP-MS analyses and calculated ages for zircon separates from the granulite migmatites of the Beni Boussera unit

Sample KSL

grain	L-No	Texture/Position	²³⁸ Pu (ppm)	U ¹ (ppm)	Pb ² (ppm)	Th ³ (ppm)	²⁰⁶ Pb/ ²³⁸ U		²⁰⁷ Pb/ ²³⁵ U		²⁰⁶ Pb/ ²³⁵ U		Age (Ma)							
							±1σ	±2σ	±1σ	±2σ	±1σ	±2σ	±1σ	±2σ						
Z61	a1	oscillatory	5082	562	18	0.033	0.0361	3.2	0.256	4.1	0.014	2.6	0.77	229	7	231	9	267	60	
Z62	a2	oscillatory	3328	491	18	0.037	0.0401	3.0	0.291	4.4	0.026	3.4	0.68	24	7	259	10	314	73	
Z70	a3	oscillatory	3965	391	15	0.034	0.0414	2.3	0.293	3.6	0.013	2.7	0.66	281	6	261	8	254	62	
Z74	a4	oscillatory	3239	371	13	0.028	0.0391	2.8	0.279	4.0	0.017	2.9	0.69	247	6	250	7	273	66	
Z75	a5	oscillatory	5131	1000	41	0.032	0.0446	2.8	0.322	3.9	0.023	2.7	0.72	281	8	283	10	300	61	
Z8a	a6	oscillatory	1102	145	5	0.024	0.0345	3.4	0.467	7.4	0.017	2.4	0.62	18	3	223	8	283	18	
Z8a1	a7	overgrowth	1184	716	23	0.002	0.00349	2.6	0.023	1.5	0.0476	1.7	0.15	22.5	0.6	230	4.0			
Z8a2	a8	oscillatory	203	263	7.7	0.028	0.0391	4.9	0.421	5.0	0.027	3.0	0.46	20	3	211	11	316	115	
Z8b	a9	oscillatory	3373	357	13	0.030	0.0411	2.5	0.301	4.3	0.021	3.0	0.60	260	6	267	10	333	78	
Z8b1	a10	overgrowth	1244	688	21	0.010	0.00332	3.0	0.021	6.9	0.0461	6.2	0.43	21.4	0.6	214	1.5			
Z8b2	a11	oscillatory	889	991	32	0.041	0.0570	2.8	0.260	3.4	0.029	2.4	0.63	234	6	235	6	237	80	
Z8a1	a12	overgrowth	2136	312	11	0.022	0.0432	3.6	0.316	5.0	0.031	3.5	0.72	272	10	279	12	323	79	
Z8a	a13	oscillatory	2662	362	12	0.041	0.0561	2.6	0.293	4.6	0.013	3.8	0.56	209	6	210	8	263	87	
Z4b1	a14	oscillatory	6875	1290	49	0.013	0.0422	3.5	0.301	4.5	0.017	2.8	0.78	287	9	287	11	270	74	
Z4a2	a15	oscillatory	4167	369	38	0.026	0.0336	3.3	0.302	4.6	0.044	3.2	0.92	269	9	269	11	257	73	
Z4b	a16	oscillatory	1067	70	30	0.005	0.0461	2.6	0.337	5.9	0.031	5.3	0.44	291	7	295	15	332	121	
Z4b1	a17	oscillatory	3499	360	14	0.031	0.044	2.7	0.302	4.9	0.026	4.7	0.51	281	7	289	13	305	106	
Z4a2	a18	oscillatory	1935	200	8.4	0.018	0.050	2.7	0.460	5.4	0.024	2.1	0.55	284	8	286	12			
Z4b1	a19	overgrowth	1170	411	15	0.027	0.0383	3.3	0.0267	6.7	0.005	5.9	0.49	247	0.8	267	1.8			
Z2a1	a20	oscillatory	1136	307	1.2	0.008	0.00349	3.4	0.016	6.4	0.060	5.4	0.52	31.9	0.7	21.7	1.4			
Z2a2	a21	oscillatory	6756	454	18	0.034	0.0441	2.5	0.324	3.2	0.032	2.0	0.79	278	7	285	8	337	44	
Z2b	a22	oscillatory	5267	591	21	0.036	0.0458	2.5	0.307	4.2	0.026	3.4	0.59	289	7	288	11	278	78	
Z2b1	a23	oscillatory	2355	234	10	0.022	0.0458	2.7	0.330	4.8	0.023	4.0	0.56	289	8	290	12	299	91	
Z2b2	a24	oscillatory	1909	192	8.1	0.027	0.0457	2.5	0.333	4.4	0.028	3.5	0.58	288	7	292	11	321	80	
Z10a	a25	overgrowth	1115	332	1.1	0.014	0.00344	3.3	0.018	8.1	0.049	7.4	0.40	22.1	0.7	21.9	1.8			
Z10a1	a26	oscillatory	4115	487	20	0.024	0.0457	3.1	0.326	4.5	0.017	3.3	0.69	288	9	286	11	272	75	
Z10a2	a27	oscillatory	1172	392	1.3	0.009	0.00344	3.9	0.029	7.2	0.048	6.1	0.35	21.4	0.9	23.0	1.6	113	143	
Z14a	a28	overgrowth	1215	719	23.3	0.007	0.00350	2.7	0.016	9.2	0.048	8.8	0.29	22.5	0.6	21.7	2.0			
Z14a1	a29	oscillatory	4266	465	16	0.023	0.0416	2.4	0.424	6.4	0.027	3.6	0.65	201	1	218	8	318	83	
Z2a	a30	overgrowth	2312	382	10	0.012	0.0284	3.6	0.207	4.7	0.030	3.0	0.77	180	5	191	6	328	83	
Z2a1	a31	oscillatory	1608	263	6.1	0.046	0.0162	7.4	0.102	8.2	0.020	3.5	0.90	30	1	88	8	286	80	
Z2a2	a32	oscillatory	1840	74	7.1	0.44	0.0936	2.4	0.783	4.1	0.060	3.3	0.58	57	13	587	18	627	71	
Z2b	a33	outer rim	580	71	6.0	0.067	0.029	4.9	0.426	4.7	0.036	3.4	0.68	50	1	488	26	399	78	
Z2b1	a34	inner rim	533	275	24	0.025	0.039	2.6	0.287	3.7	0.034	6.0	0.70	339	9	339	11	344	60	
Z2a2	a35	oscillatory	2762	229	4.8	0.016	0.0229	4.4	0.166	5.2	0.026	2.8	0.84	146	6	156	8	311	64	
Z2a	a36	overgrowth	316	29	2.1	0.057	0.020	6.9	0.097	8.2	0.013	2.9	0.62	115	1	149	54			
Z2a1	a37	overgrowth	1302	45	0.7	0.11	0.0160	4.8	0.116	6.0	0.028	3.7	0.80	102	5	112	6	321	83	
Z2b	a38	oscillatory	2841	263	11	0.048	0.0342	3.8	0.282	4.7	0.012	4.2	0.81	217	8	217	8	281	63	
Z2b1	a39	oscillatory	4628	206	15	0.35	0.0736	3.6	0.592	4.3	0.008	2.2	0.85	40	1	472	16	632	48	
Z4a	a40	oscillatory	804	305	41	0.010	0.068	3.8	0.102	6.0	0.018	3.8	0.68	624	6	635	10	638	68	
Z4a1	a41	oscillatory	3964	156	16	0.35	0.104	3.1	0.860	4.1	0.000	2.7	0.75	637	19	604	19	604	58	
Z4a2	a42	overgrowth	194	145	10.8	0.048	0.0374	4.8	0.278	6.6	0.066	4.4	0.76	11	24	4	478	28		
Z4a1	a43	lamellar inner rim	3413	169	26.1	0.044	0.157	5.5	0.221	3.2	0.027	3.8	0.48	1185	45	1668	58			
Z8a1	a44	overgrowth	2217	185	17	0.029	0.100	5.4	0.056	6.4	0.019	3.4	0.85	616	32	628	30	672	72	
Z8a2	a45	oscillatory	1047	244	42	0.05	0.177	4.0	0.105	2.4	0.02	4.0	1029	60	174	50	174	50		
Z8a	a46	oscillatory	6047	94	15	0.32	0.151	3.9	2.10	4.7	0.101	2.7	0.82	306	33	1150	33	1647	50	
Z7a	a47	oscillatory	12395	30	1.7	0.43	0.040	2.6	0.5	1.4	0.244	4.4	0.14	258	20	309	37	309	37	
Z7a1	a48	overgrowth	466	204	2.9	0.48	0.0151	7.2	0.114	11.4	0.050	8.9	0.63	96	7	110	12	412	198	
Z7a2	a49	overgrowth	1848	458	28	0.46	0.08	7.8	0.468	28	0.018	4.2	0.88	604	45	632	48	632	48	
Z6a1	a50	inner rim	1834	306	5.3	0.054	0.185	5.4	0.137	7.3	0.036	3.7	0.87	118	7	130	9	355	83	
Z6a2	a51	overgrowth	12410	457	1.5	0.015	0.00350	5.4	0.022	6.0	0.040	2.6	0.80	22.5	1.2	22.3	1.3			
Z6b	a52	oscillatory	102	18	0.18	0.037	0.39	0.016	1.3	0.20	0.16	1.3	0.55	0.16	0.18	0.16	0.18	0.16	0.18	

Sample MA09/20L

grain	L-No	Texture/Position	²³⁸ Pu (ppm)	U ¹ (ppm)	Pb ² (ppm)	Th ³ (ppm)	²⁰⁶ Pb/ ²³⁸ U		²⁰⁷ Pb/ ²³⁵ U		²⁰⁶ Pb/ ²³⁵ U		Age (Ma)							
							±1σ	±2σ	±1σ	±2σ	±1σ	±2σ	±1σ	±2σ						
Z1	a05	oscillatory	8786	464	17	0.01	0.03996	4.4	0.285	4.8	0.0164	1.8	0.52	253	11	254	11	269	42	
Z2	A06	oscillatory	7877	389	18	0.01	0.03664	3.0	0.354	4.0	0.0154	1.0	0.77	315	11	310	10	346	44	
Z2	A07	oscillatory	6747	380	19	0.01	0.04865	2.1	0.3597	2.7	0.0254	1.7	0.78	312	7	312	7	309	38	
Z3	A08	oscillatory	6719	436	19	0.01	0.0414	2.5	0.3466	3.2	0.0223	3.0	0.72	292	7	292	7	292	7	
Z3	A09	oscillatory	8722	429	19	0.01	0.04717	2.6	0.3414	3.4	0.0250	2.2	0.75	297	7	298	9	307	45	
Z4	A10	oscillatory	2411	484	19	0.01	0.0441	19	0.3589	4.3	0.0274	19	0.3589	4.3	0.0274	19	0.3589	4.3	0.0274	19
Z4	A11	oscillatory	21202	1121	35.0	0.003	0.03731	4.3	0.2470	5.0	0.0513	2.0	0.86	214	9	224	10	334	57	
Z4	A12	oscillatory	8931	429	20	0.01	0.04991	2.4	0.3692	3.3	0.0265	2.4	0.70	314	7	319	9	307	54	
Z5	A13	oscillatory	8474	840	21	0.01	0.04664	1.8	0.4242	3.5	0.0245	3.0	0.61	231	6	245	8	305	69	
Z6	A14	oscillatory	17782	1022	36	0.003	0.03897	4.1	0.2761	4.6	0.0138	2.2	0.88	246	10	248	10	258	51	
Z7	A15	oscillatory	8941	429	20	0.01	0.04664	1.8	0.4242	3.5	0.0245	3.0	0.61	231	6	245	8	305	69	
Z5	A16	oscillatory	7185	363	14	0.01	0.04238	3.4	0.3100	4.2	0.0196	2.5	0.80	273	9	274	10	283	57	
Z5	A17	oscillatory	426	426	19	0.01	0.0398	3.0	0.358	4.0	0.0265	2.3	0.74	297	7	297	7	297	7	
Z5	A18	oscillatory	11215	608	24	0.01	0.04302	2.0	0.3105	2.4	0.0234	1.3	0.84	272	5	275	6	300	31	
Z5	A19	oscillatory	9693	489	22	0.01	0.04729	1.9	0.3461	3.3	0.0210	2.7	0.58	298	6	302	9	333	61	
Z5	A20	oscillatory	8386	430	19	0.01	0.04773	2.2	0.343	3.0	0.0218	2.4	0.71	291	6	292	9	293	49	
Z7	A21	oscillatory	21081	1266	44	0.00														

Table 4

Table 4 - Selected Trace and REE elements of garnets and zircon from leucosomes as obtained through in situ LA-ICPMS analyses and corresponding Zircon/Garnet REEs distribution coefficients (D_{REE})

Sample Mineral	K3L - MA09/28L - MA09/30L Zircon		K3L				MA09/28L				MA09/30L		Average	
			Grt-2 cores		Grt-2 rim				Grt-3					
	Average (n=22)	Range	Average (n=6)	Range	Average (n=9)	Range	Average (n=14)	Range	Average (n=3)	Range	Average (n=5)	Range	Average (n=22)	Range
REE elements (ppm)														
La	0.09	0-1.02	0.01	0-0.02	0.04	0-0.11	0.35	0.03-2.39	0.12	0.05-0.16	0.02	0.01-0.03	0.27	0.01-2.39
Ce	1.21	0.29-3.39	0.11	0.03-0.31	0.22	0.12-0.33	0.84	0.28-3.84	0.35	0.18-0.45	0.10	0.05-0.16	0.61	0.05-3.84
Pr	0.05	0.01-0.18	0.11	0.02-0.28	0.22	0.13-0.33	0.28	0.16-0.49	0.10	0.06-0.13	0.12	0.05-0.24	0.22	0.05-0.49
Nd	1.11	0.42-3.06	2.60	0.48-7.6	5.36	2.67-9.2	5.73	3.31-8.64	1.63	1.48-1.8	4.25	1.79-7.38	4.83	1.48-8.64
Sm	4.49	1.74-8.56	5.11	1.47-17.31	10.65	3.98-18.98	18.67	13.91-24.69	7.34	7.27-7.43	13.36	6.29-21.47	15.92	6.29-24.69
Eu	0.28	0.07-0.38	0.54	0.25-1.45	0.89	0.46-1.42	1.11	0.65-1.62	0.97	0.86-1.1	1.37	0.58-2.92	1.15	0.58-2.92
Gd	36.38	12.48-48.1	19.63	14.24-29.57	20.42	12.83-31.46	43.04	28-52	30.94	30.26-32.15	33.94	26.84-39.12	39.32	26.84-52
Tb	14.18	4.41-19.48	8.58	6.03-11.24	6.51	5.12-9.45	6.71	4.63-8.26	6.00	5.42-6.63	6.70	2.95-8.78	6.61	2.95-8.78
Dy	140.57	45.05-178.02	142.26	129.88-168.64	53.62	25.02-76.25	30.41	18.03-41.36	27.39	21.33-33.65	39.23	11.77-57.83	32.00	11.77-57.83
Ho	42.07	14.66-56.68	57.36	29.33-72.38	10.66	4.58-18.77	4.12	2.17-6.94	3.68	2.52-4.8	6.74	1.83-11.59	4.65	1.83-11.59
Er	188.00	69.05-277.14	271.11	113.14-342.46	23.52	8.74-50.72	8.25	4.07-17.61	7.37	4.1-10.59	17.98	4.27-32.51	10.34	4.07-32.51
Tm	38.11	14.81-57.38	53.11	21.33-69.96	2.77	0.89-5.93	0.80	0.39-2.22	0.80	0.32-1.27	2.26	0.53-3.83	1.13	0.32-3.83
Yb	369.68	148.87-543.59	411.99	191.61-593.51	17.13	5.33-39.43	4.46	1.87-11.71	4.85	2.98-7.29	15.69	3.87-26.71	7.07	1.87-26.71
Lu	64.75	25.83-100.62	69.03	36.68-94.42	2.17	0.65-4.22	0.51	0.2-1.23	0.58	0.29-0.98	1.81	0.43-3.06	0.82	0.2-3.06
Σ LREE	2.44	0.74-6.87	2.83	0.54-8.19	5.84	2.96-9.78	7.20	4.34-12.01	2.20	1.78-2.49	4.48	1.96-7.77	5.90	1.78-12.01
Σ HREE	893.73	335.16-1264.24	1033.07	552.19-1365.66	136.80	80.94-218.36	98.29	63.26-137.11	81.60	67.37-97.34	124.35	52.49-180.62	101.94	52.49-180.62
(La/Sm) _N	0.01	0-0.15	0.002	0-0.003	0.003	0-0.007	0.12	0.06-0.29	0.19	0.12-0.27	0.53	0.17-0.88	0.01	0.001-0.099
(Yb/Gd) _N			26.94	8.75-38.02	1.12	0.42-2.85	5.23	2.36-7.7	4.05	3.09-4.79	1.88	1.17-2.88	0.22	0.06-0.88
(Dy/Yb) _N	0.27	0.19-0.38												
Eu/Eu*	0.07	0.05-0.11	0.17	0.12-0.20	0.19	0.09-0.27	0.12	0.08-0.20	0.20	0.18-0.22	0.19	0.13-0.37	0.15	0.08-0.37
Ti	5.31	3.38-13.81												
T °C [± 70 °C] ^a	684	654-770												
$D_{REE}^{Zrn/Grt}$														
La			13.35	6.11-28.36	7.19	0.84-22.63	0.99	0.04-3.72	0.98	0.57-1.76	9.03	3.27-15.7	2.19	0.04-15.70
Ce			19.75	3.95-37.05	6.14	3.62-9.86	2.56	0.31-4.34	4.03	2.70-6.60	14.35	7.55-25.94	5.44	0.31-25.94
Pr			1.07	0.18-2.94	0.26	0.16-0.41	0.22	0.11-0.32	0.58	0.41-0.83	0.57	0.22-1.00	0.35	0.11-1.00
Nd			1.03	0.15-2.29	0.24	0.12-0.42	0.21	0.13-0.33	0.69	0.62-0.75	0.34	0.15-0.62	0.30	0.13-0.75
Sm			1.76	0.26-3.05	0.52	0.24-1.13	0.25	0.18-0.32	0.61	0.60-0.62	0.40	0.21-0.71	0.33	0.18-0.71
Eu			0.78	0.20-1.11	0.36	0.20-0.62	0.27	0.17-0.43	0.29	0.26-0.33	0.28	0.1-0.49	0.28	0.1-0.49
Gd			1.98	1.23-2.55	1.95	1.16-2.84	0.87	0.70-1.30	1.18	1.13-1.20	1.10	0.93-1.36	0.96	0.70-1.36
Tb			1.72	1.26-2.35	2.25	1.50-2.77	2.17	1.72-3.06	2.38	2.14-2.62	2.47	1.61-4.80	2.27	1.61-4.80
Dy			1.00	0.83-1.08	2.97	1.84-5.62	4.84	3.40-7.80	5.31	4.18-6.59	4.96	2.43-11.95	4.93	2.43-11.95
Ho			0.84	0.58-1.43	4.85	2.24-9.19	11.08	6.06-19.39	12.27	8.77-16.68	9.32	3.63-22.96	10.84	3.63-22.96
Er			0.84	0.55-1.66	10.72	3.71-21.51	26.29	10.67-46.17	29.64	17.76-45.83	17.00	5.78-44.05	24.64	5.78-46.17
Tm			0.91	0.54-1.79	18.71	6.43-42.62	57.87	17.2-97.77	65.41	30.01-118.31	27.48	9.96-71.33	51.99	9.96-118.31
Yb			1.09	0.62-1.93	29.25	9.38-69.38	103.34	31.57-198.07	87.13	50.71-123.98	37.66	13.84-95.56	86.20	13.84-198.07
Lu			1.10	0.69-1.77	39.35	15.34-100.04	161.31	52.7-325.73	142.08	66.27-225.52	56.82	21.15-149.37	134.94	21.15-325.73

^aTi-in-zircon thermometry (Ferry and Watson, 2007).